IMPROVING NON-VIRAL GENE DELIVERY: POLYMER CARRIERS FOR SPATIAL AND TEMPORAL CONTROL OF NUCLEIC ACID RELEASE

by

Abbygail A. A. Foster

A dissertation submitted to the Faculty of the University of Delaware in partial fulfillment of the requirements for the degree of Doctor of Philosophy in Chemical Engineering

Spring 2014

ProQuest LLC.
789 East Eisenhower Parkway
P.O. Box 1346
Ann Arbor, MI 48106 - 1346

IMPROVING NON-VIRAL GENE DELIVERY:

POLYMER CARRIERS FOR SPATIAL AND TEMPORAL

CONTROL OF NUCLEIC ACID RELEASE

by

Abbygail A. A. Foster

Approved: _____

Abraham M. Lenhoff, Ph.D.
Chair of the Department of Chemical and Biomolecular Engineering

Approved: _____

Babatunde A. Ogunnaike, Ph.D.
Dean of the College of Engineering

Approved: _____

James G. Richards, Ph.D.
Vice Provost for Graduate and Professional Education

I certify that I have read this dissertation and that in my opinion it meets the academic and professional standard required by the University as a dissertation for the degree of Doctor of Philosophy.

Signed: _____

Millicent O. Sullivan, Ph.D.
Professor in charge of dissertation

I certify that I have read this dissertation and that in my opinion it meets the academic and professional standard required by the University as a dissertation for the degree of Doctor of Philosophy.

Signed: _____

Eric M. Furst, Ph.D.
Member of dissertation committee

I certify that I have read this dissertation and that in my opinion it meets the academic and professional standard required by the University as a dissertation for the degree of Doctor of Philosophy.

Signed: _____

April M. Kloxin, Ph.D.
Member of dissertation committee

I certify that I have read this dissertation and that in my opinion it meets the academic and professional standard required by the University as a dissertation for the degree of Doctor of Philosophy.

Signed: _____

Kelvin H. Lee, Ph.D.
Member of dissertation committee

I certify that I have read this dissertation and that in my opinion it meets the academic and professional standard required by the University as a dissertation for the degree of Doctor of Philosophy.

Signed: _____

Robert E. Akins, Ph.D.
Member of dissertation committee

ACKNOWLEDGMENTS

I would like to offer my thanks to a number of people without whom this dissertation would not have been possible:

First, I would like to thank my advisor, Dr. Millicent Sullivan for her guidance, patience, and support that have helped me to hone my skills as a researcher and provided a wonderful atmosphere for graduate study. Millie has been a kind and approachable mentor and I am sincerely grateful for the opportunity to have worked in her lab.

I would like to thank my committee members, Dr. April Kloxin, Dr. Robert Akins, Dr. Eric Furst, and Dr. Kelvin Lee for their valuable feedback and insight throughout my graduate work, and for the numerous discussions that have helped to directly guide and improve the studies detailed in this dissertation. Additionally, I would like to thank Dr. Thomas Epps, III for taking an interest in my work and growth as a researcher. I truly appreciate the many useful discussions over the years.

Throughout my time at the University of Delaware I have benefited from interactions with several graduate students who have all enriched my graduate career. I would like to thank my fellow Sullivan lab mates – those who have moved on, those in the middle, and those just beginning – for their insightful discussion, humor and continued support that made it a pleasure to work in the Sullivan lab. I would specifically like to thank Dr. Peter Millili, Dr. Kory Blocker, Dr. Meghan Reilly and Dr. John Larsen for their mentorship in my early years of graduate school. My graduate career would not have been the same without them. I would also like to

acknowledge Dr. Scott Crown, Andrea Naranjo, Patrick McNeely, and Kyle Doolan for their friendship, enthusiasm, and comments on my work.

I would like to thank my family and friends who have been a constant source of inspiration and have provided tremendous support for as long as I can remember. Thanks go to my parents and younger brother who have always supported me and never doubted my potential for success. I am also grateful to my grandparents and a large collection of aunts and uncles for their wisdom and guidance in all of my pursuits. Thank you to my dear friends Andrea and Monique who have treated me like a sister for as long as I have known them. I hope our friendship continues until we are old and gray.

Finally, to Andrew, my biggest fan, drill sergeant, voice of reason, and life coach. Thank you for always being in my corner. I look forward to beginning this next chapter of our lives together.

TABLE OF CONTENTS

LIST OF FIGURES

LIST OF TABLES

ABSTRACT

Gene therapy has garnered significant interest over the past few decades as an innovative approach for regulating protein expression towards the treatment of (i) genetic disorders – including cystic fibrosis, severe combined immunodeficiency (SCID), and muscular dystrophy, (ii) acquired/infectious diseases – such as Hepatitis and HIV/AIDS, and (iii) multiple varieties of cancer. Non-viral gene delivery approaches have received particular attention due their low toxicity, high nucleic acid storage capacity, and tailorability as compared to their viral counterparts. However, the efficiency and clinical realization of non-viral delivery vehicles has been limited by an incomplete understanding of their assembly, subcellular trafficking, and intracellular release mechanisms. Thus, the goal of this work was to develop strategies to understand and direct gene association and release using non-viral carriers, with the aim of improving current delivery platforms. Specific milestones of these studies include (1) the identification of the structural and functional consequences of fluorescent labeling of polymeric carriers for intracellular investigations, (2) the development of materials with tunable gene association and release capacity, as well as (3) the identification of novel non-viral approaches to address the functional requirements of gene transfer while promoting versatile preparation methods and facile cell-responsive delivery.

A systematic investigation of the impact of fluorescent modification of an established polymer carrier, polyethylenimine, indicated that the incorporation of

hydrophobic labeling moieties weakened gene association and promoted increased heterogeneity in polyplex structure. Additionally, cellular investigations identified extracellular aggregation and reduced polyplex uptake as a result of this routinely employed structural modification. In the design of controllable methods for promoting gene association and release, a polymeric delivery platform with light-responsive groups along the cationic segment of the polymer backbone was designed to provide controlled nucleic acid assembly and a user-defined method for intracellular release. Additionally, light-mediated polyplex destabilization demonstrated significant utility in siRNA delivery as observed through efficient siRNA release and enhanced protein silencing compared to a commercial Lipofectamine lipoplex. The demonstrated benefits of this stimuli-responsive delivery method motivated a cell-responsive approach to control gene association and release. A novel polymer-peptide conjugate with functional capabilities for controlled release, cell targeting, and endosomal escape was developed to address the numerous functional requirements in the gene delivery pathway.

Ultimately, the clinical realization of gene therapies will rely on the development of methods to elucidate and control gene association and release along the delivery pathway. This will require the development of delivery vehicles whose physical and biochemical properties enable them to appropriately navigate the intra- and extracellular space. In total, this dissertation provides new evidence of the role of structural modifications (including fluorescent probes, targeting ligands and stimuli-responsive groups) for promoting efficient gene association and subsequent delivery and contributes to the growing body of literature to improve our fundamental understanding of the processing of non-viral carriers.

Chapter 1

CURRENT STRATEGIES FOR NON-VIRAL GENE DELIVERY

1.1 Motivation and Overall Goal of Thesis

Gene transfer is a promising therapeutic approach and experimental tool for introducing plasmid DNA, oligonucleotides, short interfering RNA (siRNA), or messenger RNA (mRNA) into eukaryotic cells for a variety of research and drug discovery applications. Specifically, gene therapy presents researchers with the opportunity to: (1) study gene function, (2) establish disease models, and (3) regulate protein expression. Therapeutic strategies have been geared toward applications in disease treatment and regenerative medicine, including the development of materials for wound healing, infectious disease, as well as a range of acquired and heritable genetic diseases ailments.

The vast majority of current gene delivery vehicles involve genetic modification of viruses, which have naturally evolved efficient mechanisms for internalization and transfer of their genetic material. Modification of these viral vectors then involves replacement of the viral genome with therapeutic nucleic acid prior to therapeutic application. As of January 2014, ~67% of ongoing worldwide clinical trials involved viral vectors and a number of these strategies have seen recent success in the clinic.[1] In one such example, researchers at Amgen have developed a re-engineered virus for the selective infection of cancer cells demonstrating reduction in tumor occurrence, delivery to metastatic sites and complete tumor disappearance in 11% of the patients in the study.[2] Similar successes have been observed with the

improvement in vision of patients of the Children's Hospital of Philadelphia being treated for Leber's congenital amaurosis.[3-6] Despite these encouraging results and the high efficiency of transduction using viral methods, it is of note that there are no FDA approved gene therapies on the US market. Unfortunately the viral delivery has faced several adverse effects associated with non-specific viral DNA insertion,[7-9] the occurrence of carcinomas in a number of patients thought to be successfully treated,[10, 11] and in some cases patient death.[12, 13] These roadblocks to the application of viral methods have led to increasing interest into non-viral delivery approaches.

Non-viral gene delivery strategies use synthetic components to facilitate delivery. These vectors are an attractive alternative to their viral counterparts due to several advantageous properties, including low toxicity and a lack of innate immunogenicity.[14] Additionally, these synthetic approaches can be molecularly tuned for improved control over gene delivery. Specifically, cell or tissue-specific functionalities can be incorporated into the design of non-viral vectors and other chemical modifications can be used to allow for spatial and temporal control of delivery. Furthermore, non-viral polymer and lipid packaging materials are also easier to scale-up and have a higher stability for long-term storage compared to their viral counterparts.

Unfortunately, the low gene transfer efficiency of non-viral delivery methods represents a major limitation towards their clinical application. While viruses have naturally evolved to transport their genetic material to intracellular targets non-viral carriers are much less efficient at overcoming the various stages of transport along the delivery pathway. Additionally, there are several poorly understood aspects of subcellular delivery and inconsistent behaviors across a number of non-viral carriers.

It has become increasingly evident that the success of non-viral gene therapy depends on effectively linking vector design and delivery approaches to address the complexity of the cellular space. Thus, the presented studies aimed to develop: (i) methods to understand gene association/release and (ii) novel design strategies to control gene association/release for improved delivery. The following sections will detail the current understanding of the delivery process, as well as some of the state-of-the-art methods that have been used to address the physiological barriers to efficient delivery.

1.2 Improving Delivery: Addressing the Physiological Barriers to Non-viral Transfer

The majority of non-viral carriers currently being explored for nucleic acid delivery are cationic in nature. These systems assemble by electrostatic interactions between the cationic groups in a lipid or polymer (N) and the anionic phosphates in the nucleic acid (P), leading to the formation of condensed lipoplexes (for lipid assemblies) or polyplexes (for polymer-based carriers). The assembly of polyplex structures is routinely reported in terms of an N/P ratio, where efficiently condensed complexes possess a net positive charge (positive N/P) and are able to tightly condense and protect the nucleic acid during the stages of delivery. However, several extracellular and intracellular barriers restrict gene transfer from these structures.[15-20] As seen in Figure 1.1, the polyplexes must address multiple challenges including efficient transport through the blood stream and the extracellular space, cellular recognition and adhesion to the cell surface, cellular internalization, trafficking to the appropriate intracellular target, and unpackaging of the nucleic acid. The following sections will highlight the various physiological barriers to delivery as well as current

strategies and attempts to overcome these barriers to improve non-viral delivery methods.

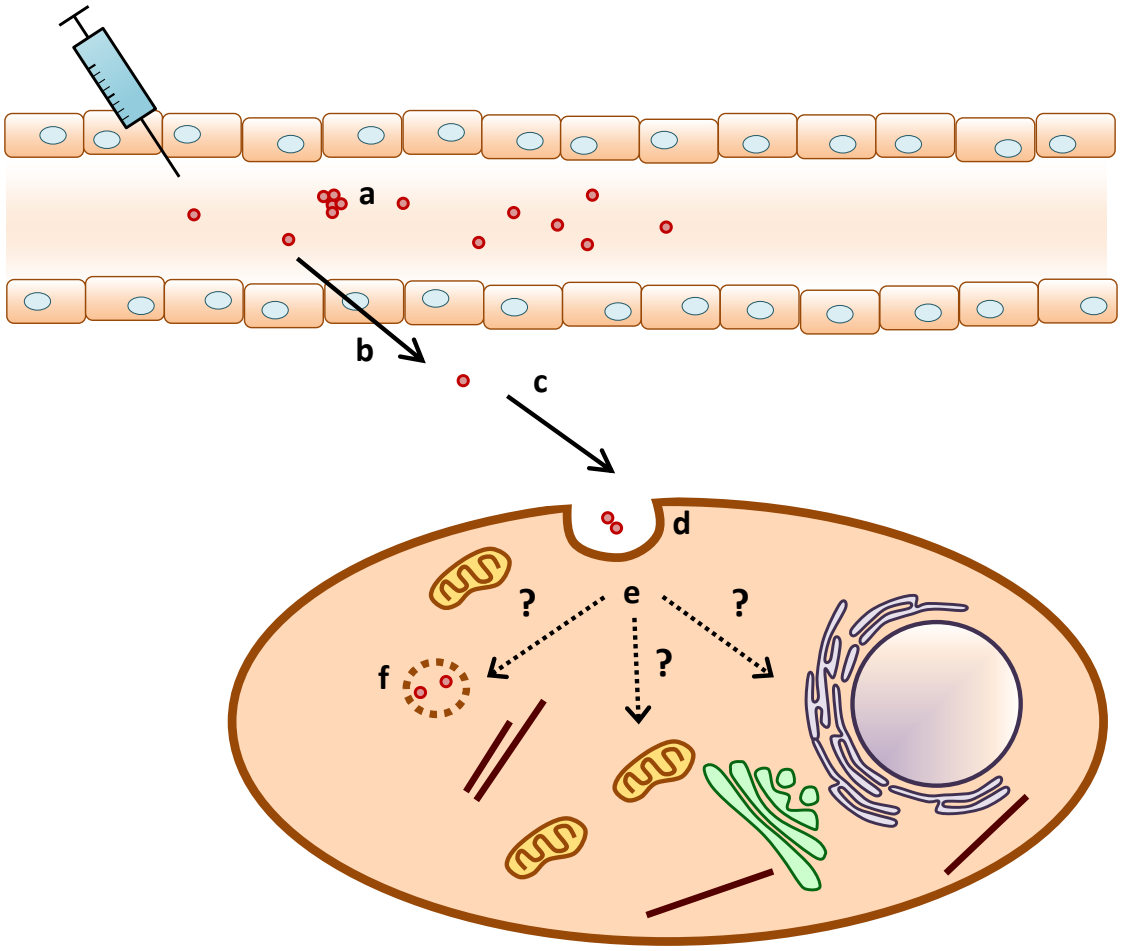

Figure 1.1 **The physiological barriers that decrease the efficiency of non-viral gene delivery include a) stability in the bloodstream, b) accumulation into the target tissue, c) transport in the extracellular space, d) cellular adhesion and uptake, e) intracellular trafficking, and f) vector unpackaging.**

1.2.1 Improving Extracellular Transport

Although a number of non-viral vectors provide high gene transfer activity *in vitro*, there have been several limitations for *in vivo* applications.[21] In particular, *in vivo* applications do not allow for the large therapeutic dosages and excess DNA which are possible *in vitro,* and also face several physiological barriers along the delivery pathway. Barriers to delivery exist in the epithelial space, endothelial cell linings and the extracellular matrix surrounding the cells, which prevent direct access of macromolecules to the target cells. Additionally, nucleases in the extracellular space can degrade free nucleic acids rapidly, within 20 min following administration.[22] Therapies delivered via intravenous administration must travel through the bloodstream and overcome these physiological barriers for successful delivery at a target site.

1.2.1.1 Prolonged Circulation

One significant obstacle to effective delivery is clearance by the reticuloendothelial system (RES),[23, 24] which is initiated by interactions between foreign particles and the phagocytic cells in the blood. Phagocytic cells in the blood and tissues serve key roles in the recognition and clearance of dying cells and invading microbes.[25-27] These cells respond similarly to injected therapeutic particles, resulting in reduced therapeutic efficacy.[28, 29] Numerous studies have demonstrated clearance by the RES within minutes if the delivery vector is not protected from opsonization.[23, 24, 30, 31] Hydrophobic and/or charged nanoparticles are particularly vulnerable to opsonization resulting in shorter circulation half-lives.[32, 33]

A number of properties affect the circulation time of non-viral carriers and have been considered in the rational design of improved structures to prolong

circulation and improve transport. Specifically, the carrier size, shape and surface coating have all been identified as factors that should be considered in designing long-circulating particles. As such the following sections will discuss a number of strategies which have been used to reduce the rapid clearance from the blood stream and uptake by the liver and the spleen by modification of these properties.

1.2.1.1.1 Effects of carrier size and geometry on *in vivo* circulation

The carrier size has been shown to be a crucial determinant of the *in vivo* transport of nanostructures for drug and gene delivery, and a number of studies have demonstrated that smaller particles (10-200nm) are better at avoiding immune recognition and phagocytic clearance than larger structures.[34-36] In one particular study, Fang and coworkers developed poly(methoxypolyethyleneglycol cyanoacrylate-co-*n*-hexadecyl cyanoacrylate) (PEG-PHDCA) nanoparticles at 80, 170 and 240 nm to explore this phenomenon.[36] In this work, they demonstrated less than 20% uptake by macrophages and a 24-fold increase in the serum half-life of their 80nm particles. Similarly, Pessault *et al*. identified that smaller PEGylated nanoparticles have longer blood-circulation half-life in their preparation of PEGylated gold nanoparticles.[34]

More recent approaches to prolong circulation demonstrate that geometry plays a crucial role in the *in vivo* behavior of circulating therapies.[37] In fact, in a study using polystyrene particle of various shapes and sizes, Champion and Mitragotri demonstrate that local particle shape determines whether macrophages initiate phagocytosis of circulating particles.[38] A number of research groups have shown that non-spherical structures are favorable for prolonged circulation and exploited this result in the fabrication of delivery structures.[39-41] For example, in the comparison of soft spherical assemblies with flexible filaments, Geng and coworkers found that the

in vivo circulation time for the nonspherical filomicelles was about 10 times longer than their analogous spherical counterparts.[41]

1.2.1.1.2 Surface modifications and stealth coating

Hydrophobic or charged nanoparticles have been shown to have a shorter circulation half –life than uncharged structures due to high levels of opsonization.[32, 33] As such, a number of delivery platforms have employed modified surface coatings to improve *in vivo* circulation.

Passive "stealth coatings" have been the primary approach for prolonging *in vivo* circulation. With this strategy, therapies developed for systemic application are typically coated with an electrostatically neutral, hydrophilic surface layer to extend the circulation times of non-viral carriers *in vivo*.[42] This "stealth coating" forms a flexible layer, providing steric hindrance for the adsorption of opsonins and resisting phagocytic uptake.[43, 44] Figure 1.2 shows some of the approaches which have been used for applying a passive stealth coating. Poly(ethylene glycol) (PEG) has been used as a stealth coating for delivery in the majority of studies,[28, 45-47] however a number of polymers based on poly(oxazoline),[48] polyvinyl alcohol,[49] poly(glycerol),[50] poly-N-vinylpyrrolidone,[51] and poly[N-(2-hydroxypropyl)methacrylamide][52-54] have also been investigated. These hydrophilic polymers have been incorporated through various approaches including copolymerization in which the stealth polymer is prepared in a block copolymer architecture. This method allows for scalability in preparation, however a number of research groups have identified steric concerns with the stealth block reducing the complexation efficiency of the block copolymer.[55] Alternatively, several lipoplex and polyplex strategies have involved stealth modification following complexation.[56, 57] While this method has reduced effects on

complexation efficiency, there are challenges with the scalability of this process. In a novel approach, Davis and coworkers demonstrated the development of cyclodextrin-based polymer (CDP) inclusion complexes with current clinical applications in siRNA delivery.[58] These inclusion complexes, with surface cyclodextrins, allow for surface modification with PEG-adamantane and enable efficient siRNA and scalable preparation. Despite successful use of passive stealth coatings for surface protection of a number of gene delivery vectors, the vast majority recognize a few disadvantages of surface modification in delivery. Specifically, the polymer coating has been shown to reduce polyplex interactions with the cell surface, hinder uptake in target cells and limit subsequent drug release in a number of carriers.[59-61] Several attempts have been made to enhance the efficacy of these delivery vehicles by controlled cleavage of the polymer coating using stimuli responsive groups, which will be discussed in detail later in this chapter.

As an alternative to passive "stealth" delivery approaches, active strategies to control immune suppression have recently come to the forefront. In particular, in a recent study Discher and coworkers identified minimal "self" peptides by computational design of the CD47 membrane protein.[62] This membrane protein has been shown to impede phagocytosis in mice and is reportedly a marker of "self".[63] In this work Discher et al. demonstrate delayed macrophage-mediated clearance of nanoparticles to promote persistent circulation.[62]

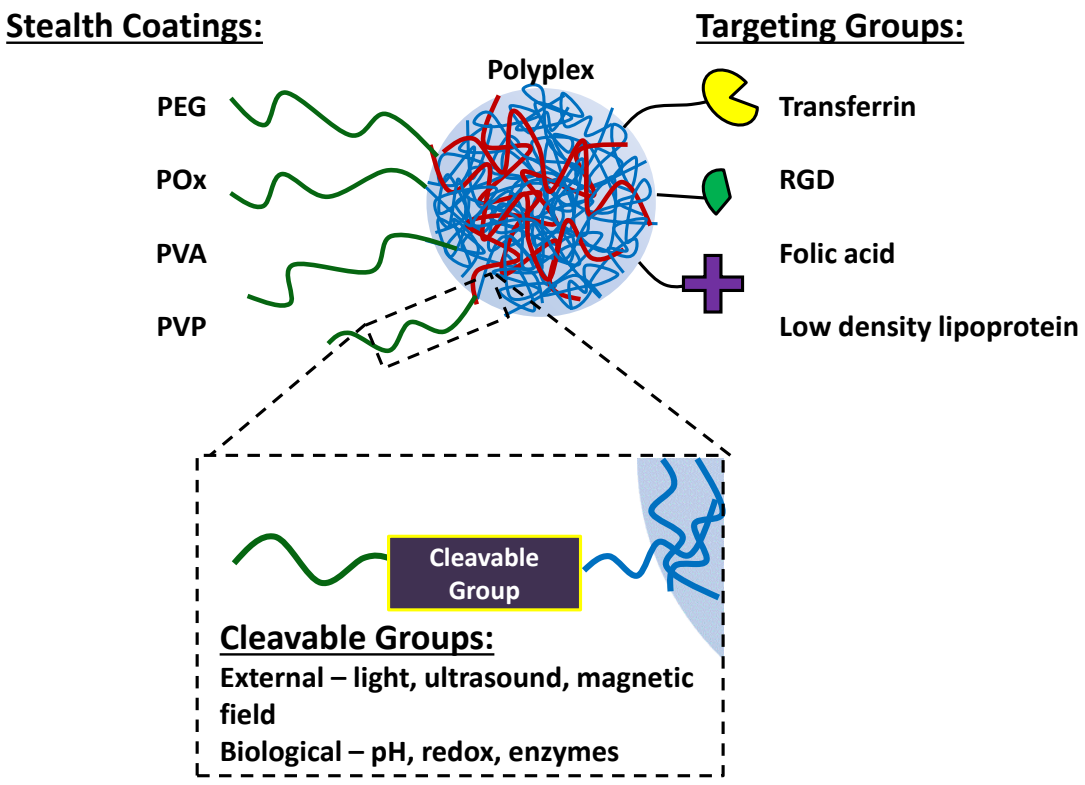

Figure 1.2 Surface modification of non-viral carriers for a) prolonged circulation and b) tissue and cell targeting. Stimuli-responsive groups allow for controlled deshielding of the stealth coating/polymers (green). Polyplex (DNA (red)-cationic polymer (blue)) shown as an example.

1.2.1.2 Tissue targeting

Provided the delivery vehicle remains stable during circulation, it must be able to navigate to a target cell. Unfortunately, developing methods to predictably control delivery to target tissues is a significant hurdle to effective delivery and there is currently no 'magic bullet' for targeted delivery. Targeted delivery approaches attempt to take advantage of the unique physical properties of the target tissues. For example, polyplex systems can be designed to passively accumulate in organs such as the liver

due to the presence of 100-200 nm sinusoidal capillaries along the endothelial wall and absence of basal lamina.[64] Similarly, passive targeting approaches are often employed for delivery to tumor tissue due to the increased levels of vascularization and enhanced vascular permeability. Tumor vessels are highly disorganized, with poor lymphatic drainage and enlarged gap junctions between endothelial cells. This 'leaky' vascularization, as well poor lymphatic drainage leads to enhanced accumulation in the tumor vasculature, and is termed the enhanced permeability and retention (EPR) effect. The EPR effect allows for the passive migration of macromolecules up to 400 nm in diameter into the tumor tissue. [65] However, efforts to utilize passive targeting approaches such as those employing the EPR effect suffer poor control over delivery and place restrictions on the types of therapies that can be delivered by this method. Specifically, this targeting approach requires that therapies are long-circulating to provide sufficient accumulation in the tumor tissue.

Active targeting approaches can enhance the therapeutic efficacy of polyplexes by increasing accumulation at target sites. High affinity ligands including antibodies, aptamers, peptides, and various small molecules that bind to receptors on the cell surface have been incorporated into a number of polyplex delivery vehicles to improve targeting. [66, 67] Interestingly, a number of studies have indicated that the target ligand does not influence biodistribution and bulk localization, but instead influences the distribution within the tissue (i.e. in targeted cells versus non-targeted). For example, Bartlett and coworkers demonstrated similar whole body distribution using untargeted and transferrin-targeted siRNA nanoparticles, but more pronounced gene inhibition in cancer cells using the targeted strategy.[68] Similarly, Park *et al*. showed enhanced localization of targeted liposomes in tumor cells despite no enhancements in

accumulation in tumor tissues compared to untargeted controls.[69] In a novel active targeting approach, studies by Schnitzer and coworkers demonstrate the utility in targeting caveolae to overcome the restrictive endothelial cell barrier and mediate active pumping of nanoparticles into the lung.[70] Specifically, they use quantitative proteomics to identify aminopeptidase P (APP) concentrated in caveolae of the lung endothelium and demonstrate rapid caveolae-mediate transport (within seconds) of APP-targeted nanoparticles against a concentration gradient.

Unfortunately, active targeting approaches have yet to demonstrate significant utility in a clinical setting. Specifically, active targeting requires the identification of unique molecular targets that are expressed exclusively, or at significantly higher levels, in a target tissue. Only then can these methods provide predictable control over targeted non-viral delivery.

1.2.2 Cellular Adhesion and Uptake

Following arrival at a target cell, polyplexes must bind to the cell surface, be internalized, and traffic towards the specific intracellular target – typically either the nucleus (gene-encoding DNA) or cytosol (mRNA, siRNA, antisense DNA). However, transport across the cell membrane is one of the biggest hurdles to efficient gene transfer, as the lipophilic nature of the plasma membrane restricts cellular entry of most macromolecular therapeutics. Adhesion to the cell surface and subsequent endocytic internalization is typically accomplished by one of two methods: targeted binding to receptors on the cell surface to facilitate directed uptake;[71] or non-specific electrostatic binding to the anionic glycosaminoglycan (GAG) residues on the cell surface followed by non-selective endocytosis.[72] During cellular uptake, the cell

invaginates portions of the plasma membrane and accompanying extracellular fluid. Endocytosis then delivers internalized cargo to sorting compartments within the cell, followed by trafficking to various subcellular destinations. The following sections discuss the various modes of cellular entry and the subsequent subcellular trafficking of internalized molecules.

1.2.2.1 Ligand-mediated cellular uptake

There has been considerable effort focused on designing carriers to improve the efficiency and specificity of cellular uptake. A number of ligands have been shown to stimulate targeted and non-specific uptake of therapeutic agents. These materials can be divided into two distinct classes. The first class consists of targeting ligands with the potential to bind to specific cell-surface receptors with high affinity and selectivity. These include antibodies, small molecules, and a number of cell targeted peptides (CTPs) demonstrating high affinity for a targeted cell surface receptor. The second class utilizes materials with the ability to non-specifically interact with the cell surface and enhance cell entry. The majority of these materials are peptides derived from protein transduction domains (PTDs), or cell-penetrating peptides (CPPs).

1.2.2.1.1 CTP-mediated uptake

CTPs and conjugated structures primarily internalize by a receptor-mediated process. This delivery strategy is an attractive option since it allows for cell-specific therapeutic delivery. Various CTPs have been identified by combinatorial approaches to take advantage of this process. These CTPs show high affinity and specificity upon interaction with cell surface receptors, and are internalized by receptor-mediated endocytosis. Such sequences are designed to take advantage of differences in the

expression levels of key cell surface receptors that occur during the progression of various diseases.[73] For example, in the last decade, receptor targeted strategies for cancer therapy have been widely researched. Perhaps the most notable CTP for this application is the arginine-glycine-aspartic acid (RGD) tripeptide is derived from the binding domain of fibronectin, and collagen and is also present in some isoforms of the basement membrane protein laminin.[74] RGD serves as a ligand for the $\alpha_v\beta_3$ and $\alpha_5\beta_1$ integrins which are upregulated in cancer cells.[75-78] For targeted cancer therapy, researchers have demonstrated enhanced transfection when RGD moieties are grafted onto nanocarriers such as polymer conjugates, polyplexes, liposomes and micelles.[79] In addition to peptide-mediated targeting, there are also a number of well-characterized targeting groups including cholera toxin B, folic acid, low-density lipoprotein, nicotinic acid, riboflavin and transferrin[80-82] with potential utility for targeted gene delivery. Additionally, a few of these targeting systems have seen translation to the clinic and are now being investigated in human trials. One particularly well known targeting system is the cyclodextrin-based siRNA delivery system in clinical development at Arrowhead Pharmaceuticals. This formulation, termed CALAA-01 utilizes a transferrin displayed on the nanoparticle surface to target transferrin receptors that are overexpressed in tumor cells,[83-86] and has been shown to provide tumor-specific gene knockdown in patients with metastatic melanoma.[58]

1.2.2.1.2 CPP/PTD-mediated uptake

In the second strategy for stimulating cellular internalization, many carriers incorporate CPPs due to their demonstrated robust cellular uptake. These PTDs/CPPs are rich in positively charged amino acids such as lysine (K) and arginine (R), and initiate translocation across cell membranes by binding to anionic cell surface residues

through electrostatic interactions. The specific mechanisms for CPP-mediated delivery are very diverse and have not been completely elucidated. In fact, the preferred mechanism of CPP-mediated uptake has been shown to vary based on physicochemical properties, cargo, as well as cell type.[17, 87-92]

The library of CPPs can be further dived into two groups according to their binding properties. The first group of CPPs, classified by their non-amphipathic polycationic structure, consists of highly charged peptides, which show a high affinity for the anionic GAG chains on the cell surface. This group of CPPs shows tremendous diversity in their mode of cellular entry depending on the attached therapeutic cargo, as well as the mode of CPP incorporation into the nanostructure[90, 91, 93-99] One such example, the transactivator of transcription (TAT) peptide has been one of the most widely studied CPPs due to its ability to transport a wide range of cargo across cell membranes.[95, 100] TAT is derived from the transcriptional activator protein that is encoded by human immunodeficiency virus type 1 (HIV-1), and it has been used to deliver multiple therapeutics including genetic material, proteins, and the anticancer drugs doxorubicin and paclitaxcel.[98, 101] TAT peptide has directed different internalization routes dependent on the attached cargo. Specifically, it has been suggested that TAT complexes with larger cargo preferentially internalize through endocytosis, whereas TAT complexes carrying smaller cargo internalize via direct membrane penetration/fusion[91] which is a common uptake route for the second group of CPPs that will be discussed below. Researchers have also identified cargo-dependent differences in the cellular distribution of TAT-associated structures following cellular uptake. For example, Guterstam and coworkers prepared a fluorescein isothiocyanate (FITC) labeled TAT peptide which displayed a diffuse

cellular distribution following uptake.[87] In contrast, the delivery of TAT-Cre constructs prepared using Cre recombinase of bacteriophage P1 and TAT fused to quantum dots demonstrated a vesicular distribution of peptide within the cell, suggesting the involvement of endocytosis and vesicular entrapment.[91]

The second group of CPPs consists of amphipathic peptides with sequential hydrophobic and hydrophilic residues along their primary structure. The proposed cellular entry mechanism for this group of CPPs is direct membrane penetration. These peptides are thought to bind to and insert themselves into neutral and anionic membranes via hydrophobic interactions and have been shown to form transmembrane pores. For example, a synthetic peptide derived from the hydrophobic fusion peptide of HIV-1 gp41 and the hydrophilic nuclear localization sequence of SV40 large T antigen, known as MPG, is thought to form a β-barrel structure as part of a transient pore facilitating cell uptake.[102] Structural and chemical investigations with and without an associated cargo have demonstrated strong MPG interactions and spontaneous penetration of lipid-phase and natural membranes.[103] Specifically, circular dichroism analysis by Deshayes and coworkers using free peptide and MPG-oligonucleotide complexes revealed a transition from a non-structured conformation to a β-sheet upon interaction with phospholipids leading to induced membrane permeability.[102]

1.2.2.2 Cellular uptake routes and subcellular trafficking

There are multiple pathways through which polyplexes can actively enter cells and the precise mechanism is dependent on numerous factors including the size, charge, and surface functionality of the internalized molecule.[104, 105] The most commonly discussed and extensively studied methods of internalization are shown in Figure 1.3. These include macropinocytosis, clathrin-mediated endocytosis, and

caveolae-mediated endocytosis,[106-109] which can shuttle cargo into cells following either non-specific internalization (in the case of macropinocytosis) or receptor-mediated uptake. Carriers displaying a positive surface charge, such as cationic polyplexes, have the ability to non-specifically interact with the negatively charged cell surface and can be internalized by macropinocytosis. This process involves the formation of actin-coated vesicles on the surface and is usually preceded by membrane ruffling due to actin polymerization. Macropinosomes vary in their eventual intracellular fate and may merge into endosomes and lysosomes or recycle cargo back to the cell surface for exocytosis.[82, 88, 110-113]

Cellular uptake may also occur through receptor–mediated endocytosis by binding to cell surface receptors and trafficking through clathrin or caveloae mediated endocytosis. Clathrin-mediated endocytosis is currently the most well understood of the intracellular trafficking pathways. Unfortunately, a disadvantage of targeting this mechanism for non-viral gene delivery is the eventual trafficking to lysosomes.[114, 115] The clathrin-mediated delivery route begins with binding to a cell surface receptor followed by receptor clustering and formation of a clathrin-coated pit. These pits pinch off from the plasma membrane to form clathrin-coated vesicles which sequentially traffic towards early endosomes, late endosomes and lysosomes.[114, 115]

The formation of caveolae is believed to be receptor-mediated and is dynamin- and actin-dependent.[116-119] The past few years have seen a tremendous increase in understanding of caveolae and their diverse trafficking pathways; however the exact mechanisms and pathway have not been completely elucidated. Prior to internalization molecules associate with the cell membrane and then become trapped in relatively static caveolae on the plasma surface. These caveolae experience short

range shuttling cycles as individual caveolae continuously internalize and fuse with the plasma membrane. Ligand-stimulated phosphorylation of caveolae, caveolar association with dynamin at the neck of the caveolae, and cytoskeletal reorganization results in pinching off from the plasma membrane.[120-122] Caveolae may then fuse with early endosomes and traffic through acidifying vesicles or fuse with pre-existing multicaveolae clusters known as caveosomes,[123, 124] These caveosomes may then further traffic through a non-degradative pathway to the endoplasmic reticulum (ER) or Golgi complex.[125-129]

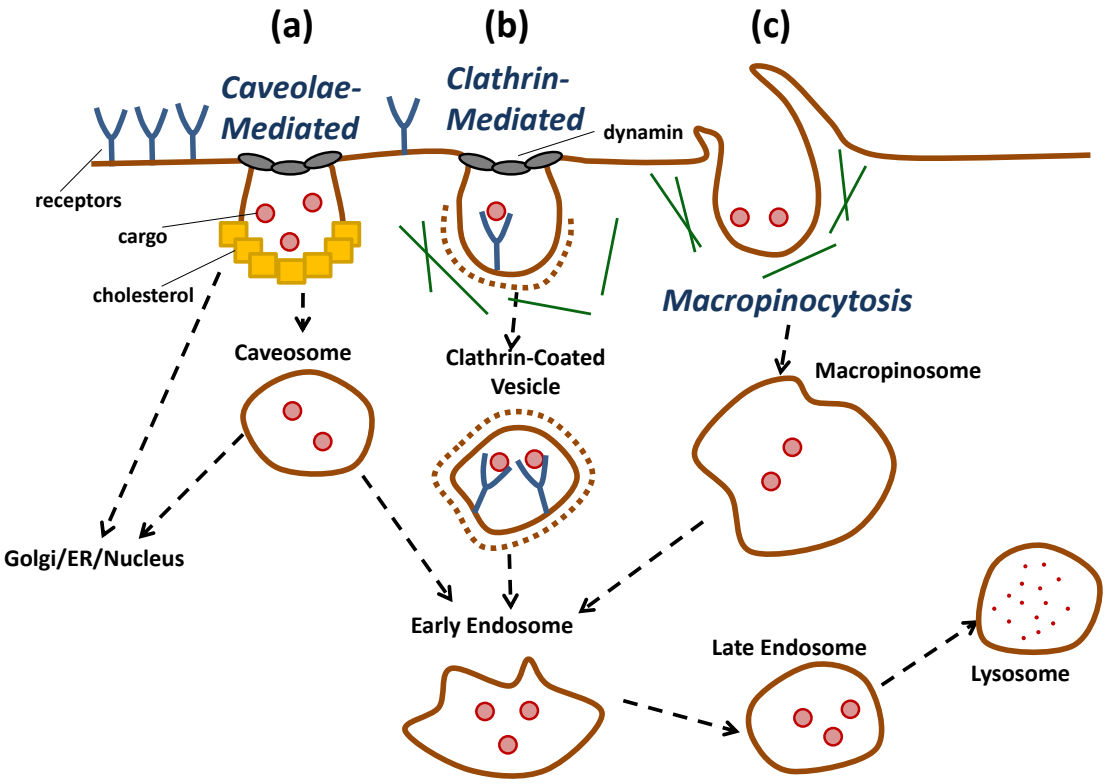

Figure 1.3 The cellular uptake routes and trafficking pathways of non-viral gene delivery materials include (a) caveolae-mediated, (b) clathrin-mediated, and (c) macropinocytotic endocytosis.

1.2.3 Intracellular Transport and Targeting

Cellular entry through one of the previously discussed internalization routes initiates the trafficking of the internalized carriers through endocytic vesicles. These vesicles must then navigate the intracellular space to a specific subcellular target location. Navigating the intracellular space presents different requirements based on the type of genetic cargo. For instance, DNA delivery requires transport to the nucleus for transcription, while siRNA therapies require delivery to the cytosolic space of target cells for RNA interference (RNAi) and gene silencing. However, the subcellular trafficking of non-viral carriers is not completely understood and presents a major challenge for improving their efficacy. The following sections will outline several key barriers to intracellular transport and will discuss current methods to effectively target cargo to desired subcellular locations.

1.2.3.1 Endosomal Escape

A number of endocytic trafficking pathways have the potential to lead to entrapment in the lysosome where the acidic pH can lead to degradation of nucleic acids. Endosomal escape has been identified in numerous delivery systems as one of the major bottlenecks to successful delivery. Specifically, the transport of siRNA-based therapies from endosomes into the cytoplasm is considered a major rate-limiting step for many delivery approaches.[130]

As such, understanding the mechanisms for endosomal escape and designing features to aid in release are key requirements for improving cellular delivery of therapeutic agents and preventing lysosomal degradation. Several approaches have been employed using known or hypothesized mechanisms to facilitate endosomal

escape and release of therapeutics into the cytoplasm. The following sections outline the various strategies currently employed to promote cytosolic release.

Cationic carriers including polyethylenimine (PEI),[131] polyamidoamine (PAMAM) dendrimers[132] and imidazole-containing polymers[133, 134] contain protonatable amines with a pK_a between 5 and 7. These polymers can buffer endosomal acidification by taking up protons and have been shown to be effective in stimulating endosomal escape of the associated polyplexes.[135] Specifically, this buffering process is known as the 'proton sponge effect' and is the most widely reported mechanism for the endosomal escape of non-viral delivery structures. In the endosome, protonation induces an influx of chloride ions and water. This then leads to an increase in osmotic pressure and eventually results in endosomal rupture and release of the contents of the endosome into the cytosol. Numerous publications support this buffering effect,[136-138] although it is heavily debated and there are contradictory reports on its validity. In recent work, Andresen and coworkers cast doubt on the hypothesis through measurements of PEI concentrations in the lysosome and lysosomal pH.[139] Their study shows that despite high levels of PEI accumulation in the lysosome, a small fraction may escape the endosomal pathway before reaching the lysosomes. They suggest that it is this fraction of polyplexes that may mediate transfection. Additionally, they demonstrate that PEI does not induce changes in lysosomal pH as previously suggested. A number of publications argue that although the osmotic pressure built up during the acidification may be a contributing factor to eventual disruption; it is theoretically insufficient to cause endosome disruption on its own.[139] Overall, the validity of this hypothesis requires rigorous testing as no conclusive evidence of this mechanism has been demonstrated.

As an alternative to endosomal buffering, a number of peptides, polymers and lipids have been identified with the capacity to directly destabilize the endosomal membrane. This process is thought to occur through one of two methods. Specifically, these materials may destabilize the membrane directly or do so in response to an environmental trigger. Cationic peptides, such as polylysine (PLL) and melittin, possess an inherent ability to directly destabilize and penetrate the endosomal membrane. These materials are thought to bind perpendicular to the anionic membrane, followed by direct insertion to form a pore.[140] Covalently binding these peptides to a number of carriers has been shown to be particularly advantageous. In fact, incorporation with lipids and polymer carriers such as PEI was shown to significantly increase reporter gene expression in a range of cells.[141] Specifically, the incorporation of melittin into PEI polyplexes led to a 700-fold increase in gene transfer of a luciferase reporter gene.[142]

The second mechanism, triggered destabilization, has been shown to play an important role in intracellular delivery of pathogens. In particular, the majority of viruses have protein domains that undergo conformational changes upon exposure to an environmental trigger such as a change in pH. These conformational changes allow the protein to fuse with the lipid bilayer to facilitate membrane disruption.[143] A number of lipids and short peptides derived from lytic domains in viruses display this fusogenic property. For example, the HA2 subunit of the hemagglutinin (HA) glycoprotein on the surface of influenza viruses has been shown to contain most of the membrane fusion capability of the protein.[144, 145] This glycoprotein undergoes a conformational change from a random coil to an α-helix, thereby exposing the N-terminal lytic segment of HA2 upon acidification. A number of pH-sensitive

amphipathic α-helical peptides were designed based on this subunit to facilitate membrane disruption. For example, the glutamic acid enriched HA2 analog, INF7, has been used in a number of gene delivery systems to facilitate triggered endosomal escape. Glutamic acid residues in the peptide sequence protonate under the acidic conditions in the endosome, triggering a conformational change from a random coil to an α-helix.[145] In the α-helical conformation, the INF7 peptide has been shown to fuse with and penetrate the endosomal membrane to form pores.[145]

Enhancements in gene transfection based on increased endosomal escape have also been demonstrated for a number of fusogenic lipids.[146-149] For example, the neutral helper lipid dioleoyl phosphatidylethanolamine (DOPE) has been used in a number of non-viral lipoplex formulations, as well as in the commercial transfection agent Lipofectamine™ as a gene delivery carrier. This lipid forms a stable bilayer at pH 7 and undergoes a transition to an inverted hexagonal structure below pH 6 leading to membrane fusion and destabilization.[150, 151] Researchers have demonstrated the utility of this fusogenic lipid in a number of applications. Specifically, the addition of DOPE to quaternized lipidoids – a combinatorial library of lipid-like materials screened for their siRNA and DNA transfection ability – was shown to significantly enhance DNA transfection.[152]

1.2.3.2 Cytoplasmic Trafficking and Targeting the Nucleus

Many types of therapeutic cargo require targeting to destinations other than the cytosol. For example, plasmid DNA and antisense therapies require nuclear delivery, enzyme replacement therapies function in endosomal and lysosomal compartments and proapoptotic drugs are active in mitochondria. However, subcellular targeting often proves to be an elusive goal. Due to the complexity of the intracellular space,

objects greater than 26 nm in radius cannot effectively diffuse in the cytoplasm[153] and require active transport mechanisms to reach their intracellular target.

Therapies which are active in the nucleus face the additional barrier of the nuclear membrane. Passive transport of molecules less than 9 nm in diameter or less than 40 kDa can occur through nuclear pore complexes (NPC),[154, 155] which span the nuclear envelope. In contrast, larger macromolecules require active transport for nuclear entry, which can be accomplished by utilizing nuclear localization signals (NLSs).[156] Delivery mediated by NLSs involves a widening of the nuclear pore promoting uptake of macromolecules as large as 50 MDa.[157] A number of research groups have investigated the utility of synthetic NLSs for delivery to the nucleus.[158-160] By utilizing NLSs, nuclear uptake occurs via the importin-β pathway. Import may involve binding directly to importin-β or indirectly through the adapter protein importin-α to guide the import substrate through the nuclear pore.

NLSs present an advantageous targeting strategy for therapies which do not have free access or affinity for the nuclear compartment. This targeting method is particularly useful for delivery of DNA and antisense therapies which are active in the nucleus of the cell. Early strategies in developing nuclear targeted therapies involved the direct conjugation of the NLS to the therapeutic. Perhaps the most widely studied and well–characterized NLSs are the simian virus 40 large tumor antigen sequence (PKKKRKV), and M9 derived from nuclear ribonucleoprotein. The incorporation of these and other NLSs has enabled the development of a number of non-viral carriers with improved nuclear targeting capacity. NLSs have been incorporated through electrostatic interactions with the DNA molecule and have shown utility for nuclear delivery[161] and retention.[162] For example, in a study using PLL, the mu peptide (μ) – a

polypeptide demonstrating high efficiency for DNA condensation –and NLS-modified mu (NLS-μ), Akita and coworkers demonstrated enhanced levels of transgene expression following cytoplasmic delivery of NLS-μ polyplexes compared to PLL- and μ-containing structures.[163] In a study to further understand the role of NLSs for the nuclear entry of polyplexes, Larsen and coworkers demonstrated a necessity for NLSs in promoting post-mitotic nuclear retention.[162] Specifically, using polyplexes and nanoparticles of various sizes they demonstrated post-mitotic exclusion of PEI-DNA polyplexes and untargeted nanoparticles and retention of histone H3 NLS/DNA polyplexes using a nuclear microinjection technique.

Alternatively, the NLS can be incorporated through covalent conjugation methods, which have demonstrated utility in a number of studies.[164] When using this method, care must be taken to avoid conjugation to the transcription cassette and subsequent hindrance of DNA activity. A particularly interesting approach to incorporating NLS is the use of NLS-peptide nucleic acids (PNA), and this allows for control of the number of attached NLSs and their binding site on the DNA. For example, in a study by Brandén and coworkers, DNA hybridization with this NLS-PNA conjugate and complexation with PEI resulted in increased uptake and up to 8-fold enhanced plasmid transfection efficiency.[165]

1.2.4 Approaches for Controlled Vehicle Unpackaging

The final step of vector unpackaging presents a considerable challenge for non-viral polyplex and lipoplex delivery systems. Unfortunately, the electrostatic interactions that promote tight packaging and strong association in non-viral complexes limit accessibility to cellular machinery (e.g. transcriptional proteins, components of the RNA-induced silencing complex [RISC], etc.), thereby inhibiting

the intracellular activity of the therapeutic nucleic acid.[166, 167] For example, Zabner *et al*. demonstrated the challenge of nucleic acid release due to tight electrostatic interactions using lipid DNA complexes.[167] In this work, they showed that these complexes were unable to facilitate transgene expression following direct microinjection into the nucleus. Larsen and coworkers found similar results in a complementary study using DNA/PEI polyplexes.[166] Following nuclear microinjection of polyplexes and naked DNA, these researchers demonstrated 40% lower transfection efficiency for the complex compared to the free plasmid, highlighting a major need for an unpackaging mechanism.

Although delayed unpackaging may hinder gene transfer, premature unpackaging can lead to nucleic acid release and degradation. In fact, a number of studies have resulted in disassembly of non-viral materials due to interactions with extracellular components and rapid nucleic acid degradation.[168, 169] As such, non-viral therapies face contradictory demands on delivery. These materials must avoid destabilization by extacellular components and nuclease-mediated degradation, but also promote efficient release at an intracellular target. This requires that these structures provide controlled methods to alter their presentation of nucleic acids; however this has proven to be a difficult task for a number of non-viral carriers. In fact, there are limited materials that effectively control the time and location of nucleic acid release. For example, Zabner *et al*. demonstrated the challenge of nucleic acid release due to tight electrostatic interactions using lipid DNA complexes. In this work, they showed that these complexes were unable to facilitate transgene expression following direct microinjection into the nucleus.[167] These delivery challenges

necessitate the design of structures with the ability to adapt to the evolving needs of the delivery pathway and controllably deshield the nucleic acid to promote its activity.

Several strategies have been proposed for non-viral vector design to actively control the packaging and release of nucleic acids and maximize their delivery at a target site. In particular, a number of stimuli-responsive non-viral vectors have been developed to reduce carrier association in response to biological or applied stimuli, and release nucleic acids via changes in molecular self-assembly or surface charge. Figure 1.2 depicts some of the design approaches used for these responsive structures. The following sections will detail specific carriers that have been developed to address the key barrier of controlled release along the delivery pathway.

1.2.4.1 Controlled release in response to biological stimuli

The cellular environment provides a range of signals that can be employed to promote changes in carrier structure and drive nucleic acid release. In particular, cell-responsive carriers have been developed to change their molecular conformation in response to local changes in biological signals including pH,[170-172] redox potential[173] or enzyme concentration.[174-176] These systems provide complementary functionality for both encapsulation and triggered release of nucleic acids.

Numerous pH-responsive materials have been employed for intracellular nucleic acid release. These systems take advantage of the decrease in pH afforded by endocytic processing. One such example is the pH-sensitive, comb-like polymer developed by El-Sayed and coworkers to deliver siRNA.[177] These polymers were demonstrated to degrade in acidic conditions due to hydrolysis of the hydrazone linkages connecting the cationic grafts to the polymer backbone. Additionally, these materials were able to reduce targeted gene expression by 36-40% at both the mRNA

and protein levels following efficient polyplex uptake. Similarly, Chen *et al*. described the development of antisense oligonucleotide therapeutics that provide time- and dose-dependent transfection in human adenocarcinoma cells demonstrating higher efficacy and lower cytotoxicity when compared to structures prepared with poly(D,L-lactide-co-glycolide), 25 kDa branched PEI and Lipofectamine 2000 lacking pH-responsiveness.[170]

Systems with enzyme-responsive capability provide an attractive strategy for controlled release in response to local changes in enzyme concentration. For example, Grinstaff *et al*. reported several lipid-based amphiphiles containing both cationic headgroups to encapsulate DNA and terminal esters susceptible to enzymatic hydrolysis and charge reversal in the carrier. [175] These amphiphiles (within lipoplexes) successfully released DNA following enzymatic hydrolysis, and enhanced transfection efficiency 100-fold in comparison to amphiphiles without responsive groups. In another strategy to incorporate enzyme responsiveness into carrier design, Chu and coworkers selected Cathepsin B, an endosomal/lysosomal endopeptidase,[178-180] as an enzyme target for triggered DNA release.[176] Specifically, they developed copolymers containing an oligolysine capped with the liner peptide Phenylalanine-Lysine-Phenylalanine-Leucine (FKFL), a Cathepsin B substrate, and demonstrated rapid polymer degradation in the presence of Cathepsin B. Furthermore, these polymers were less toxic than the non-degradable controls and PEI used in their study despite no significant improvement in transfection efficiency. In work from the Sullivan and Kiick labs, Blocker and coworkers described an enzyme-responsive system for applications in wound healing. In this work, surface immobilization of

DNA polyplexes using a cell-responsive tether provided higher transfection in NIH/3T3 cells compared to non-labile tethers.[174]

1.2.4.2 External or applied stimuli

Additional advantages can be provided by non-viral gene delivery systems that respond to external or applied stimuli. Specifically, these systems provide the benefits of user-defined spatial and temporal control over delivery. Various materials have been developed to change their properties in response to an external or applied stimulus such as light, magnetic field, or ultrasound. Photo-responsive gene carriers are particularly appealing because of the versatility and spatial resolution afforded by light. In particular, these systems provide the ability to minimize off-target effects by controllably releasing the nucleic acid therapy.

Photoactive functional groups can undergo isomeric rearrangements or photochemical cleavage reactions depending on the specific functional group utilized.[181] One particular example is the *o*-nitrobenzyl (*o*-NB) ester which absorbs UV and near-infrared light to form a carboxylic acid and a nitrosobenzaldehyde.[182] The potential for spatial and temporal control of nucleic acid release using light-triggered carriers has made photo-responsive carriers of great interest. As such, there have increasing studies aimed towards successful incorporation of these photo-responsive moieties for drug and gene delivery. In one such example, Liu *et al*. synthesized a photocleavable azobenzene-containing "catanionic" surfactant (consisting of a cationic and anionic mixture) /DNA complex for DNA delivery.[183] Following a 2-8 hour incubation with cells and subsequent 365 nm UV irradiation, these complexes were able to unpackage the vector and provide enhanced transfection.

1.3 Dissertation Synopsis

Non-viral gene delivery presents a promising yet unrealized approach to disease treatment. Despite the significant strides in the field of non-viral delivery, the therapeutic application of these materials is limited by an incomplete understanding of current carriers and their delivery mechanisms, as well as a lack of controllable delivery methods. The previous sections detailed our current understanding of the delivery process as well as several unresolved challenges in understanding the specific mechanisms of delivery and developing effective therapeutic materials. This dissertation presents the developments of methods to understand gene association/release mechanisms and novel design strategies to control gene association/release. The general outline for this work can be seen in Figure 1.4. Chapter 2 explores the structure/function relationship of fluorescent labeling tools that have been commonly utilized to understand the mechanisms of endocytic processing, using a traditional gene transfer polyplex as a model system. This chapter investigates conditions necessary for maintaining polyplex structure and activity, while providing efficient and accurate reporting tools to improve our understanding of the intracellular pathway. The development of a light-responsive polymeric carrier for nucleic acid release is detailed in Chapter 3. This chapter details a versatile synthetic scheme for polymers with high affinity for DNA and demonstrates light-responsive release from these structures. Chapter 4 then examines the cellular delivery potential of this light-responsive polymer platform, and identifies an improved silencing capacity with this external trigger. Taken together, these two chapters highlight an adaptable delivery system with tunable affinity for both DNA and siRNA. Combining the knowledge of the extra- and intracellular requirements of the delivery pathway, Chapter 5 details key

aspects to the synthesis of modular carriers that combine stealth polymers, cell targeting ligands (e.g. RGD) and biologically responsive release linkers for controlled siRNA release. Collectively, these studies address some of the key requirements for promoting high efficacy gene transfer and highlight several novel biomimetic materials as useful tools for controlling, investigating, and understanding gene delivery in the complex cellular environment.

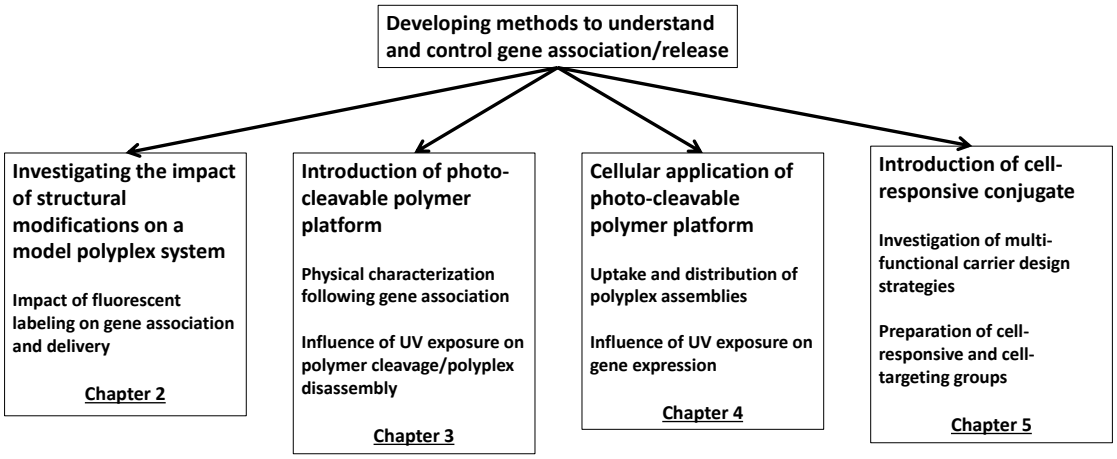

Figure 1.4 Outline of investigations of the gene association and release of non-viral carriers.

REFERENCES

1. Gene Therapy Clinical Trials Worldwide. http://www.wiley.com/legacy/wileychi/genmed/clinical/ (April 7, 2014)

2. Andtbacka, R. I. In *OpTiM: A randomized phase III trial of talimogene laherparepvec (T-VEC) versus subcutaneous (SC) granulocyte-macrophage colony-stimulating factor (GM-CSF) for the treatment (tx) of unresected stage IIIB/C and IV melanoma*, American Society of Clinical Oncology Annual Meeting, Chicago, IL, 2013; Chicago, IL, 2013.

3. Maguire, A. M.; Simonelli, F.; Pierce, E. A.; Pugh, E. N., Jr.; Mingozzi, F.; Bennicelli, J.; Banfi, S.; Marshall, K. A.; Testa, F.; Surace, E. M.; Rossi, S.; Lyubarsky, A.; Arruda, V. R.; Konkle, B.; Stone, E.; Sun, J.; Jacobs, J.; Dell'Osso, L.; Hertle, R.; Ma, J. X.; Redmond, T. M.; Zhu, X.; Hauck, B.; Zelenaia, O.; Shindler, K. S.; Maguire, M. G.; Wright, J. F.; Volpe, N. J.; McDonnell, J. W.; Auricchio, A.; High, K. A.; Bennett, J., Safety and efficacy of gene transfer for Leber's congenital amaurosis. *N Engl J Med* **2008,** 358, (21), 2240-8.

4. Simonelli, F.; Maguire, A. M.; Testa, F.; Pierce, E. A.; Mingozzi, F.; Bennicelli, J. L.; Rossi, S.; Marshall, K.; Banfi, S.; Surace, E. M.; Sun, J.; Redmond, T. M.; Zhu, X.; Shindler, K. S.; Ying, G. S.; Ziviello, C.; Acerra, C.; Wright, J. F.; McDonnell, J. W.; High, K. A.; Bennett, J.; Auricchio, A., Gene therapy for Leber's congenital amaurosis is safe and effective through 1.5 years after vector administration. *Mol Ther* **2010,** 18, (3), 643-50.

5. Hufnagel, R. B.; Ahmed, Z. M.; Correa, Z. M.; Sisk, R. A., Gene therapy for Leber congenital amaurosis: advances and future directions. *Graefes Arch Clin Exp Ophthalmol* **2012,** 250, (8), 1117-28.

6. Bennett, J.; Ashtari, M.; Wellman, J.; Marshall, K. A.; Cyckowski, L. L.; Chung, D. C.; McCague, S.; Pierce, E. A.; Chen, Y.; Bennicelli, J. L.; Zhu, X.; Ying, G. S.; Sun, J.; Wright, J. F.; Auricchio, A.; Simonelli, F.; Shindler, K. S.; Mingozzi, F.; High, K. A.; Maguire, A. M., AAV2 gene therapy readministration in three adults with congenital blindness. *Sci Transl Med* **2012,** 4, (120), 120ra15.

7. Hackett, C. S.; Geurts, A. M.; Hackett, P. B., Predicting preferential DNA vector insertion sites: implications for functional genomics and gene therapy. *Genome Biol* **2007,** 8 Suppl 1, S12.

8. Yi, Y.; Hahm, S. H.; Lee, K. H., Retroviral gene therapy: safety issues and possible solutions. *Curr Gene Ther* **2005,** 5, (1), 25-35.

9. Berns, A., Good news for gene therapy. *N Engl J Med* **2004,** 350, (16), 1679-80.

10. Hacein-Bey-Abina, S.; von Kalle, C.; Schmidt, M.; Le Deist, F.; Wulffraat, N.; McIntyre, E.; Radford, I.; Villeval, J. L.; Fraser, C. C.; Cavazzana-Calvo, M.; Fischer, A., A serious adverse event after successful gene therapy for X-linked severe combined immunodeficiency. In *N Engl J Med*, United States, 2003; Vol. 348, pp 255-6.

11. Hacein-Bey-Abina, S.; Le Deist, F.; Carlier, F.; Bouneaud, C.; Hue, C.; De Villartay, J. P.; Thrasher, A. J.; Wulffraat, N.; Sorensen, R.; Dupuis-Girod, S.; Fischer, A.; Davies, E. G.; Kuis, W.; Leiva, L.; Cavazzana-Calvo, M., Sustained correction of X-linked severe combined immunodeficiency by ex vivo gene therapy. *N Engl J Med* **2002,** 346, (16), 1185-93.

12. Kaiser, J., Clinical research. Death prompts a review of gene therapy vector. In *Science*, United States, 2007; Vol. 317, p 580.

13. Lehrman, S., Virus treatment questioned after gene therapy death. *Nature* **1999,** 401, (6753), 517-8.

14. Medina-Kauwe, L. K.; Xie, J.; Hamm-Alvarez, S., Intracellular trafficking of nonviral vectors. *Gene Ther* **2005,** 12, (24), 1734-51.

15. Akinc, A.; Thomas, M.; Klibanov, A. M.; Langer, R., Exploring polyethylenimine-mediated DNA transfection and the proton sponge hypothesis. *J Gene Med* **2005,** 7, (5), 657-63.

16. Dauty, E.; Verkman, A. S., Actin cytoskeleton as the principal determinant of size-dependent DNA mobility in cytoplasm: a new barrier for non-viral gene delivery. *J Biol Chem* **2005,** 280, (9), 7823-8.

17. Mueller, J.; Kretzschmar, I.; Volkmer, R.; Boisguerin, P., Comparison of cellular uptake using 22 CPPs in 4 different cell lines. *Bioconjug Chem* **2008,** 19, (12), 2363-74.

18. Munkonge, F. M.; Amin, V.; Hyde, S. C.; Green, A. M.; Pringle, I. A.; Gill, D. R.; Smith, J. W.; Hooley, R. P.; Xenariou, S.; Ward, M. A.; Leeds, N.; Leung, K. Y.; Chan, M.; Hillery, E.; Geddes, D. M.; Griesenbach, U.; Postel, E. H.; Dean, D. A.; Dunn, M. J.; Alton, E. W., Identification and functional characterization of

cytoplasmic determinants of plasmid DNA nuclear import. *J Biol Chem* **2009,** 284, (39), 26978-87.

19. Schaffer, D. V.; Lauffenburger, D. A., Optimization of cell surface binding enhances efficiency and specificity of molecular conjugate gene delivery. *J Biol Chem* **1998,** 273, (43), 28004-9.

20. Schaffer, D. V.; Fidelman, N. A.; Dan, N.; Lauffenburger, D. A., Vector unpacking as a potential barrier for receptor-mediated polyplex gene delivery. *Biotechnol Bioeng* **2000,** 67, (5), 598-606.

21. Al-Dosari, M. S.; Gao, X., Nonviral Gene Delivery: Principle, Limitations, and Recent Progress. *AAPS J* **2009,** 11, (4), 671-81.

22. Chiou, H. C.; Tangco, M. V.; Levine, S. M.; Robertson, D.; Kormis, K.; Wu, C. H.; Wu, G. Y., Enhanced resistance to nuclease degradation of nucleic acids complexed to asialoglycoprotein-polylysine carriers. *Nucleic Acids Res* **1994,** 22, (24), 5439-46.

23. Kao, Y. J.; Juliano, R. L., Interactions of liposomes with the reticuloendothelial system. Effects of reticuloendothelial blockade on the clearance of large unilamellar vesicles. *Biochim Biophys Acta* **1981,** 677, (3-4), 453-61.

24. Senior, J. H., Fate and behavior of liposomes in vivo: a review of controlling factors. *Crit Rev Ther Drug Carrier Syst* **1987,** 3, (2), 123-93.

25. Bartneck, M.; Keul, H. A.; Zwadlo-Klarwasser, G.; Groll, J., Phagocytosis independent extracellular nanoparticle clearance by human immune cells. *Nano Lett* **2010,** 10, (1), 59-63.

26. Dobrovolskaia, M. A.; Aggarwal, P.; Hall, J. B.; McNeil, S. E., Preclinical studies to understand nanoparticle interaction with the immune system and its potential effects on nanoparticle biodistribution. *Mol Pharm* **2008,** 5, (4), 487-95.

27. Pratten, M. K.; Lloyd, J. B., Pinocytosis and phagocytosis: the effect of size of a particulate substrate on its mode of capture by rat peritoneal macrophages cultured in vitro. *Biochim Biophys Acta* **1986,** 881, (3), 307-13.

28. Essa, S.; Rabanel, J. M.; Hildgen, P., Characterization of rhodamine loaded PEG-g-PLA nanoparticles (NPs): effect of poly(ethylene glycol) grafting density. *Int J Pharm* **2011,** 411, (1-2), 178-87.

29. Patel, H. M.; Moghimi, S. M., Serum-mediated recognition of liposomes by phagocytic cells of the reticuloendothelial system - The concept of tissue specificity. *Adv Drug Deliv Rev* **1998,** 32, (1-2), 45-60.

30. Medina, O. P.; Pillarsetty, N.; Glekas, A.; Punzalan, B.; Longo, V.; Gonen, M.; Zanzonico, P.; Smith-Jones, P.; Larson, S. M., Optimizing tumor targeting of the lipophilic EGFR-binding radiotracer SKI 243 using a liposomal nanoparticle delivery system. *J Control Release* **2011,** 149, (3), 292-8.

31. Cullis, P. R.; Chonn, A.; Semple, S. C., Interactions of liposomes and lipid-based carrier systems with blood proteins: Relation to clearance behaviour in vivo. *Adv Drug Deliv Rev* **1998,** 32, (1-2), 3-17.

32. Yamamoto, Y.; Nagasaki, Y.; Kato, Y.; Sugiyama, Y.; Kataoka, K., Long-circulating poly(ethylene glycol)-poly(D,L-lactide) block copolymer micelles with modulated surface charge. *J Control Release* **2001,** 77, (1-2), 27-38.

33. Sheng, Y.; Yuan, Y.; Liu, C.; Tao, X.; Shan, X.; Xu, F., In vitro macrophage uptake and in vivo biodistribution of PLA-PEG nanoparticles loaded with hemoglobin as blood substitutes: effect of PEG content. *J Mater Sci Mater Med* **2009,** 20, (9), 1881-91.

34. Perrault, S. D.; Walkey, C.; Jennings, T.; Fischer, H. C.; Chan, W. C., Mediating tumor targeting efficiency of nanoparticles through design. *Nano Lett* **2009,** 9, (5), 1909-15.

35. Moghimi, S. M.; Hedeman, H.; Muir, I. S.; Illum, L.; Davis, S. S., An investigation of the filtration capacity and the fate of large filtered sterically-stabilized microspheres in rat spleen. *Biochim Biophys Acta* **1993,** 1157, (3), 233-40.

36. Fang, C.; Shi, B.; Pei, Y. Y.; Hong, M. H.; Wu, J.; Chen, H. Z., In vivo tumor targeting of tumor necrosis factor-alpha-loaded stealth nanoparticles: effect of MePEG molecular weight and particle size. *Eur J Pharm Sci* **2006,** 27, (1), 27-36.

37. Longmire, M. R.; Ogawa, M.; Choyke, P. L.; Kobayashi, H., Biologically optimized nanosized molecules and particles: more than just size. *Bioconjug Chem* **2011,** 22, (6), 993-1000.

38. Champion, J. A.; Mitragotri, S., Role of target geometry in phagocytosis. *Proc Natl Acad Sci U S A* **2006,** 103, (13), 4930-4.

39. Decuzzi, P.; Godin, B.; Tanaka, T.; Lee, S. Y.; Chiappini, C.; Liu, X.; Ferrari, M., Size and shape effects in the biodistribution of intravascularly injected particles. *J Control Release* **2010,** 141, (3), 320-7.

40. Devarajan, P. V.; Jindal, A. B.; Patil, R. R.; Mulla, F.; Gaikwad, R. V.; Samad, A., Particle shape: a new design parameter for passive targeting in splenotropic drug delivery. *J Pharm Sci* **2010,** 99, (6), 2576-81.

41. Geng, Y.; Dalhaimer, P.; Cai, S.; Tsai, R.; Tewari, M.; Minko, T.; Discher, D. E., Shape effects of filaments versus spherical particles in flow and drug delivery. *Nat Nanotechnol* **2007,** 2, (4), 249-55.

42. Amoozgar, Z.; Yeo, Y., Recent advances in stealth coating of nanoparticle drug delivery systems. *Wiley Interdiscip Rev Nanomed Nanobiotechnol* **2012,** 4, (2), 219-33.

43. Kenausis, G. L.; Vörös, J.; Elbert, D. L.; Huang, N.; Hofer, R.; Ruiz-Taylor, L.; Textor, M.; Hubbell, J. A.; Spencer, N. D., Poly(l-lysine)-g-Poly(ethylene glycol) Layers on Metal Oxide Surfaces: Attachment Mechanism and Effects of Polymer Architecture on Resistance to Protein Adsorption. *The Journal of Physical Chemistry B* **2000,** 104, (14), 3298-3309.

44. Drobek, T.; Spencer, N. D.; Heuberger, M., Compressing PEG Brushes. *Macromolecules* **2005,** 38, (12), 5254-5259.

45. Harvie, P.; Wong, F. M.; Bally, M. B., Use of poly(ethylene glycol)-lipid conjugates to regulate the surface attributes and transfection activity of lipid-DNA particles. *J Pharm Sci* **2000,** 89, (5), 652-63.

46. Gref, R.; Luck, M.; Quellec, P.; Marchand, M.; Dellacherie, E.; Harnisch, S.; Blunk, T.; Muller, R. H., 'Stealth' corona-core nanoparticles surface modified by polyethylene glycol (PEG): influences of the corona (PEG chain length and surface density) and of the core composition on phagocytic uptake and plasma protein adsorption. *Colloids Surf B Biointerfaces* **2000,** 18, (3-4), 301-313.

47. Ebrahimnejad, P.; Dinarvand, R.; Jafari, M. R.; Tabasi, S. A.; Atyabi, F., Characterization, blood profile and biodistribution properties of surface modified PLGA nanoparticles of SN-38. *Int J Pharm* **2011,** 406, (1-2), 122-7.

48. Bauer, M.; Lautenschlaeger, C.; Kempe, K.; Tauhardt, L.; Schubert, U. S.; Fischer, D., Poly(2-ethyl-2-oxazoline) as alternative for the stealth polymer poly(ethylene glycol): comparison of in vitro cytotoxicity and hemocompatibility. *Macromol Biosci* **2012,** 12, (7), 986-98.

49. Takeuchi, H.; Kojima, H.; Yamamoto, H.; Kawashima, Y., Evaluation of circulation profiles of liposomes coated with hydrophilic polymers having different molecular weights in rats. *J Control Release* **2001,** 75, (1-2), 83-91.

50. Maruyama, K.; Okuizumi, S.; Ishida, O.; Yamauchi, H.; Kikuchi, H.; Iwatsuru, M., Phosphatidyl polyglycerols prolong liposome circulation in vivo. *International Journal of Pharmaceutics* **1994,** 111, (1), 103-107.

51. Torchilin, V. P.; Levchenko, T. S.; Whiteman, K. R.; Yaroslavov, A. A.; Tsatsakis, A. M.; Rizos, A. K.; Michailova, E. V.; Shtilman, M. I., Amphiphilic poly-N-vinylpyrrolidones: synthesis, properties and liposome surface modification. *Biomaterials* **2001,** 22, (22), 3035-44.

52. Johnson, R. N.; Chu, D. S.; Shi, J.; Schellinger, J. G.; Carlson, P. M.; Pun, S. H., HPMA-oligolysine copolymers for gene delivery: optimization of peptide length and polymer molecular weight. *J Control Release* **2011,** 155, (2), 303-11.

53. Kostka, L.; Konak, C.; Subr, V.; Spirkova, M.; Addadi, Y.; Neeman, M.; Lammers, T.; Ulbrich, K., Removable nanocoatings for siRNA polyplexes. *Bioconjug Chem* **2011,** 22, (2), 169-79.

54. Schellinger, J. G.; Pahang, J. A.; Johnson, R. N.; Chu, D. S.; Sellers, D. L.; Maris, D. O.; Convertine, A. J.; Stayton, P. S.; Horner, P. J.; Pun, S. H., Melittin-grafted HPMA-oligolysine based copolymers for gene delivery. *Biomaterials* **2013,** 34, (9), 2318-26.

55. Kursa, M.; Walker, G. F.; Roessler, V.; Ogris, M.; Roedl, W.; Kircheis, R.; Wagner, E., Novel shielded transferrin-polyethylene glycol-polyethylenimine/DNA complexes for systemic tumor-targeted gene transfer. *Bioconjug Chem* **2003,** 14, (1), 222-31.

56. Wolfert, M. A.; Schacht, E. H.; Toncheva, V.; Ulbrich, K.; Nazarova, O.; Seymour, L. W., Characterization of vectors for gene therapy formed by self-assembly of DNA with synthetic block co-polymers. *Hum Gene Ther* **1996,** 7, (17), 2123-33.

57. Mignet, N.; Richard, C.; Seguin, J.; Largeau, C.; Bessodes, M.; Scherman, D., Anionic pH-sensitive pegylated lipoplexes to deliver DNA to tumors. *Int J Pharm* **2008,** 361, (1-2), 194-201.

58. Davis, M. E.; Zuckerman, J. E.; Choi, C. H.; Seligson, D.; Tolcher, A.; Alabi, C. A.; Yen, Y.; Heidel, J. D.; Ribas, A., Evidence of RNAi in humans from systemically administered siRNA via targeted nanoparticles. *Nature* **2010,** 464, (7291), 1067-70.

59. Mishra, S.; Webster, P.; Davis, M. E., PEGylation significantly affects cellular uptake and intracellular trafficking of non-viral gene delivery particles. *Eur J Cell Biol* **2004,** 83, (3), 97-111.

60. Hatakeyama, H.; Akita, H.; Harashima, H., A multifunctional envelope type nano device (MEND) for gene delivery to tumours based on the EPR effect: a strategy for overcoming the PEG dilemma. *Adv Drug Deliv Rev* **2011,** 63, (3), 152-60.

61. Fella, C.; Walker, G. F.; Ogris, M.; Wagner, E., Amine-reactive pyridylhydrazone-based PEG reagents for pH-reversible PEI polyplex shielding. *Eur J Pharm Sci* **2008,** 34, (4-5), 309-20.

62. Rodriguez, P. L.; Harada, T.; Christian, D. A.; Pantano, D. A.; Tsai, R. K.; Discher, D. E., Minimal "Self" peptides that inhibit phagocytic clearance and enhance delivery of nanoparticles. *Science* **2013,** 339, (6122), 971-5.

63. Oldenborg, P. A.; Zheleznyak, A.; Fang, Y. F.; Lagenaur, C. F.; Gresham, H. D.; Lindberg, F. P., Role of CD47 as a marker of self on red blood cells. *Science* **2000,** 288, (5473), 2051-4.

64. Jacobs, F.; Wisse, E.; De Geest, B., The role of liver sinusoidal cells in hepatocyte-directed gene transfer. *Am J Pathol* **2010,** 176, (1), 14-21.

65. Yuan, F.; Dellian, M.; Fukumura, D.; Leunig, M.; Berk, D. A.; Torchilin, V. P.; Jain, R. K., Vascular permeability in a human tumor xenograft: molecular size dependence and cutoff size. *Cancer Res* **1995,** 55, (17), 3752-6.

66. Beduneau, A.; Saulnier, P.; Benoit, J. P., Active targeting of brain tumors using nanocarriers. *Biomaterials* **2007,** 28, (33), 4947-67.

67. Peer, D.; Karp, J. M.; Hong, S.; Farokhzad, O. C.; Margalit, R.; Langer, R., Nanocarriers as an emerging platform for cancer therapy. *Nat Nanotechnol* **2007,** 2, (12), 751-60.

68. Kirpotin, D. B.; Drummond, D. C.; Shao, Y.; Shalaby, M. R.; Hong, K.; Nielsen, U. B.; Marks, J. D.; Benz, C. C.; Park, J. W., Antibody targeting of long-circulating lipidic nanoparticles does not increase tumor localization but does increase internalization in animal models. *Cancer Res* **2006,** 66, (13), 6732-40.

69. Bartlett, D. W.; Su, H.; Hildebrandt, I. J.; Weber, W. A.; Davis, M. E., Impact of tumor-specific targeting on the biodistribution and efficacy of siRNA nanoparticles measured by multimodality in vivo imaging. *Proc Natl Acad Sci U S A* **2007,** 104, (39), 15549-54.

70. Oh, P.; Borgstrom, P.; Witkiewicz, H.; Li, Y.; Borgstrom, B. J.; Chrastina, A.; Iwata, K.; Zinn, K. R.; Baldwin, R.; Testa, J. E.; Schnitzer, J. E., Live dynamic imaging of caveolae pumping targeted antibody rapidly and specifically across endothelium in the lung. *Nat Biotechnol* **2007,** 25, (3), 327-37.

71. Harbottle, R. P.; Cooper, R. G.; Hart, S. L.; Ladhoff, A.; McKay, T.; Knight, A. M.; Wagner, E.; Miller, A. D.; Coutelle, C., An RGD-oligolysine peptide: a prototype construct for integrin-mediated gene delivery. *Hum Gene Ther* **1998,** 9, (7), 1037-47.

72. Lorenz, M. R.; Holzapfel, V.; Musyanovych, A.; Nothelfer, K.; Walther, P.; Frank, H.; Landfester, K.; Schrezenmeier, H.; Mailander, V., Uptake of functionalized, fluorescent-labeled polymeric particles in different cell lines and stem cells. *Biomaterials* **2006,** 27, (14), 2820-8.

73. Ogris, M.; Wagner, E., To be targeted: is the magic bullet concept a viable option for synthetic nucleic acid therapeutics? *Hum Gene Ther* **2011,** 22, (7), 799-807.

74. Barczyk, M.; Carracedo, S.; Gullberg, D., Integrins. *Cell Tissue Res* **2010,** 339, (1), 269-80.

75. Roman, J.; Ritzenthaler, J. D.; Roser-Page, S.; Sun, X.; Han, S., alpha5beta1-integrin expression is essential for tumor progression in experimental lung cancer. *Am J Respir Cell Mol Biol* **2010,** 43, (6), 684-91.

76. Leavesley, D. I.; Ferguson, G. D.; Wayner, E. A.; Cheresh, D. A., Requirement of the integrin beta 3 subunit for carcinoma cell spreading or migration on vitronectin and fibrinogen. *J Cell Biol* **1992,** 117, (5), 1101-7.

77. Gasparini, G.; Brooks, P. C.; Biganzoli, E.; Vermeulen, P. B.; Bonoldi, E.; Dirix, L. Y.; Ranieri, G.; Miceli, R.; Cheresh, D. A., Vascular integrin alpha(v)beta3: a new prognostic indicator in breast cancer. *Clin Cancer Res* **1998,** 4, (11), 2625-34.

78. Brooks, P. C.; Stromblad, S.; Klemke, R.; Visscher, D.; Sarkar, F. H.; Cheresh, D. A., Antiintegrin alpha v beta 3 blocks human breast cancer growth and angiogenesis in human skin. *J Clin Invest* **1995,** 96, (4), 1815-22.

79. Park, J.; Singha, K.; Son, S.; Kim, J.; Namgung, R.; Yun, C. O.; Kim, W. J., A review of RGD-functionalized nonviral gene delivery vectors for cancer therapy. *Cancer Gene Ther* **2012,** 19, (11), 741-8.

80. Bareford, L. M.; Swaan, P. W., Endocytic mechanisms for targeted drug delivery. *Adv Drug Deliv Rev* **2007,** 59, (8), 748-58.

81. Bellocq, N. C.; Pun, S. H.; Jensen, G. S.; Davis, M. E., Transferrin-containing, cyclodextrin polymer-based particles for tumor-targeted gene delivery. *Bioconjug Chem* **2003,** 14, (6), 1122-32.

82. Gabrielson, N. P.; Pack, D. W., Efficient polyethylenimine-mediated gene delivery proceeds via a caveolar pathway in HeLa cells. *J Control Release* **2009,** 136, (1), 54-61.

83. Bueno, R.; Appasani, K.; Mercer, H.; Lester, S.; Sugarbaker, D., The alpha folate receptor is highly activated in malignant pleural mesothelioma. *J Thorac Cardiovasc Surg* **2001,** 121, (2), 225-33.

84. Dainty, L. A.; Risinger, J. I.; Morrison, C.; Chandramouli, G. V.; Bidus, M. A.; Zahn, C.; Rose, G. S.; Fowler, J.; Berchuck, A.; Maxwell, G. L., Overexpression of folate binding protein and mesothelin are associated with uterine serous carcinoma. *Gynecol Oncol* **2007,** 105, (3), 563-70.

85. Inoue, T.; Cavanaugh, P. G.; Steck, P. A.; Brunner, N.; Nicolson, G. L., Differences in transferrin response and numbers of transferrin receptors in rat and human mammary carcinoma lines of different metastatic potentials. *J Cell Physiol* **1993,** 156, (1), 212-7.

86. Ross, J. F.; Wang, H.; Behm, F. G.; Mathew, P.; Wu, M.; Booth, R.; Ratnam, M., Folate receptor type beta is a neutrophilic lineage marker and is differentially expressed in myeloid leukemia. *Cancer* **1999,** 85, (2), 348-57.

87. Guterstam, P.; Madani, F.; Hirose, H.; Takeuchi, T.; Futaki, S.; El Andaloussi, S.; Graslund, A.; Langel, U., Elucidating cell-penetrating peptide mechanisms of action for membrane interaction, cellular uptake, and translocation utilizing the hydrophobic counter-anion pyrenebutyrate. *Biochim Biophys Acta* **2009,** 1788, (12), 2509-17.

88. Jones, A. T., Macropinocytosis: searching for an endocytic identity and role in the uptake of cell penetrating peptides. *J Cell Mol Med* **2007,** 11, (4), 670-84.

89. Madani, F.; Lindberg, S.; Langel, U.; Futaki, S.; Graslund, A., Mechanisms of cellular uptake of cell-penetrating peptides. *J Biophys* **2011,** 2011, 414729.

90. Richard, J. P.; Melikov, K.; Vives, E.; Ramos, C.; Verbeure, B.; Gait, M. J.; Chernomordik, L. V.; Lebleu, B., Cell-penetrating peptides. A reevaluation of the mechanism of cellular uptake. *J Biol Chem* **2003,** 278, (1), 585-90.

91. Tunnemann, G.; Martin, R. M.; Haupt, S.; Patsch, C.; Edenhofer, F.; Cardoso, M. C., Cargo-dependent mode of uptake and bioavailability of TAT-containing proteins and peptides in living cells. *Faseb j* **2006,** 20, (11), 1775-84.

92. Vives, E.; Schmidt, J.; Pelegrin, A., Cell-penetrating and cell-targeting peptides in drug delivery. In *Biochim Biophys Acta*, Netherlands, 2008; Vol. 1786, pp 126-38.

93. Brooks, H.; Lebleu, B.; Vives, E., Tat peptide-mediated cellular delivery: back to basics. *Adv Drug Deliv Rev* **2005,** 57, (4), 559-77.

94. Cardarelli, F.; Serresi, M.; Bizzarri, R.; Giacca, M.; Beltram, F., In vivo study of HIV-1 Tat arginine-rich motif unveils its transport properties. In *Mol Ther*, United States, 2007; Vol. 15, pp 1313-22.

95. Frankel, A. D.; Pabo, C. O., Cellular uptake of the tat protein from human immunodeficiency virus. *Cell* **1988,** 55, (6), 1189-93.

96. Gump, J. M.; June, R. K.; Dowdy, S. F., Revised role of glycosaminoglycans in TAT protein transduction domain-mediated cellular transduction. In *J Biol Chem*, United States, 2010; Vol. 285, pp 1500-7.

97. Kaplan, I. M.; Wadia, J. S.; Dowdy, S. F., Cationic TAT peptide transduction domain enters cells by macropinocytosis. In *J Control Release*, Netherlands, 2005; Vol. 102, pp 247-53.

98. Lee, J. Y.; Choi, Y. S.; Suh, J. S.; Kwon, Y. M.; Yang, V. C.; Lee, S. J.; Chung, C. P.; Park, Y. J., Cell-penetrating chitosan/doxorubicin/TAT conjugates for efficient cancer therapy. *Int J Cancer* **2011,** 128, (10), 2470-80.

99. Richard, J. P.; Melikov, K.; Brooks, H.; Prevot, P.; Lebleu, B.; Chernomordik, L. V., Cellular uptake of unconjugated TAT peptide involves clathrin-dependent endocytosis and heparan sulfate receptors. In *J Biol Chem*, United States, 2005; Vol. 280, pp 15300-6.

100. Green, M.; Loewenstein, P. M., Autonomous functional domains of chemically synthesized human immunodeficiency virus tat trans-activator protein. *Cell* **1988,** 55, (6), 1179-88.

101. Niu, R.; Zhao, P.; Wang, H.; Yu, M.; Cao, S.; Zhang, F.; Chang, J., Preparation, characterization, and antitumor activity of paclitaxel-loaded folic acid modified and TAT peptide conjugated PEGylated polymeric liposomes. *J Drug Target* **2011,** 19, (5), 373-81.

102. Deshayes, S.; Gerbal-Chaloin, S.; Morris, M. C.; Aldrian-Herrada, G.; Charnet, P.; Divita, G.; Heitz, F., On the mechanism of non-endosomial peptide-mediated cellular delivery of nucleic acids. *Biochim Biophys Acta* **2004,** 1667, (2), 141-7.

103. Deshayes, S.; Morris, M. C.; Divita, G.; Heitz, F., Interactions of primary amphipathic cell penetrating peptides with model membranes: consequences on the mechanisms of intracellular delivery of therapeutics. *Curr Pharm Des* **2005,** 11, (28), 3629-38.

104. He, C.; Hu, Y.; Yin, L.; Tang, C.; Yin, C., Effects of particle size and surface charge on cellular uptake and biodistribution of polymeric nanoparticles. *Biomaterials* **2010,** 31, (13), 3657-66.

105. Adler, A. F.; Leong, K. W., Emerging links between surface nanotechnology and endocytosis: impact on nonviral gene delivery. *Nano Today* **2010,** 5, (6), 553-569.

106. Conner, S. D.; Schmid, S. L., Regulated portals of entry into the cell. *Nature* **2003,** 422, (6927), 37-44.

107. Rejman, J.; Conese, M.; Hoekstra, D., Gene transfer by means of lipo- and polyplexes: role of clathrin and caveolae-mediated endocytosis. *J Liposome Res* **2006,** 16, (3), 237-47.

108. Khalil, I. A.; Kogure, K.; Futaki, S.; Harashima, H., High density of octaarginine stimulates macropinocytosis leading to efficient intracellular trafficking for gene expression. *J Biol Chem* **2006,** 281, (6), 3544-51.

109. Harush-Frenkel, O.; Debotton, N.; Benita, S.; Altschuler, Y., Targeting of nanoparticles to the clathrin-mediated endocytic pathway. *Biochem Biophys Res Commun* **2007,** 353, (1), 26-32.

110. Swanson, J. A.; Watts, C., Macropinocytosis. *Trends Cell Biol* **1995,** 5, (11), 424-8.

111. Meier, O.; Greber, U. F., Adenovirus endocytosis. *J Gene Med* **2003,** 5, (6), 451-62.

112. Wadia, J. S.; Stan, R. V.; Dowdy, S. F., Transducible TAT-HA fusogenic peptide enhances escape of TAT-fusion proteins after lipid raft macropinocytosis. *Nat Med* **2004,** 10, (3), 310-5.

113. Hillaireau, H.; Couvreur, P., Nanocarriers' entry into the cell: relevance to drug delivery. *Cell Mol Life Sci* **2009,** 66, (17), 2873-96.

114. Maxfield, F. R.; McGraw, T. E., Endocytic recycling. *Nat Rev Mol Cell Biol* **2004,** 5, (2), 121-32.

115. Luzio, J. P.; Mullock, B. M.; Pryor, P. R.; Lindsay, M. R.; James, D. E.; Piper, R. C., Relationship between endosomes and lysosomes. *Biochem Soc Trans* **2001,** 29, (Pt 4), 476-80.

116. Hansen, C. G.; Nichols, B. J., Molecular mechanisms of clathrin-independent endocytosis. *J Cell Sci* **2009,** 122, (Pt 11), 1713-21.

117. Lamaze, C.; Fujimoto, L. M.; Yin, H. L.; Schmid, S. L., The actin cytoskeleton is required for receptor-mediated endocytosis in mammalian cells. *J Biol Chem* **1997,** 272, (33), 20332-5.

118. Takei, K.; McPherson, P. S.; Schmid, S. L.; De Camilli, P., Tubular membrane invaginations coated by dynamin rings are induced by GTP-gamma S in nerve terminals. *Nature* **1995,** 374, (6518), 186-90.

119. Damke, H.; Baba, T.; Warnock, D. E.; Schmid, S. L., Induction of mutant dynamin specifically blocks endocytic coated vesicle formation. *J Cell Biol* **1994,** 127, (4), 915-34.

120. Rothberg, K. G.; Heuser, J. E.; Donzell, W. C.; Ying, Y. S.; Glenney, J. R.; Anderson, R. G., Caveolin, a protein component of caveolae membrane coats. *Cell* **1992,** 68, (4), 673-82.

121. Orlandi, P. A.; Fishman, P. H., Filipin-dependent inhibition of cholera toxin: evidence for toxin internalization and activation through caveolae-like domains. *J Cell Biol* **1998,** 141, (4), 905-15.

122. Parton, R. G.; Richards, A. A., Lipid rafts and caveolae as portals for endocytosis: new insights and common mechanisms. *Traffic* **2003,** 4, (11), 724-38.

123. Pelkmans, L.; Kartenbeck, J.; Helenius, A., Caveolar endocytosis of simian virus 40 reveals a new two-step vesicular-transport pathway to the ER. *Nat Cell Biol* **2001,** 3, (5), 473-83.

124. Pelkmans, L.; Puntener, D.; Helenius, A., Local actin polymerization and dynamin recruitment in SV40-induced internalization of caveolae. *Science* **2002,** 296, (5567), 535-9.

125. Le, P. U.; Guay, G.; Altschuler, Y.; Nabi, I. R., Caveolin-1 is a negative regulator of caveolae-mediated endocytosis to the endoplasmic reticulum. *J Biol Chem* **2002,** 277, (5), 3371-9.

126. Le, P. U.; Nabi, I. R., Distinct caveolae-mediated endocytic pathways target the Golgi apparatus and the endoplasmic reticulum. *J Cell Sci* **2003,** 116, (Pt 6), 1059-71.

127. McLendon, P. M.; Fichter, K. M.; Reineke, T. M., Poly(glycoamidoamine) vehicles promote pDNA uptake through multiple routes and efficient gene expression via caveolae-mediated endocytosis. *Mol Pharm* **2010,** 7, (3), 738-50.

128. Nichols, B. J.; Lippincott-Schwartz, J., Endocytosis without clathrin coats. *Trends Cell Biol* **2001,** 11, (10), 406-12.

129. Nichols, B. J., A distinct class of endosome mediates clathrin-independent endocytosis to the Golgi complex. *Nat Cell Biol* **2002,** 4, (5), 374-8.

130. Dominska, M.; Dykxhoorn, D. M., Breaking down the barriers: siRNA delivery and endosome escape. *J Cell Sci* **2010,** 123, (Pt 8), 1183-9.

131. Boussif, O.; Lezoualc'h, F.; Zanta, M. A.; Mergny, M. D.; Scherman, D.; Demeneix, B.; Behr, J. P., A versatile vector for gene and oligonucleotide transfer into cells in culture and in vivo: polyethylenimine. *Proc Natl Acad Sci U S A* **1995,** 92, (16), 7297-301.

132. Zhou, J.; Wu, J.; Hafdi, N.; Behr, J. P.; Erbacher, P.; Peng, L., PAMAM dendrimers for efficient siRNA delivery and potent gene silencing. *Chem Commun (Camb)* **2006**, (22), 2362-4.

133. Moreira, C.; Oliveira, H.; Pires, L. R.; Simoes, S.; Barbosa, M. A.; Pego, A. P., Improving chitosan-mediated gene transfer by the introduction of intracellular buffering moieties into the chitosan backbone. *Acta Biomater* **2009,** 5, (8), 2995-3006.

134. Yang, S. R.; Lee, H. J.; Kim, J. D., Histidine-conjugated poly(amino acid) derivatives for the novel endosomolytic delivery carrier of doxorubicin. *J Control Release* **2006,** 114, (1), 60-8.

135. Won, Y. Y.; Sharma, R.; Konieczny, S. F., Missing pieces in understanding the intracellular trafficking of polycation/DNA complexes. *J Control Release* **2009,** 139, (2), 88-93.

136. Pack, D. W.; Hoffman, A. S.; Pun, S.; Stayton, P. S., Design and development of polymers for gene delivery. *Nat Rev Drug Discov* **2005,** 4, (7), 581-93.

137. Remy, J. S.; Sirlin, C.; Vierling, P.; Behr, J. P., Gene transfer with a series of lipophilic DNA-binding molecules. *Bioconjug Chem* **1994,** 5, (6), 647-54.

138. Sonawane, N. D.; Szoka, F. C., Jr.; Verkman, A. S., Chloride accumulation and swelling in endosomes enhances DNA transfer by polyamine-DNA polyplexes. *J Biol Chem* **2003,** 278, (45), 44826-31.

139. Benjaminsen, R. V.; Mattebjerg, M. A.; Henriksen, J. R.; Moghimi, S. M.; Andresen, T. L., The possible "proton sponge " effect of polyethylenimine (PEI) does not include change in lysosomal pH. *Mol Ther* **2013,** 21, (1), 149-57.

140. van den Bogaart, G.; Guzmán, J. V.; Mika, J. T.; Poolman, B., On the Mechanism of Pore Formation by Melittin. *Journal of Biological Chemistry* **2008,** 283, (49), 33854-33857.

141. Boeckle, S.; Fahrmeir, J.; Roedl, W.; Ogris, M.; Wagner, E., Melittin analogs with high lytic activity at endosomal pH enhance transfection with purified targeted PEI polyplexes. *J Control Release* **2006,** 112, (2), 240-8.

142. Ogris, M.; Steinlein, P.; Carotta, S.; Brunner, S.; Wagner, E., DNA/polyethylenimine transfection particles: influence of ligands, polymer size, and PEGylation on internalization and gene expression. *AAPS PharmSci* **2001,** 3, (3), E21.

143. Wagner, E., Application of membrane-active peptides for nonviral gene delivery. *Adv Drug Deliv Rev* **1999,** 38, (3), 279-289.

144. Oehlke, J.; Scheller, A.; Wiesner, B.; Krause, E.; Beyermann, M.; Klauschenz, E.; Melzig, M.; Bienert, M., Cellular uptake of an alpha-helical amphipathic model peptide with the potential to deliver polar compounds into the cell interior non-endocytically. *Biochim Biophys Acta* **1998,** 1414, (1-2), 127-39.

145. Plank, C.; Oberhauser, B.; Mechtler, K.; Koch, C.; Wagner, E., The influence of endosome-disruptive peptides on gene transfer using synthetic virus-like gene transfer systems. *J Biol Chem* **1994,** 269, (17), 12918-24.

146. Farhood, H.; Serbina, N.; Huang, L., The role of dioleoyl phosphatidylethanolamine in cationic liposome mediated gene transfer. *Biochim Biophys Acta* **1995,** 1235, (2), 289-95.

147. Hassani, Z.; Lemkine, G. F.; Erbacher, P.; Palmier, K.; Alfama, G.; Giovannangeli, C.; Behr, J. P.; Demeneix, B. A., Lipid-mediated siRNA delivery down-regulates exogenous gene expression in the mouse brain at picomolar levels. *J Gene Med* **2005,** 7, (2), 198-207.

148. Heyes, J.; Palmer, L.; Bremner, K.; MacLachlan, I., Cationic lipid saturation influences intracellular delivery of encapsulated nucleic acids. *J Control Release* **2005,** 107, (2), 276-87.

149. Litzinger, D. C.; Huang, L., Phosphatidylethanolamine liposomes: drug delivery, gene transfer and immunodiagnostic applications. *Biochim Biophys Acta* **1992,** 1113, (2), 201-27.

150. Bailey, A. L.; Cullis, P. R., Membrane fusion with cationic liposomes: effects of target membrane lipid composition. *Biochemistry* **1997,** 36, (7), 1628-34.

151. Wattiaux, R.; Jadot, M.; Warnier-Pirotte, M. T.; Wattiaux-De Coninck, S., Cationic lipids destabilize lysosomal membrane in vitro. *FEBS Lett* **1997,** 417, (2), 199-202.

152. Sun, S.; Wang, M.; Alberti, K. A.; Choy, A.; Xu, Q., DOPE facilitates quaternized lipidoids (QLDs) for in vitro DNA delivery. *Nanomedicine* **2013,** 9, (7), 849-54.

153. Luby-Phelps, K.; Castle, P. E.; Taylor, D. L.; Lanni, F., Hindered diffusion of inert tracer particles in the cytoplasm of mouse 3T3 cells. *Proc Natl Acad Sci U S A* **1987,** 84, (14), 4910-3.

154. Bonner, W. M., Protein migration into nuclei. I. Frog oocyte nuclei in vivo accumulate microinjected histones, allow entry to small proteins, and exclude large proteins. *J Cell Biol* **1975,** 64, (2), 421-30.

155. Bastos, R.; Pante, N.; Burke, B., Nuclear pore complex proteins. *Int Rev Cytol* **1995,** 162b, 257-302.

156. Wente, S. R., Gatekeepers of the nucleus. *Science* **2000,** 288, (5470), 1374-7.

157. Lechardeur, D.; Verkman, A. S.; Lukacs, G. L., Intracellular routing of plasmid DNA during non-viral gene transfer. *Adv Drug Deliv Rev* **2005,** 57, (5), 755-67.

158. Bremner, K. H.; Seymour, L. W.; Logan, A.; Read, M. L., Factors influencing the ability of nuclear localization sequence peptides to enhance nonviral gene delivery. *Bioconjug Chem* **2004,** 15, (1), 152-61.

159. Cartier, R.; Reszka, R., Utilization of synthetic peptides containing nuclear localization signals for nonviral gene transfer systems. *Gene Ther* **2002,** 9, (3), 157-67.

160. Chan, C. K.; Jans, D. A., Using nuclear targeting signals to enhance non-viral gene transfer. *Immunol Cell Biol* **2002,** 80, (2), 119-30.

161. Akita, H.; Tanimoto, M.; Masuda, T.; Kogure, K.; Hama, S.; Ninomiya, K.; Futaki, S.; Harashima, H., Evaluation of the nuclear delivery and intra-nuclear

transcription of plasmid DNA condensed with micro (mu) and NLS-micro by cytoplasmic and nuclear microinjection: a comparative study with poly-L-lysine. *J Gene Med* **2006,** 8, (2), 198-206.

162. Larsen, J. D.; Ross, N. L.; Sullivan, M. O., Requirements for the nuclear entry of polyplexes and nanoparticles during mitosis. *J Gene Med* **2012,** 14, (9-10), 580-9.

163. Akita, H.; Tanimoto, M.; Masuda, T.; Kogure, K.; Hama, S.; Ninomiya, K.; Futaki, S.; Harashima, H., Evaluation of the nuclear delivery and intra-nuclear transcription of plasmid DNA condensed with μ (mu) and NLS-μ by cytoplasmic and nuclear microinjection: a comparative study with poly-L-lysine. *J Gene Med* **2006,** 8, (2), 198-206.

164. Zanta, M. A.; Belguise-Valladier, P.; Behr, J. P., Gene delivery: a single nuclear localization signal peptide is sufficient to carry DNA to the cell nucleus. *Proc Natl Acad Sci U S A* **1999,** 96, (1), 91-6.

165. Brandén, L. J.; Mohamed, A. J.; Smith, C. I., A peptide nucleic acid-nuclear localization signal fusion that mediates nuclear transport of DNA. *Nat Biotechnol* **1999,** 17, (8), 784-7.

166. Larsen, J. D.; Reilly, M. J.; Sullivan, M. O., Using the epigenetic code to promote the unpackaging and transcriptional activation of DNA polyplexes for gene delivery. *Mol Pharm* **2012,** 9, (5), 1041-51.

167. Zabner, J.; Fasbender, A. J.; Moninger, T.; Poellinger, K. A.; Welsh, M. J., Cellular and molecular barriers to gene transfer by a cationic lipid. *J Biol Chem* **1995,** 270, (32), 18997-9007.

168. Burke, R. S.; Pun, S. H., Extracellular Barriers to in Vivo PEI and PEGylated PEI Polyplex-Mediated Gene Delivery to the Liver. *Bioconjugate Chemistry* **2008,** 19, (3), 693-704.

169. Zuckerman, J. E.; Choi, C. H.; Han, H.; Davis, M. E., Polycation-siRNA nanoparticles can disassemble at the kidney glomerular basement membrane. *Proc Natl Acad Sci U S A* **2012,** 109, (8), 3137-42.

170. Chen, H.; Liu, X.; Dou, Y.; He, B.; Liu, L.; Wei, Z.; Li, J.; Wang, C.; Mao, C.; Zhang, J.; Wang, G., A pH-responsive cyclodextrin-based hybrid nanosystem as a nonviral vector for gene delivery. *Biomaterials* **2013,** 34, (16), 4159-72.

171. Gaspar, V. M.; Marques, J. G.; Sousa, F.; Louro, R. O.; Queiroz, J. A.; Correia, I. J., Biofunctionalized nanoparticles with pH-responsive and cell penetrating blocks for gene delivery. *Nanotechnology* **2013,** 24, (27), 275101.

172. Liu, Z.; Zhang, N., pH-Sensitive polymeric micelles for programmable drug and gene delivery. *Curr Pharm Des* **2012,** 18, (23), 3442-51.

173. Dong, R.; Su, Y.; Yu, S.; Zhou, Y.; Lu, Y.; Zhu, X., A redox-responsive cationic supramolecular polymer constructed from small molecules as a promising gene vector. *Chem Commun (Camb)* **2013,** 49, (84), 9845-7.

174. Blocker, K. M.; Kiick, K. L.; Sullivan, M. O., Surface Immobilization of Plasmid DNA with a Cell-Responsive Tether for Substrate-Mediated Gene Delivery. *Langmuir* **2011**.

175. Prata, C. A.; Zhao, Y.; Barthelemy, P.; Li, Y.; Luo, D.; McIntosh, T. J.; Lee, S. J.; Grinstaff, M. W., Charge-reversal amphiphiles for gene delivery. *J Am Chem Soc* **2004,** 126, (39), 12196-7.

176. Chu, D. S.; Johnson, R. N.; Pun, S. H., Cathepsin B-sensitive polymers for compartment-specific degradation and nucleic acid release. *J Control Release* **2012,** 157, (3), 445-54.

177. Lin, Y. L.; Jiang, G.; Birrell, L. K.; El-Sayed, M. E., Degradable, pH-sensitive, membrane-destabilizing, comb-like polymers for intracellular delivery of nucleic acids. *Biomaterials* **2010,** 31, (27), 7150-66.

178. Lautwein, A.; Kraus, M.; Reich, M.; Burster, T.; Brandenburg, J.; Overkleeft, H. S.; Schwarz, G.; Kammer, W.; Weber, E.; Kalbacher, H.; Nordheim, A.; Driessen, C., Human B lymphoblastoid cells contain distinct patterns of cathepsin activity in endocytic compartments and regulate MHC class II transport in a cathepsin S-independent manner. *J Leukoc Biol* **2004,** 75, (5), 844-55.

179. Authier, F.; Metioui, M.; Bell, A. W.; Mort, J. S., Negative regulation of epidermal growth factor signaling by selective proteolytic mechanisms in the endosome mediated by cathepsin B. *J Biol Chem* **1999,** 274, (47), 33723-31.

180. Blum, J. S.; Fiani, M. L.; Stahl, P. D., Proteolytic cleavage of ricin A chain in endosomal vesicles. Evidence for the action of endosomal proteases at both neutral and acidic pH. *J Biol Chem* **1991,** 266, (33), 22091-5.

181. Zhao, Y., Light-Responsive Block Copolymer Micelles. *Macromolecules* **2012,** 45, (9), 3647-3657.

182. Il'ichev, Y. V.; Schworer, M. A.; Wirz, J., Photochemical reaction mechanisms of 2-nitrobenzyl compounds: methyl ethers and caged ATP. *J Am Chem Soc* **2004,** 126, (14), 4581-95.

183. Liu, Y. C.; Le Ny, A. L.; Schmidt, J.; Talmon, Y.; Chmelka, B. F.; Lee, C. T., Jr., Photo-assisted gene delivery using light-responsive catanionic vesicles. *Langmuir* **2009,** 25, (10), 5713-24.

Chapter 2

STRUCTURE/FUNCTION RELATIONSHIP OF NON-VIRAL CARRIERS: WEAKENED GENE ASSOCIATION THROUGH THE INCORPORATION OF HYDROPHOBIC FLUORESCENT LABELS

Recent research has highlighted a clear need for an improved understanding of the intracellular trafficking of non-viral structures. However, the intracellular space is very complex and necessitates controllable structures to effectively elucidate the stages of the delivery pathway. Fluorescent labeling is a regularly used approach to monitor delivery and disassembly; yet few studies investigate the effects of label incorporation on the structure and activity of gene transfer polyplexes. Herein, the impacts of label incorporation on polyplex assembly and gene transfer were detailed through the utilization of a model DNA-polyethylenimine (PEI) delivery system. This provides evidence that routine labeling strategies for polyplexes weakened the DNA-PEI binding affinity and induced significant polyplex aggregation, particularly in the cellular environment. Additionally, cellular internalization studies showed that increased labeling fractions led to reductions in polyplex uptake due to weakened complexation. These results not only provide insight into the assembly of these structures, but also help to identify labeling strategies sufficient to preserve activity while enabling detailed studies of trafficking and disassembly.

2.1 Introduction

Non-viral gene delivery carriers have attracted significant interest due to several advantageous properties not offered by their viral counterparts. Specifically,

non-viral vectors lack an innate immunogenicity, have a larger nucleic acid cargo capacity, are easier to produce and scale up, and offer molecular tunability in vector design.[1] Despite these advantageous properties, non-viral vectors have seen low transfection efficiencies as a result of inefficient nucleic acid trafficking to intracellular targets such as the nucleus and cytosol. In fact, the detailed subcellular trafficking and subsequent nucleic acid release mechanisms are still largely unknown for a number of non-viral carriers. A number of studies demonstrate the need for controlling subcellular trafficking and vector release.[2-5] In particular, early work by Schaffer and Lauffenburger identified inefficient polyplex trafficking to the nucleus and insufficient plasmid release as key challenges preventing the activity of polycationic gene carriers.[6] Using a series of fluorescently labeled polylysines as carriers for labeled DNA to monitor colocalization and intracellular compartmentalization, they reported high levels of polyplex accumulation within vesicular compartments in NR6 fibroblast cells. Interestingly, a number of the polyplexes unpackaged in the cytosol prior to nuclear localization. Additionally, their results indicated that very few polyplexes localized in the cell nucleus despite the high levels of cellular accumulation. Recent studies by Peng and coworkers presented complementary results.[7] Using two well-established transfection agents, PEI and Lipofectamine 2000, these authors demonstrated minimal levels of nuclear localization in bone mesenchymal stem cells (BMSCs) (20.69% and 30% for PEI and Lipofectamine, respectively) despite noting that as many as 80% of the MSCs internalized PEI polyplexes and 50% internalized Lipofectamine assemblies. These examples highlight a challenge that is common to a number of non-viral carriers: a

need for an improved understanding of subcellular trafficking and release to enhance the efficiency of gene delivery.

Delivery vehicles are required to provide adequate control during cellular uptake, and subsequently traffic through a complex intracellular space consisting of a dense cytoskeletal network to enable compartment-specific delivery.[4, 6, 8-11] Endocytosis has been identified as the primary internalization mechanism for the majority of non-viral carriers including polyplexes and lipoplexes, and the specific mode of internalization is an important determinant of intracellular fate.[2, 4, 12-16] However, researchers are still unclear as to the precise endocytic pathways to target to promote efficacious gene transfer. As outlined in chapter 1, cellular entry through endocytosis introduces the possibility to shuttle through an acidifying intracellular trafficking route. A number of studies identify carriers that traffic to the lysosome and establish the proton sponge mechanism – with its characteristic cytoplasmic release event – as the mode of DNA release from polyplexes.[17-20] Utilizing the proton-sponge effect, gene delivery carriers with a high buffering capacity – due to the presence of protonable amines – are thought to induce an influx of chloride ions and water as a result of protonation leading to an increase in osmotic pressure and eventual endosomal rupture. However, a number of other reports question the role of endosomal acidification in polyplex release and ultimate gene expression. For example, the work of Andresen and coworkers disputes the possible proton-sponge hypothesis through measurements in the use of PEI which reportedly possesses an endosomal buffering capactity.[21] Specifically, they identify low concentrations of PEI colocalized with the lysosomal compartment and minimal changes in lysosomal pH. Furthermore, a number of non-viral structures designed to exploit the acidification

process show limited or no improvements in activity. For example, Subramanian and coworkers demonstrate that the incorporation of endosomolytic HA-2 peptide does not increase transgene expression despite demonstrations of endosomal release.[22] Improving the efficacy of these vectors requires a mechanistic understanding of intracellular processing towards the rational design of improved therapies for gene transfer.

A number of different approaches have been used to probe the endocytic processing of gene delivery vectors. These involve labeling vector components with radioactive, fluorescent, or electron-dense markers such as gold so that the localization of the markers (and carriers) can be easily monitored in cells by fluorimetric or other detection methods.[2, 12, 23, 24] These labeling techniques are often used in combination with separation techniques – such as subcellular fractionation and flow cytometry – or endocytic inhibition studies. For example, radiolabeling methods provide quantitative determination of subcellular trafficking, yet these techniques typically require cellular separation by subcellular fractionation or other organelle isolation methods.[25] A number of studies employ electron microscopy imaging of gold-labeled DNA or other carrier components to monitor endocytic processing. For example, in work by Friend *et al*. imaging of gold-labeled DNA clearly indicates the presence of gold in vesicular compartments.[26] Furthermore, through the use of this imaging technique they propose that their delivered liposomes may enter the nucleus by fusion with the nuclear envelope, creating vesicular and reticular intranuclear membranes. The favorable optical properties of gold have also expanded their use in nanoparticle formulations for bioimaging. However, a number of studies report toxicity of these structures due to their physicochemical properties. For example in a study by Uboldi *et al*., they

report compromised cell viability and proliferation in alveolar type-II cell lines A549 and NCIH441 as a result of the stabilizing agent used for gold nanoparticle synthesis. An additional concern with the use of these systems to probe endocytic processing is the potential for differences in internalization and trafficking due to structural changes in these nanoparticles.[27] Another strategy to probe endocytic processing involves the use of chemical inhibitors. Chemical inhibitors such as chlorpromazine, filipin, and genistein have the ability to block key steps within specific endocytic pathways and hence identify the endocytic processing steps that direct intracellular activity. However, these inhibitors may also have indirect effects on other cellular processes that may confuse the results of these experiments. For example, chlorpromazine, which is often used to block clathrin-mediated endocytosis by depleting adaptor proteins on the plasma membrane, has been shown to cause an inhibition of receptor recycling[28] and inhibit clathrin-independent endocytosis in some cell lines.[29] Similarly, Fujimoto *et al*. demonstrated that inhibitors of actin polymerization have variable effects on cellular processes and can alter transferrin-mediated endocytosis depending on the cell line examined and experimental conditions used.[30]

Fluorescent labeling methods have been widely explored to probe intracellular trafficking and correlate specific vehicle transport pathways with gene transfer activity. Additionally, these techniques offer the ability to differentiate the behavior of the cargo and carrier with spectrally distinct labels. Fluorescent tracking of non-viral structures is typically performed by applying a fluorescent tag to the nucleic acid, the carrier molecule, or both structures to probe colocalization or unpackaging.[6, 31] However, the addition of these labels has the potential to alter assembly and activity. Specifically, fluorescent molecules are typically hydrophobic, and have the potential

to promote polyplex aggregation, reduce the efficiency of complexation, and alter unpackaging in the cellular environment. In fact, several lines of evidence suggest that incorporation of fluorescent tags and other hydrophobic molecules alters assembly or activity of both free plasmids and plasmid-based assemblies.[31-34] In work by Godfrey and coworkers employing the Oregon Green® 488 tag to monitor colocalization with labeled plasmids, they demonstrate a reduction in complexation ability of DNA-PEI polyplexes with the introduction of fluorescent labels and also identify the nuclear localization of PEI molecules with and without associated plasmid. The impact of fluorescent labeling on gene association and subsequent trafficking is not directly addressed in this work, yet characterization of their assembled structures indicate the need for additional cationic PEI to efficiently condense the DNA compared to polyplexes formed with unmodified structures.[12] Pack *et al*. also demonstrated the effects on DNA binding affinity of including hydrophobic residues in DNA-packaging molecules. In this study, acetylation of up to 57% of the primary amines in 25 kDa PEI increased gene transfection efficiency due to weakened PEI-DNA binding interactions and enhanced intracellular unpackaging.[33] Zheng and coworkers demonstrated a similar reduction in DNA binding affinity and enhancement in gene transfection following lipoylation of 1.8 kDa PEI, but also highlight the need to balance the charge density and the degree of modification due to an observed impaired DNA retardation in agarose gel electrophoresis.[32] These studies emphasize concerns in the study of non-viral vectors that are often unaddressed in current studies of endocytic processing. Specifically, they indicate that hydrophobic molecules, including fluorescent dyes, impact the gene association of delivered DNA and may be a determinant of ultimate gene transfer efficiency due to the need to balance stable

DNA complexation with efficient intracellular release. These studies further indicate the need to systematically probe the structure/function relationships of these hydrophobically-modified polymers towards the development of improved delivery structures. While the size and hydrophobicity of the fluorescent label is a major factor in selection prior to conjugation, there are limited studies that explore the structure/function relationship of these modified polymers.

In the work presented in this chapter, the influence of a common hydrophobic fluorophore [e.g. Oregon Green® (OG) 488 labeled PEI] on DNA binding, complexation, and cellular activity was systematically investigated. The OG fluorescent dye has been routinely used as an optical reporter for probing internalization and intracellular trafficking when conjugated to various polymers,[35, 36] proteins,[37] and therapeutic drugs.[38] It also offers comparable green fluorescence to fluorescein with increased photostability and ready conjugation to amine-containing polymers by straightforward protocols. The impacts of label incorporation on polyplex assembly and cellular delivery in the use of a model DNA-PEI delivery system are detailed in this chapter. Specifically, these studies identify the interesting phenomenon of extracellular losses and intracellular aggregation with increasing label incorporation. With these new insights this study provides an improved understanding of the structural and functional effects of label incorporation in non-viral carriers with the potential to improve current methods to elucidate intracellular processing.

2.2 Materials and Methods

2.2.1 Materials

Branched PEI (25 kDa) was obtained from Sigma (St. Louis, MO). The gWIZ mammalian expression plasmid encoding luciferase (6732 bps) was obtained from Genlantis (San Diego, CA), amplified in DH5α Escherichia coli in Lysogeny Broth, and purified with a QIAGEN Plasmid Maxi Kit (QIAGEN Inc., Valencia, CA) following the manufacturer's protocols. The gWIZ vector contains 10 sequential copies of the repeated peptide nucleic acid (PNA) binding site (5′-AGAGAGAG-3′). PNA labeled with Alexa Fluor®555 (PNA-AF555) was obtained at >90% purity from Panagene (Daejeon, Korea). The PNA consisted of a maleimide-TCTCTCTC-OOOJTJTJTJT-Lys with Alexa Fluor® covalently attached to the Lys terminus [O = 8-amino-3,6-dioxactanoic acid; J = pseudoisocytosine]. The Oregon Green® 488 dye (carboxylic acid, succinimidyl ester) was purchased from Life Technologies (Carlsbad, CA). All other reagents were obtained from Fisher Scientific (Pittsburgh, PA) unless otherwise noted.

2.2.2 Methods

2.2.2.1 PEI and Plasmid Labeling

PEI was fluorescently labeled with Oregon Green 488 according to the manufacturer's protocols. Briefly, 60 μL of prepared Oregon Green tag (10 mg/mL Oregon Green 488 in dimethyl sulfoxide) was added to 1.2 mL of a 10 mg/mL stirred solution of 25 kDa branched PEI in 0.1 M sodium bicarbonate. The mixture was stirred for 1 h in the dark at 25°C and subsequently was incubated for a second hour without stirring. The solution was dialyzed against water in 3000 MWC tubing,

lyophilized, and dissolved at 0.45 mg/mL in 20 mM HEPES, pH=6.0 for further experiments. For experiments involving dual labeled polyplexes, polyplexes were formed with DNA that was prelabeled with PNA-Alexa-Fluor555 (PNA-AF555) at a weight ratio of 1:20 (DNA:PNA), as previously described.[39]

2.2.2.2 Polyplex Formation and Characterization

Polyplexes were formed at a concentration of 20 μg of DNA/mL with the gWIZ luciferase plasmid and mixtures of PEI according to a modification of established protocols.[39] DNA solutions were formulated at 40 μg/mL in 20 mM HEPES buffer at a pH of 6. Polyplexes were then prepared in a stepwise fashion. First, Oregon Green 488-labeled PEI (PEI-488) solutions were added dropwise while vortexing. Polyplex solutions were incubated for 10 minutes at room temperature. Unlabeled PEI was subsequently added and the resulting polyplexes were incubated for a further 10 minutes prior to further analyses. Polyplexes were prepared to maintain a final DNA concentration of 20 μg/mL.

2.2.2.3 Monitoring DNA Condensation using the Ethidium Bromide (EtBr) Exclusion Assay

The polyplexes were analyzed by agarose gel electrophoresis according to standard protocols. For gel electrophoresis, 1% w/v agarose gels containing 0.5 μg of ethidium bromide/mL were formed in 1× tris/borate/ethylenediaminetetraacetic acid (Tris borate EDTA, or TBE) buffer. 20 μL of each polyplex solution was added to 5 μL of gel loading buffer, and 20 μL of the mixture was added to a well of the gel. The gels were run at 100 V for 1 h and subsequently imaged using a BioRad Gel Doc XR (Hercules, CA).

2.2.2.4 Preparation of Polyplexes for Dynamic Light Scattering (DLS)

Polyplex solutions (1.5 μg DNA, 75 μL of solution) were mixed with 200 μL HEPES buffer and subsequently incubated at room temperature for 20 min prior to particle size determination. DLS experiments were performed using a Melles Griot, 632.8 nm, 75 mW laser, coupled with a Brookhaven Instruments Corporation BI-200SM goniometer that had an inline 632 nm filter from Intor, Inc. The intensity auto-correlation function was recorded at 90˚ and analyzed using a quadratic cumulant fit. All light scattering experiments were performed at 25 ˚C.

2.2.2.5 Cell Culture, Synchronization and Transfection

CHO-K1 cells were obtained from the American Type Culture Collection (ATCC, Manassas, VA). The cells were cultured according to ATCC protocols at 37°C and 5% CO_2 in Dulbecco's modified Eagle's medium (DMEM) supplemented with 10% fetal bovine serum (FBS) and 1% penicillin−streptomycin. Cells were passaged when they reached ~80% confluency. For cell synchronization, CHO cells were plated at ~7200 cells/cm^2. 24 h after plating, lovastatin (Sigma) solutions in growth medium (e.g. serum/antibiotic-supplemented DMEM) were added to cells at a final concentration of 10 μM, and the cells were incubated for 32 – 36 h.[40, 41] Subsequently, the medium containing lovastatin was removed, the cells were washed with phosphate buffered saline (PBS), and fresh medium was added to cells to resume the cell division cycle. Cells were incubated for an additional 16 h so that transfection could take place during the S phase of cell division.

Transfections were performed with PNA-AF555 labeled polyplexes and varying amounts of labeled PEI according to previously reported protocols.[39, 42-44] Immediately prior to transfection, the cells were washed with PBS and the media was

replaced with reduced serum Opti-MEM (Life Technologies). Subsequently, prepared polyplex solutions containing 1 μg of DNA/cm^2 of the plate area were added dropwise to each well. Polyplex solutions were incubated with the cells for 30 minutes. Extracellularly-bound polyplexes were removed with a 10 μg/mL heparin wash for 15 min at 37°C. Polyplex uptake was subsequently analyzed by immunocytochemistry (ICC) and flow cytometry. For flow cytometry, uptake was analyzed in two ways. To calculate the fraction of cells that had internalized polyplexes, scatter plots from untransfected cells were gated for autofluorescence, and the gates were used to determine the percentages of transfected cells that had internalized particles. To calculate the average polyplex concentrations per transfected cell, the mean fluorescence intensity (MFI) per cell of each transfected cell sample was calculated. A total of 10,000 cells were analyzed for each sample.

2.2.2.6 Immunocytochemistry (ICC) and Cell Staining

For ICC analyses, cells were fixed with 4% paraformaldehyde for 10 min following transfection. Cells were subsequently permeabilized with 0.2% Tween-20 in PBS (PBSt) and blocked with 3% BSA in 0.2% PBSt.

2.2.2.7 Z-Stack Deconvolution and Fluorescence Microscopy

The localization of polyplexes was monitored through Z-stack deconvolution microscopy on a Leica DMI 6000B inverted fluorescence microscope (Leica, Wetzlar, Germany) with a 63×/1.4-0.6 oil objective. Deconvolution procedures were performed in accordance with manufacturer algorithms using an automatically generated point spread function (PSF).

2.3 Results

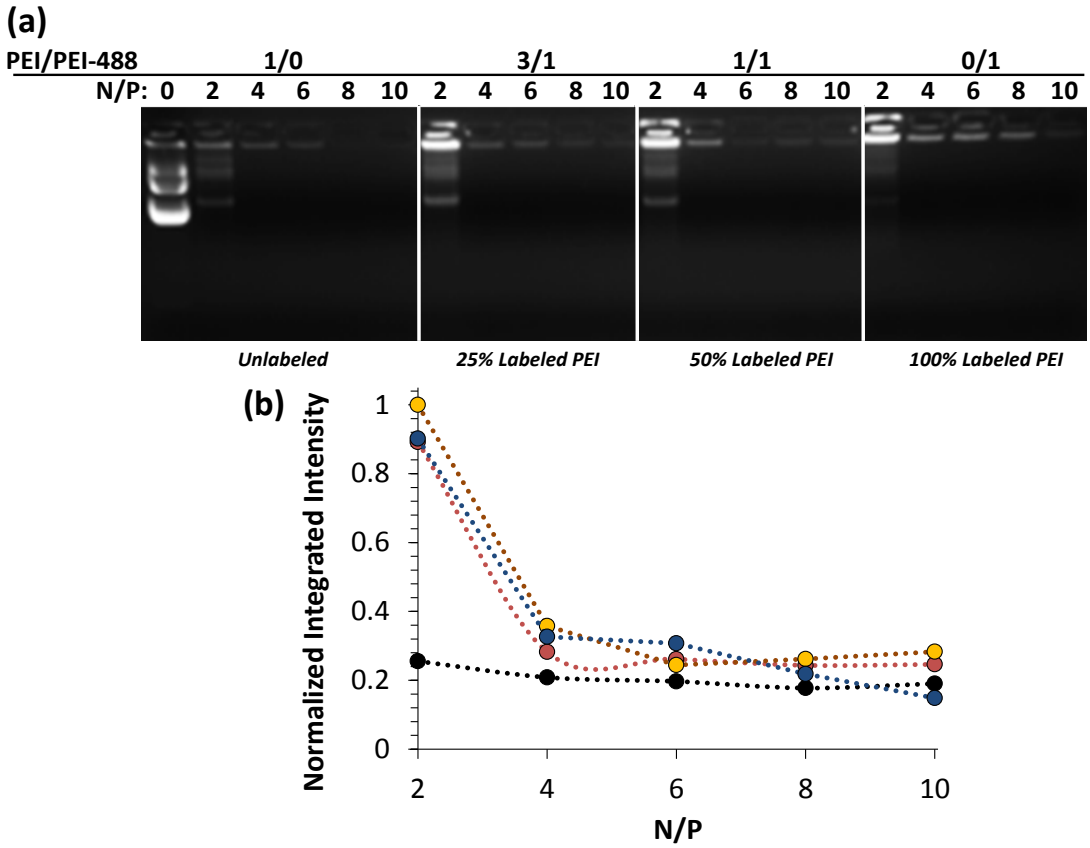

Figure 2.1 **(a) Representative ethidium bromide (EtBr) fluorescence images showing the electrophoretic mobility of plasmid DNA in polyplexes formed at various N/P ratios. Polyplexes were formed with increasing ratios of PEI-488 to unlabeled PEI as shown. (b) Integrated optical density quantification of EtBr fluorescence in the wells of the gel for polyplexes containing unmodified PEI (black), 25% PEI-488 (red), 50% PEI-488 (yellow), and 100% PEI-488 (blue). Optical densities are normalized to the highest well fluorescence in the gel.**

2.3.1 Fluorescent Labeling Decreases Polyplex Complexation Efficiency

Agarose gel electrophoresis was performed to characterize DNA/PEI polyplexes and to determine the extent to which PEI-488 was capable of condensing

DNA. Mixtures of PEI-488 and unlabeled PEI were used to form polyplexes at N/P ratios of 2, 4, 6, 8 and 10. Gel electrophoresis (Figure 2.1) demonstrated the reduced mobility of DNA within all polyplex formulations as a function of increasing N/P ratio. Specifically, for polyplexes prepared with unmodified PEI, reduced DNA mobility was observed at N/P = 2 and structures at N/P > 2 showed no DNA migration as tighter complexes were formed. For structures prepared with unmodified PEI, minimal fluorescence was observed for structures formed at N/P ≥ 6, in agreement with typical studies of DNA complexation with 25 kDa PEI.

As anticipated, the incorporation of fluorescent PEI-488 induced weakened DNA-PEI binding and caused the formation looser polyplex structures as indicated by the increasing fluorescence in the wells of the gel as a function of increasing fractions of PEI-488. Similar to the findings with the unlabeled PEI structures, attenuated migration of DNA at N/P = 2 was observed in all labeled structures, as well as an increase in DNA fluorescence in the well as compared with the unbound DNA samples (e.g. N/P = 0). At all N/P ratios, a similar general trend was observed of increased well fluorescence with increasing PEI-488. This trend becomes less apparent with increasing N/P ratio, for example in the case of structures prepared N/P = 8 where there were minimal differences in the fluorescence in the wells of the gel. Furthermore, direct comparison of unmodified and labeled structures (100% PEI-488) indicates a clear difference in the complexation efficiency of these structures as ethidium bromide is entirely excluded at N/P = 6 for the unlabeled structures compared to N/P = 10 for the modified PEI. Image analysis and quantification of EtBr fluorescence intensity (Figure 2.1b) indicates distinct differences between 100% PEI-488 labeled and unlabeled structures at all the N/P ratios tested, but deviates slightly

from visual observations for intermediate mixtures which indicate minor off-trend fluctuations with quantification. Furthermore, this quantification indicates the consistent observation of minimal changes in fluorescence for preparations above 50% labeling ratio.

2.3.2 Label Incorporation Induces Polyplex Aggregation

To further explore the effects of the weakened DNA-PEI binding that were observed in the DNA mobility studies, the polyplex sizes were examined using DLS to determine whether OG label incorporation induced polyplex aggregation. It was anticipated that the more loosely packaged (and EtBr-accessible) structures identified by electrophoresis would be more prone to aggregate due to hydrophobic interactions. For DLS analyses, polyplexes were prepared similarly to electrophoresis studies, but only at N/P ratios of 4, 6, and 8 as these ratios demonstrated polyplex formation for all formulations tested in electrophoresis (Figure 2.1a) and have previously demonstrated less toxicity than structures formed at higher N/P ratios.[45]

As anticipated based on the minimal fluorescence observed in electrophoresis, DNA-PEI structures formed at N/P 6 and 8 were appropriately sized for endocytic uptake, with average hydrodynamic diameters, D_H, below 200 nm.[46] Despite no measurable differences in the average polyplex sizes for these structures, the dispersity of the labeled structures increased markedly with the incorporation of PEI-488 at N/P = 6 (Figure 2.2). Structures prepared at N/P = 4 were notably larger than other formulations and indicated significant increases in polyplex diameter with the incorporation of PEI-488 with sizes > 200 nm for all formulation including the modified polymer.

a)

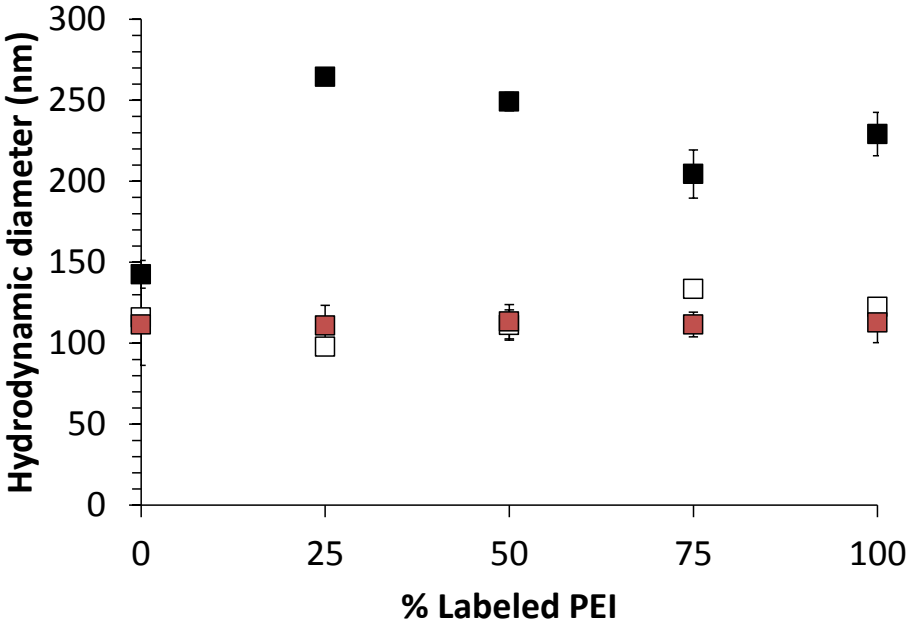

b)

% PEI-488	‡Average Dispersity
0	0.191
25	0.293
50	0.259
75	0.230
100	0.275

‡Dispersity values for N/P = 6

Figure 2.2 **(a) Hydrodynamic diameters of polyplexes prepared at N/P = 4 (black), 6 (white) and 8 (red), and (b) average dispersity of polyplexes (representative data for N/P = 6) as assessed by dynamic light scattering. Error bars represent the standard deviation of three separately prepared samples. Similarly, the dispersity represents an average of three separate samples.**

2.3.3 Looser Polyplexes are Less Efficient in Cell Entry and Result in Significant Extracellular Aggregation

It was hypothesized that the reduced polyplex packing density and increased polyplex size dispersity demonstrated in electrophoresis and DLS would correlate with altered cellular uptake. Thus, polyplex uptake efficiency was measured by fluorescence microscopy to monitor intracellular PNA-AF555 labeled DNA (DNA-555)-containing polyplexes. PNA labeling strategies have been used in a number of studies to probe the intracellular trafficking of DNA. In the preparation of PNA-labeled DNA, fluorescent PNA molecules (~5000 Da in size) label only a small fraction of DNA (~8 PNA molecules per plasmid in the work of Millili *et al*.) through sequence-specific hybridization to complementary DNA bases.[39] The labeled DNA has been shown to exhibit similar structures and transcriptional activities as unlabeled materials, in part because the PNA labels are small in size relative to the DNA plasmid.[39, 47, 48] The use of DNA-555/PEI-488 dual labeled structures provided the ability to explore the impacts of polymer labeling on both cellular uptake and intracellular colocalization of DNA and PEI.

Polyplexes were prepared at N/P 6 (Figure 2.3), at which reduced polyplex packaging density and increased dispersity were particularly apparent based on gel electrophoresis and DLS analyses due to favorable sizes as compared to preparations at N/P 4 and reduced toxicity compared to higher charge ratios.[45] Confocal imaging analyses revealed significant levels of extracellular DNA with this formulation. The quantity of extracellular DNA qualitatively appeared to increase in the presence of increasing amounts of PEI-488 up to a labeling ratio of 50% PEI-488:PEI (Figure 2.3, magnified images). For PEI-488:PEI labeling ratios greater than 50%, the amount of extracellular debris was relatively constant as the labeling ratio increased.

Intracellular polyplexes were evident in all samples; however, an increasing number of large, diffuse intracellular structures were observed with increasing PEI-488 (Figure 2.3, arrows), particularly at 100% PEI-488. Overlay images combining the DNA and PEI imaging channels revealed colocalization of both components in all samples; however, significant amounts of free extracellular DNA as well as free intracellular polymer were apparent under all labeling conditions.

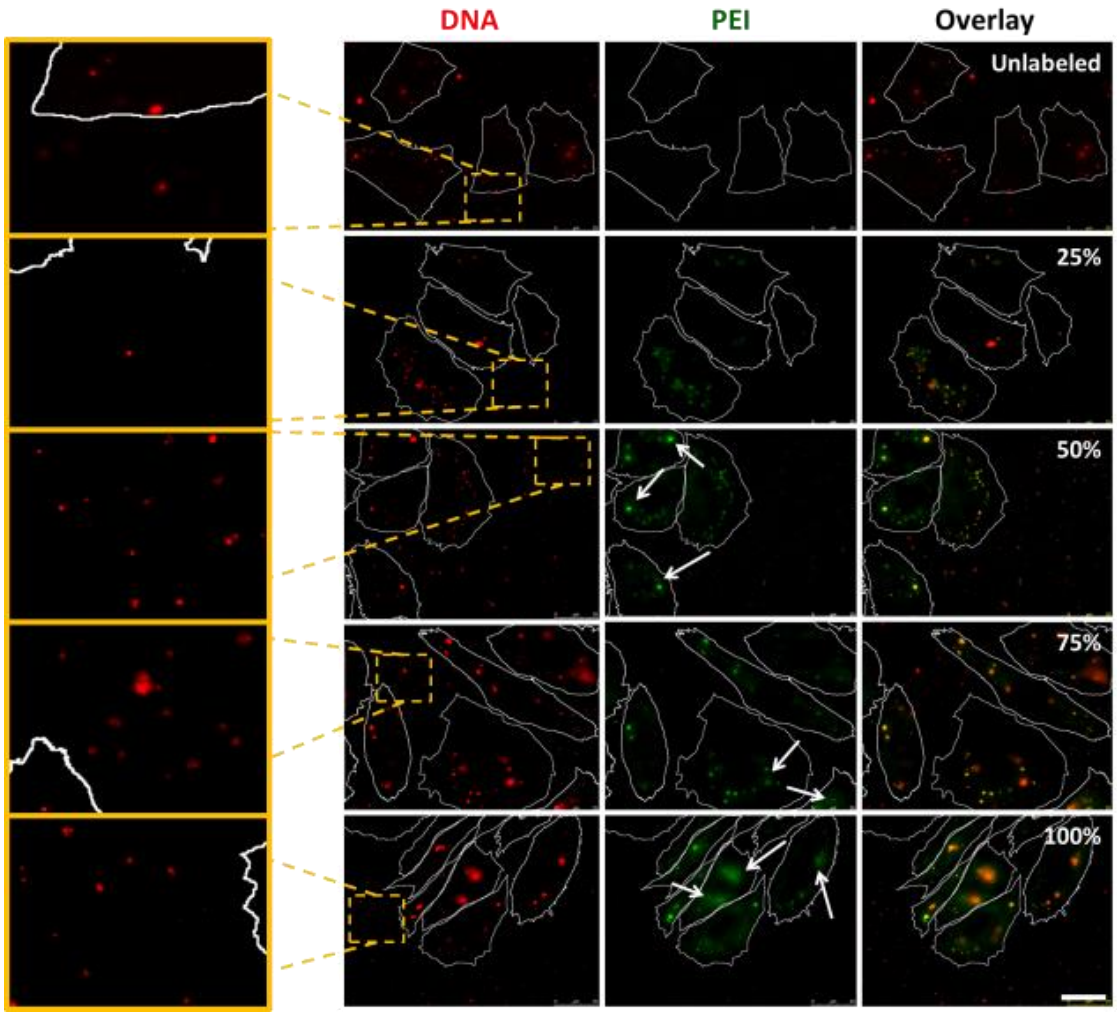

Figure 2.3 Uptake of dual labeled polyplexes with varying degrees of PEI-488 incorporation at N/P = 6. Representative fluorescence microscopy images showing a magnification of extracellular DNA-555 (far left), DNA-555 (red), PEI-488 (green), and overlaid channels (right). Arrows indicate aggregated unfocused structures. The scale bar is 25 µm.

2.3.4 High Degree of Labeling Reduces Polyplex Uptake

To investigate if the extracellular losses observed in microscopy resulted in significant reductions in DNA uptake, the amount of intracellular polyplexes were

quantified by using flow cytometry to assess DNA-555 levels within the cells. For each sample, a "pulse-chase" inspired approach was used to expose cells to polyplexes for a relatively short time period (30 min) and enable improved intracellular quantification.[49] Both the uptake efficiency (percentage of cells that internalized polyplexes) and the average quantity of intracellular polyplexes per cell (mean fluorescence intensity) were subsequently quantified (Figure 2.4). It was hypothesized that the polyplexes prepared at N/P = 4, 6, and 8, which exhibited significant extracellular aggregate formation, would be internalized to a lesser degree. Quantification of uptake efficiencies demonstrated low levels of polyplex uptake for all structures (Figure 2.4 a) commensurate with the short pulse exposure approach.

Structures prepared at low charge ratios N/P $\leq$ 4 have previously demonstrated low levels of uptake and gene transfer efficiency.[42] Consistent with these studies, polyplexes prepared at N/P = 4 exhibited negligible levels of uptake as compared with other formulations, and hence it was not possible to detect differences in polyplex uptake with varying amounts of PEI-488. Polyplexes prepared at N/P = 8 also demonstrated negligible differences in uptake for all PEI-488 formulations. This finding was consistent with the minimal differences in structure that were observed based on complexation and stability assays.

Because polyplexes prepared at N/P = 6 demonstrated inefficient complexation in the presence of PEI-488, it was hypothesized that these structures would demonstrate reduced efficacy in polyplex uptake with increasing PEI-488 incorporation. As expected, these structures exhibited differences in intracellular accumulation associated with label incorporation. Specifically, formulations prepared at $\geq$50% incorporated PEI-488 at N/P = 6 induced lower levels of uptake. Statistically

significant differences were observed in the percentage of cells which internalized polyplexes when comparing unlabeled structures to those with 50% and 100% incorporated PEI-488. Additionally, all structures prepared at ≥ 50% label demonstrated significantly lower levels of uptake than the 25% sample.

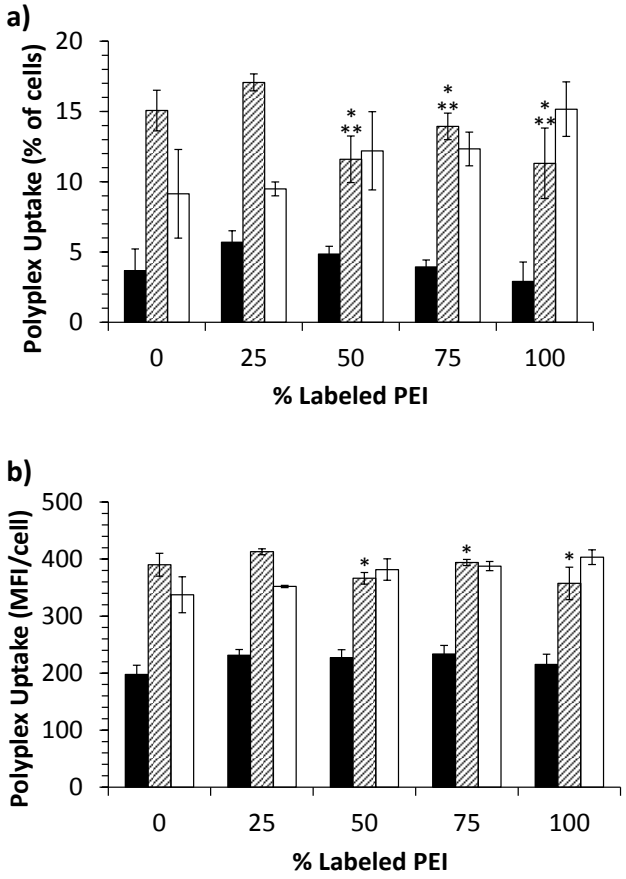

Figure 2.4 Quantification of DNA-555 uptake using dual labeled polyplexes with varying degrees of PEI-488 incorporation. (a) Percentage of CHO-K1 cells that internalize DNA-555 polyplexes, and (b) Mean fluorescent intensity per cell of CHO-K1 cells following polyplex internalization. N/P = 4 (black), 6 (diagonal stripes) and 8 (white). * indicates a statistically significant difference from samples containing 25% PEI-488 samples ($p < 0.05$). ** indicates a statistically significant difference from unlabeled PEI samples ($p < 0.1$). Samples were analyzed by one-way analysis of variance (ANOVA).

2.4 Discussion

Fluorescent tags are a routine tool for studying endocytic processing of non-viral carriers due to several favorable features. Specifically, fluorescent molecules are easy to visualize (in live and fixed cells) and they are safe compared to radioactive approaches and techniques using electron microscopy imaging. However, while published studies have demonstrated the reduced efficacy of these labeled structures,[31] little attention has been devoted to understanding the structure/function relationships in the development of these materials. A detailed exploration of the assembly and activity of fluorescently-labeled gene carriers can allow for the rational design of more efficacious and reliable tools for understanding the mechanisms of intracellular processing. Based on published studies indicating differences in gene association with label incorporation, a systemic study of the effect of label incorporation was performed and differences were identified in polyplex assembly, stability, and intracellular delivery.

This work presents a model gene delivery system using a commercially available branched 25 kDa PEI modified by the incorporation of a fluorescent tag (Oregon Green® 488) for the delivery of DNA polyplexes. It was previously demonstrated that the incorporation of hydrophobic tags has the potential to weaken polyplex binding interactions and lead to improved gene transfer due to improved DNA accessibility.[32-34] Building on this work, a systematic study of the impact of hydrophobic dye incorporation was performed. These studies aimed to determine the effects of reduced binding interactions and increased hydrophobicity on extra- and intracellular polyplex stability and endocytic processing. Polyplexes prepared with modified PEI demonstrated similar characteristics to unmodified structures, yet exhibited systematically weakened binding interactions (Figure 2.1). This was

anticipated because label incorporation sacrifices primary amines on the polymer carrier, thereby reducing the available charge for electrostatic interactions with the DNA backbone. Additionally, it was hypothesized that exposed hydrophobic residues further reduces the electrostatic condensation leading to the aggregation of these structures. Notably, polyplexes created using these labeled structures can be split into two distinct groups according to their assembly and function. Preparations greater than 50% % PEI-488 demonstrated significant differences in complexation and delivery from unlabeled structures and those prepared at 25% PEI-488. With the observation that PEI-488 has weaker DNA association that unmodified PEI, it was hypothesized that the observed groupings are a result of interactions during formulation. In particular, for low percentages of PEI-488, the addition of a larger quantity of unmodified PEI in the second stage of formulation may provide sufficient electrostatic interactions to demonstrate favorable gene association. Conversely, the addition of small fractions of unmodified PEI (for preparations at higher percentages) may be insufficient to alter association in these structures.

Interestingly, these differences in packaging efficiency manifested in structures with similar size, but increased dispersity (Figure 2.2). Although the labeled structures were slightly larger than unmodified PEI polyplexes, all samples exhibited average diameters that were less than 200 nm. It is likely that the PEI-488 might experience weakened (less efficient) interactions with DNA than unmodified PEI, leading to non-uniformity of the mixed structures and an increase in the dispersity. Furthermore, the increased polyplex dispersity is likely indicative of an enhanced tendency to aggregate as a result of exposed hydrophobic moieties from the dye.

To investigate how polyplexes with reduced packaging efficiency and increased tendency to aggregate were impacted by exposure to the cellular environment, polyplexes were delivered to cells and their uptake was monitored by fluorescence microscopy. Interestingly, fluorescence microscopy revealed the formation of extracellular aggregates in formulations prepared with the PEI-488 label. Additionally, these polyplexes showed diversity in sizes with the incorporation of the fluorescent tag (Figure 2.3). In these *in vitro* studies, the cellular environment is able to prematurely unpackage the loosened structures and thus reveal instabilities and differences in hydrophobicity in the polyplexes that are not detectable by DLS. For example, it was previously demonstrated that heparin is able to unpackage loosely associated structures more readily than those with stronger binding interactions.[50] It is likely that many of the loose polyplex aggregates are disassembled (and hence unable to enter cells) by interaction with heparin and other extracellular polyanions, leading to the significant amounts of extracellular free DNA.

The impacts of OG-488 on cellular uptake were quantified by flow cytometry (Figure 2.4). Previous work has shown that polyplexes formed at low charge ratios are less efficient at packaging and delivering nucleic acids.[42] As anticipated based on these previous observations, structures prepared at N/P = 4 demonstrated much lower levels of uptake than all other structures investigated in this study. Interestingly, there were no observed differences in polyplex uptake for formulations prepared at N/P = 8. Based on studies by Yue and coworkers indicating as much as 70% of the PEI existing in free solution following assembly (for preparations at N/P = 10), it is likely that at this high charge ratio (N/P = 8) all formulations using PEI-488 were able to overcome the unfavorable interactions of DNA with PEI-488 due to the excess free polymer in

solution.[45, 51] Interestingly, structures prepared at N/P = 6 led to a significant decrease in polyplex uptake for formulations prepared at greater than 25% incorporated label. Consistent with observations in fluorescence microscopy, it is likely that the loose extracellular structures and large aggregates that result from interactions with the cell environment are unable to efficiently enter cell due to premature unpackaging.

2.5 Conclusions

The studies detailed in this work highlight the importance of understanding structure/function relationships with diverse polymer structures, including not only fluorophores (as explored in this chapter), but also light-sensitive residues, targeting ligands and other modifying components used in the number of gene delivery applications. Ultimately, the development of improved structures relies on employing similar methods to those detailed in this study to improve our understanding of the gene association and delivery. Using the systematic studies detailed in this work, a basis has been developed for the exploration of other non-viral carriers, some of which will be detailed in the remainder of this work.

REFERENCES

1. Guo, X.; Huang, L., Recent advances in nonviral vectors for gene delivery. *Acc Chem Res* **2012,** 45, (7), 971-9.

2. Khalil, I. A.; Kogure, K.; Akita, H.; Harashima, H., Uptake pathways and subsequent intracellular trafficking in nonviral gene delivery. *Pharmacol Rev* **2006,** 58, (1), 32-45.

3. McLendon, P. M.; Fichter, K. M.; Reineke, T. M., Poly(glycoamidoamine) vehicles promote pDNA uptake through multiple routes and efficient gene expression via caveolae-mediated endocytosis. *Mol Pharm* **2010,** 7, (3), 738-50.

4. Medina-Kauwe, L. K.; Xie, J.; Hamm-Alvarez, S., Intracellular trafficking of nonviral vectors. *Gene Ther* **2005,** 12, (24), 1734-51.

5. Midoux, P.; Breuzard, G.; Gomez, J. P.; Pichon, C., Polymer-based gene delivery: a current review on the uptake and intracellular trafficking of polyplexes. *Curr Gene Ther* **2008,** 8, (5), 335-52.

6. Schaffer, D. V.; Fidelman, N. A.; Dan, N.; Lauffenburger, D. A., Vector unpacking as a potential barrier for receptor-mediated polyplex gene delivery. *Biotechnol Bioeng* **2000,** 67, (5), 598-606.

7. Peng, L. a. G. Y. a. X. Y.-N. a. H. S.-W. a. Z. R.-X., The effectiveness, cytotoxicity, and intracellular trafficking of nonviral vectors for gene delivery to bone mesenchymal stem cells. *Journal of Bioactive and Compatible Polymers* **2013,** 28, (3), 204-217.

8. Nishikawa, M.; Huang, L., Nonviral vectors in the new millennium: delivery barriers in gene transfer. *Hum Gene Ther* **2001,** 12, (8), 861-70.

9. Pouton, C. W.; Seymour, L. W., Key issues in non-viral gene delivery. *Adv Drug Deliv Rev* **2001,** 46, (1-3), 187-203.

10. Wiethoff, C. M.; Middaugh, C. R., Barriers to nonviral gene delivery. *J Pharm Sci* **2003,** 92, (2), 203-17.

11. Dauty, E.; Verkman, A. S., Actin cytoskeleton as the principal determinant of size-dependent DNA mobility in cytoplasm: a new barrier for non-viral gene delivery. *J Biol Chem* **2005,** 280, (9), 7823-8.

12. Godbey, W. T.; Wu, K. K.; Mikos, A. G., Tracking the intracellular path of poly(ethylenimine)/DNA complexes for gene delivery. *Proc Natl Acad Sci U S A* **1999,** 96, (9), 5177-81.

13. Harush-Frenkel, O.; Debotton, N.; Benita, S.; Altschuler, Y., Targeting of nanoparticles to the clathrin-mediated endocytic pathway. *Biochem Biophys Res Commun* **2007,** 353, (1), 26-32.

14. Conner, S. D.; Schmid, S. L., Regulated portals of entry into the cell. *Nature* **2003,** 422, (6927), 37-44.

15. Watson, P.; Jones, A. T.; Stephens, D. J., Intracellular trafficking pathways and drug delivery: fluorescence imaging of living and fixed cells. *Adv Drug Deliv Rev* **2005,** 57, (1), 43-61.

16. Lechardeur, D.; Verkman, A. S.; Lukacs, G. L., Intracellular routing of plasmid DNA during non-viral gene transfer. *Adv Drug Deliv Rev* **2005,** 57, (5), 755-67.

17. Haensler, J.; Szoka, F. C., Jr., Polyamidoamine cascade polymers mediate efficient transfection of cells in culture. *Bioconjug Chem* **1993,** 4, (5), 372-9.

18. Boussif, O.; Lezoualc'h, F.; Zanta, M. A.; Mergny, M. D.; Scherman, D.; Demeneix, B.; Behr, J. P., A versatile vector for gene and oligonucleotide transfer into cells in culture and in vivo: polyethylenimine. *Proc Natl Acad Sci U S A* **1995,** 92, (16), 7297-301.

19. Behr, J., The Proton Sponge: a Trick to Enter Cells the Viruses Did Not Exploit. *CHIMIA International Journal for Chemistry* **1997,** 51, 34-36.

20. Sonawane, N. D.; Szoka, F. C., Jr.; Verkman, A. S., Chloride accumulation and swelling in endosomes enhances DNA transfer by polyamine-DNA polyplexes. *J Biol Chem* **2003,** 278, (45), 44826-31.

21. Benjaminsen, R. V.; Mattebjerg, M. A.; Henriksen, J. R.; Moghimi, S. M.; Andresen, T. L., The possible "proton sponge " effect of polyethylenimine (PEI) does not include change in lysosomal pH. *Mol Ther* **2013,** 21, (1), 149-57.

22. Subramanian, A.; Ma, H.; Dahl, K. N.; Zhu, J.; Diamond, S. L., Adenovirus or HA-2 fusogenic peptide-assisted lipofection increases cytoplasmic levels of plasmid in nondividing endothelium with little enhancement of transgene expression. *J Gene Med* **2002,** 4, (1), 75-83.

23. Akita, H.; Ito, R.; Khalil, I. A.; Futaki, S.; Harashima, H., Quantitative three-dimensional analysis of the intracellular trafficking of plasmid DNA transfected by a nonviral gene delivery system using confocal laser scanning microscopy. *Mol Ther* **2004,** 9, (3), 443-51.

24. Thomas, M.; Klibanov, A. M., Conjugation to gold nanoparticles enhances polyethylenimine's transfer of plasmid DNA into mammalian cells. *Proc Natl Acad Sci U S A* **2003,** 100, (16), 9138-43.

25. Shi, J.; Chou, B.; Choi, J. L.; Ta, A. L.; Pun, S. H., Investigation of Polyethylenimine/DNA Polyplex Transfection to Cultured Cells Using Radiolabeling and Subcellular Fractionation Methods. *Mol Pharm* **2013,** 10, (6), 2145-56.

26. Friend, D. S.; Papahadjopoulos, D.; Debs, R. J., Endocytosis and intracellular processing accompanying transfection mediated by cationic liposomes. *Biochim Biophys Acta* **1996,** 1278, (1), 41-50.

27. Uboldi, C.; Bonacchi, D.; Lorenzi, G.; Hermanns, M. I.; Pohl, C.; Baldi, G.; Unger, R. E.; Kirkpatrick, C. J., Gold nanoparticles induce cytotoxicity in the alveolar type-II cell lines A549 and NCIH441. *Part Fibre Toxicol* **2009,** 6, 18.

28. Wang, L. H.; Rothberg, K. G.; Anderson, R. G., Mis-assembly of clathrin lattices on endosomes reveals a regulatory switch for coated pit formation. *J Cell Biol* **1993,** 123, (5), 1107-17.

29. Vercauteren, D.; Vandenbroucke, R. E.; Jones, A. T.; Rejman, J.; Demeester, J.; De Smedt, S. C.; Sanders, N. N.; Braeckmans, K., The use of inhibitors to study endocytic pathways of gene carriers: optimization and pitfalls. *Mol Ther* **2010,** 18, (3), 561-9.

30. Fujimoto, L. M.; Roth, R.; Heuser, J. E.; Schmid, S. L., Actin assembly plays a variable, but not obligatory role in receptor-mediated endocytosis in mammalian cells. *Traffic* **2000,** 1, (2), 161-71.

31. Gasiorowski, J. Z.; Dean, D. A., Postmitotic nuclear retention of episomal plasmids is altered by DNA labeling and detection methods. *Mol Ther* **2005,** 12, (3), 460-7.

32. Zheng, M. a. Z. Y. a. M. F. a. P. R. a. Z. Z., Lipoic Acid Modified Low Molecular Weight Polyethylenimine Mediates Nontoxic and Highly Potent in Vitro Gene Transfection. *Molecular Pharmaceutics* **2011,** 8, (6), 2434-2443.

33. Gabrielson, N. P.; Pack, D. W., Acetylation of polyethylenimine enhances gene delivery via weakened polymer/DNA interactions. *Biomacromolecules* **2006,** 7, (8), 2427-35.

34. Forrest, M. L.; Meister, G. E.; Koerber, J. T.; Pack, D. W., Partial acetylation of polyethylenimine enhances in vitro gene delivery. *Pharm Res* **2004,** 21, (2), 365-71.

35. Wang, T.; Kievit, F. M.; Veiseh, O.; Arami, H.; Stephen, Z. R.; Fang, C.; Liu, Y.; Ellenbogen, R. G.; Zhang, M., Targeted cell uptake of a noninternalizing antibody through conjugation to iron oxide nanoparticles in primary central nervous system lymphoma. *World Neurosurg* **2013,** 80, (1-2), 134-41.

36. Suk, J. S.; Suh, J.; Lai, S. K.; Hanes, J., Quantifying the intracellular transport of viral and nonviral gene vectors in primary neurons. *Exp Biol Med (Maywood)* **2007,** 232, (3), 461-9.

37. Levinson, R. T.; Olatoye, O. O.; Randles, E. G.; Howell, K. G.; DiCostanzo, A. C.; Ramirez-Alvarado, M., Role of mutations in the cellular internalization of amyloidogenic light chains into cardiomyocytes. *Sci Rep* **2013,** 3, 1278.

38. Lee, J. S.; Feijen, J., Biodegradable polymersomes as carriers and release systems for paclitaxel using Oregon Green(R) 488 labeled paclitaxel as a model compound. *J Control Release* **2012,** 158, (2), 312-8.

39. Millili, P. G.; Yin, D. H.; Fan, H.; Naik, U. P.; Sullivan, M. O., Formulation of a Peptide Nucleic Acid Based Nucleic Acid Delivery Construct. *Bioconjug Chem* **2010**.

40. Javanmoghadam-Kamrani, S.; Keyomarsi, K., Synchronization of the cell cycle using lovastatin. *Cell Cycle* **2008,** 7, (15), 2434-40.

41. Wu, J. R.; Gilbert, D. M., Lovastatin arrests CHO cells between the origin decision point and the restriction point. *FEBS Lett* **2000,** 484, (2), 108-12.

42. Reilly, M. J.; Larsen, J. D.; Sullivan, M. O., Histone H3 tail peptides and poly(ethylenimine) have synergistic effects for gene delivery. *Mol Pharm* **2012,** 9, (5), 1031-40.

43. Reilly, M. J.; Larsen, J. D.; Sullivan, M. O., Polyplexes traffic through caveolae to the Golgi and endoplasmic reticulum en route to the nucleus. *Mol Pharm* **2012,** 9, (5), 1280-90.

44. Larsen, J. D.; Reilly, M. J.; Sullivan, M. O., Using the epigenetic code to promote the unpackaging and transcriptional activation of DNA polyplexes for gene delivery. *Mol Pharm* **2012,** 9, (5), 1041-51.

45. Yue, Y.; Jin, F.; Deng, R.; Cai, J.; Chen, Y.; Lin, M. C.; Kung, H. F.; Wu, C., Revisit complexation between DNA and polyethylenimine - Effect of uncomplexed chains free in the solution mixture on gene transfection. *J Control Release* **2011,** 155, (1), 67-76.

46. Ogris, M.; Steinlein, P.; Carotta, S.; Brunner, S.; Wagner, E., DNA/polyethylenimine transfection particles: influence of ligands, polymer size, and PEGylation on internalization and gene expression. *AAPS PharmSci* **2001,** 3, (3), E21.

47. Koppelhus, U.; Nielsen, P. E., Cellular delivery of peptide nucleic acid (PNA). *Adv Drug Deliv Rev* **2003,** 55, (2), 267-80.

48. Liang, K. W.; Hoffman, E. P.; Huang, L., Targeted delivery of plasmid DNA to myogenic cells via transferrin-conjugated peptide nucleic acid. *Mol Ther* **2000,** 1, (3), 236-43.

49. Sandin, P.; Fitzpatrick, L. W.; Simpson, J. C.; Dawson, K. A., High-speed imaging of Rab family small GTPases reveals rare events in nanoparticle trafficking in living cells. *ACS Nano* **2012,** 6, (2), 1513-21.

50. Bertschinger, M.; Backliwal, G.; Schertenleib, A.; Jordan, M.; Hacker, D. L.; Wurm, F. M., Disassembly of polyethylenimine-DNA particles in vitro: implications for polyethylenimine-mediated DNA delivery. *J Control Release* **2006,** 116, (1), 96-104.

51. Thibault, M.; Astolfi, M.; Tran-Khanh, N.; Lavertu, M.; Darras, V.; Merzouki, A.; Buschmann, M. D., Excess polycation mediates efficient chitosan-based gene transfer by promoting lysosomal release of the polyplexes. *Biomaterials* **2011,** 32, (20), 4639-46.

Chapter 3

CATCH AND RELEASE: PHOTOCLEAVABLE CATIONIC DIBLOCK COPOLYMERS AS A POTENTIAL PLATFORM FOR NUCLEIC ACID DELIVERY

New approaches to polymer-based gene therapy are necessary to facilitate externally-stimulated nucleic acid release and to overcome the contradictory demands for intracellular delivery. On one hand, the binding interactions between nucleic acids and cationic polymers must be sufficiently strong to prevent nuclease-mediated degradation, while on the other hand, weak interactions are necessary to enable nucleic acid release within cells. To address this paradox, light-responsive, *o*-nitrobenzyl-containing cationic block copolymers (BCPs) were synthesized using the following design criteria: (1) complete DNA complexation into polyplexes; (2) minimized charge content to retain binding; (3) salt and serum stability; and (4) a nucleic acid release mechanism. These BCPs were subsequently investigated their potential for plasmid DNA encapsulation and triggered release. The resulting BCPs combined PEG with a novel, photo-responsive block to facilitate tunable, salt-stable complexation and light-activated release.

3.1 Introduction

Non-viral carriers such as lipids, peptides, and synthetic polymers can deliver exogenous nucleic acids to dysfunctional cells to manipulate the expression of specific genetic targets and thereby modulate cellular function.[1] Cationic polymers make up the majority of non-viral nucleic acid delivery vehicles due to their synthetic

versatility and ability to form electrostatic complexes (polyplexes) with anionic nucleic acids.[2] The encapsulation of nucleic acids within these polyplexes can prevent enzymatic degradation, reduce serum protein adsorption, and promote cell membrane interactions/endocytosis.[3] However, nucleic acid release is essential to permit binding by transcription factors (or other protein-based targets) and promote efficient gene expression.[4] Thus, balancing the competing requirements of nucleic acid binding and release is a common challenge in developing successful delivery vehicles.

Weak nucleic acid-polymer binding affinity is a substantial and well-documented roadblock to efficient delivery as it leads to polyplex instability, premature nucleic acid release, and nucleic acid degradation.[4-6] For example, Burke and Pun highlighted the importance of polyplex stability in the study of DNA/PEI polyplexes.[5] In studies of *in vivo* delivery to liver tissues, the DNA/PEI polyplexes interacted with extracellular matrix components, which displaced the DNA from the polyplexes. This premature polyplex disassembly resulted in reduced DNA internalization as well as degradation of DNA in the extracellular space. Strategies to improve nucleic acid encapsulation and polyplex stability include increasing the polymer concentration in the polyplex or the length of the polycation.[7, 8] Specifically, Abdelhady *et al*. reported the effects of an increased polymer/nucleic acid ratio, i.e. increased polyplex charge density, using polyamidoamine dendrimers and plasmid DNA.[7] That work reported degradation on the order of minutes for unprotected nucleic acids, but no degradation over several hours for polyplexes formed at nitrogen/phosphate (N/P) ratios > 1. In another example, Layman *et al*. investigated increased lengths of poly(2-dimethylaminoethyl methacrylate) that shielded DNA from degradation and increased gene expression by 20-fold as the weight-average

molecular weight (M_w) increased from 43,000 g/mol to 915,000 g/mol.[8] In other work, Rice and coworkers enhanced polyplex stability through the incorporation of hydrophobic acridine groups into polycations imposed thermodynamic penalties for disassociation and enhanced binding affinities by coupling intercalation of the hydrophobic groups with electrostatic interactions.[9-11]

Although several strategies exist to improve polyplex packaging, high affinity polymers present a challenge as they can impede nucleic acid release in the cell.[4, 10] Schaffer *et al*. and Choosakoonkriang *et al*. showed that increased polycation length (with poly(L-lysine) and polyethylenimine, respectively) decreased the transfection efficiency due to a lack of nucleic acid release from the polyplexes.[11, 12] Also, Schaffer *et al*. and Erbacher *et al*. independently concluded that reduced cationic charge on poly(L-lysine) improved DNA delivery and enhanced polyplex dissociation in solution.[11, 13] Additionally, several studies correlated increasing cytotoxicity to increasing cationic charge densities in polyplexes.[14-16] These examples suggest that alternative nucleic acid packaging strategies are necessary to enable adaptation of polyplex stability in the presence of the evolving needs during delivery.

The incorporation of stimuli-responsive functional groups into polymer/nucleic acid complexes provides complementary functionality for both stable encapsulation and triggered release of nucleic acids.[17] For example, Abbott and coworkers developed ferrocene-containing cationic lipids with reduction/oxidation (red/ox) sensitive nucleic acid binding capacity.[18] The authors showed that chemical or electrochemical oxidation/reduction of the ferrocene groups could reversibly alter the charge of the lipids and thereby produce shifts between lamellar (reduced) and amorphous (oxidized) lipoplex morphologies. In this case, the altered binding and

corresponding structural shifts were directly correlated with deactivation/activation of gene transfer due to redox triggered alterations in lipoplex stability and membrane-binding potential [19]. Subsequent studies demonstrated the ability to spatially control gene transfection *in vitro*, through application of chemical agents.[20]The above systems highlight the merits of stimuli-responsive constructs, and suggest enormous potential benefits for gene nanocarriers whose properties are sensitive to externally-applied stimuli. Photo-responsive polymers are particularly appealing because of the versatility and spatial resolution afforded by light. In particular, the *o*-nitrobenzyl (*o*-NB) ester studied in this work absorbs UV or near-infrared light and undergoes an isomeric rearrangement to form a carboxylic acid and a nitrosobenzaldehyde.[21, 22] The production of the carboxylic acid introduces a negatively charged carboxylate ion in aqueous conditions above pH ≈ 3.[21]

Recent studies have detailed the incorporation of photo-responsive moieties into various polymeric systems for drug and gene delivery.[21, 23-26] In particular, solution assemblies whose hydrophobic components contained the photo-responsive *o*-NB moiety could destabilize and release dyes or drugs upon irradiation with light.[27-29] In one such example, Johnson *et al*. synthesized a photocleavable polymer-drug conjugate that tethered doxorubicin to a poly(norbornene-PEG) bottle-brush copolymer using an *o*-NB derivative.[30] The polymer was noncytotoxic in the absence of UV irradiation and demonstrated successful release of doxorubicin in breast cancer cells *in vitro* after UV irradiation. Other *o*-NB-containing systems include photoactive dendrons, metallic nanoparticles, and peptides that facilitate nucleic acid complexation and release.[31-33] However, drawbacks preventing the clinical application of dendrimers, peptides, and nanoparticles include the difficulty of synthesis, scalability,

cost, and toxicity, which can be mediated using block copolymers (BCPs).[34-36] To that end, the controlled and scalable synthesis of a photoactive and cationic diblock copolymer has been outlined and the following experiments demonstrate its noncytotoxicity, stable and tunable DNA binding, and capacity for light-triggered release.

Based on the literature, essential criteria for new nucleic acid carriers include: (1) complete complexation and condensation of nucleic acids into polyplexes; (2) minimized charge content to reduce cytotoxicity yet retain binding capacity; (3) salt and serum stability; and (4) capability for nucleic acid unpackaging. These features were incorporated into the design of a block copolymer architecture that utilized PEG as a nonfouling/stealth component[37] and a methacrylate-based cationic block to facilitate nucleic acid complexation. A PEG macroinitiator was employed to provide access to controlled radical polymerization (CRP) techniques, i.e., atom-transfer radical polymerization (ATRP). CRP enables tunable molecular weights, compositions, dispersities, and end-group functionalities. A vital building block in this scheme was the monomer, *5*-(*3*-((*tert*-butoxycarbonyl)amino)propoxy)-2-nitrobenzyl methacrylate (Boc-APNBMA), which contained a methacrylate and protected amine functionality to facilitate ATRP. Photo-responsive character was introduced through the incorporation of an *o*-NB ester moiety. Cleavage of the Boc-protecting group following ATRP revealed the final cationic and photo-responsive block copolymer. The monomer and the subsequent protected and ionic block copolymers were prepared as depicted in Scheme 1. The placement of the photoactive *o*-NB ester between the polymer backbone and the ammonium cation is key to the block copolymer design as applied to nucleic acid delivery. This location leads to charge reversal and facilitates

the *catch and release* mechanism desired for efficiently delivering nucleic acids. Thus, this design combines the highlighted criteria, including: biocompatible/stealth PEG components; polymers with tailorable composition and molecular weights; cationic moieties that support tight polyplex formation; and photo-responsive functional groups for controlled spatiotemporal release of the nucleic acid.

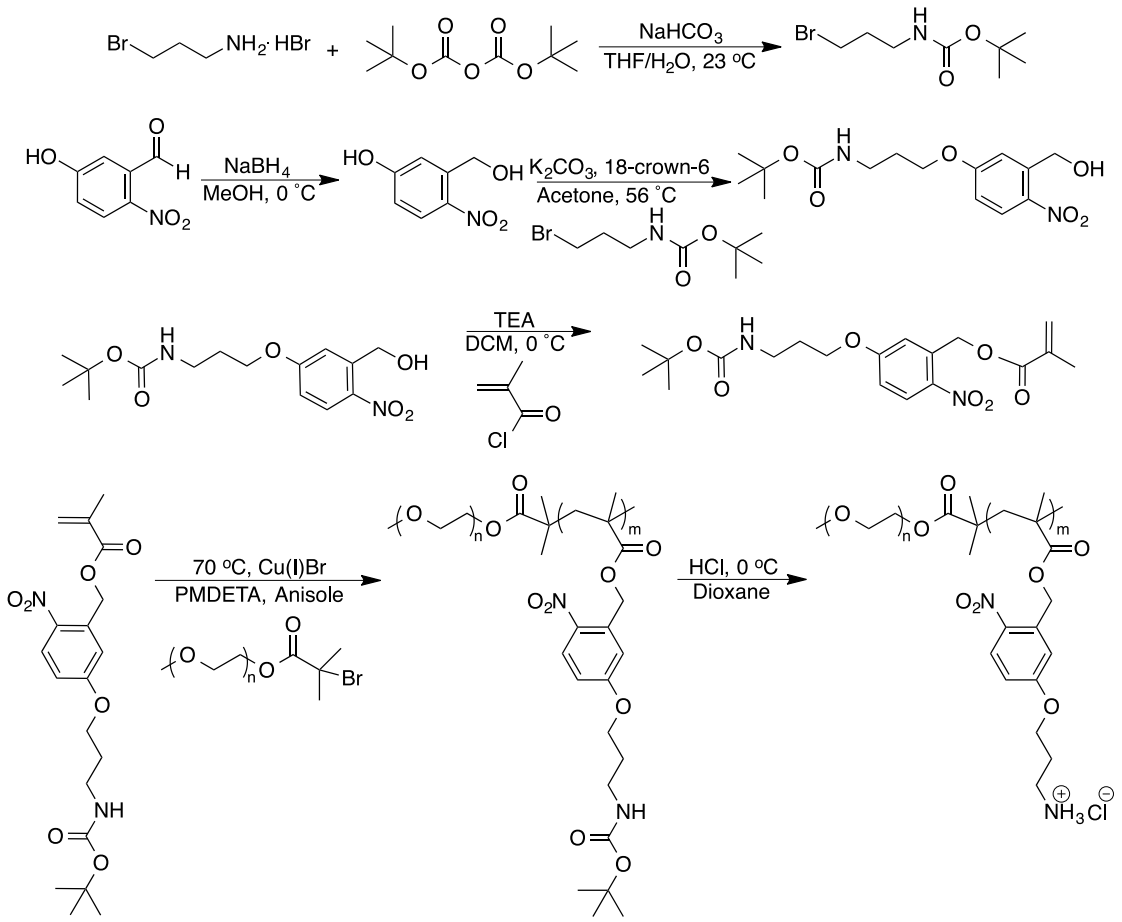

Scheme 1. Synthesis of mPEG-*b*-P(APNBMA·HCl)$_n$.

3.2 Materials and Methods

3.2.1 Materials

mPEG-*b*-P(APNBMA) copolymers were prepared by controlled radical polymerization (CRP) techniques, i.e., atom-transfer radical polymerization (ATRP) by Dr. Matthew Green as outlined in Scheme 1 (detailed synthetic methods shown in Appendix A). Intermediates and products were characterized using ^{1}H NMR spectroscopy. Water used in characterization was obtained from a Milli-Q water purification system (resistivity = 18.2 MΩ·cm). 1× Dulbecco's phosphate buffered saline (DPBS) (150 mM salt concentration, with calcium and magnesium) was purchased from Fisher, Opti-MEM® I Reduced Serum Media (buffered with HEPES and sodium bicarbonate, and supplemented with hypoxanthine, thymidine, sodium pyruvate, L-glutamine, trace elements, and growth factors) was purchased from Life Technologies. *4*-(*2*-hydroxyethyl)-*1*-piperazineethanesulfonic acid (HEPES) sodium salt was purchased from Fisher and dissolved at 20 mM in ultrapure water, and then the pH was adjusted to ≈6 using 1.0 M HCl or 1.0 M NaOH.

3.2.2 ^{1}H NMR Spectroscopy

Solutions of Boc-APNBMA, mPEG-*b*-P(Boc-APNBMA)$_n$, and mPEG-*b*-(APNBMA·HCl)$_n$ were prepared in $CDCl_3$ or DMSO-d_6. ^{1}H NMR spectra were collected at 600 MHz using a Bruker AVIII 600 MHz spectrometer.

3.2.3 Polyplex Formulation

Polyplexes were formed using mixtures of the gWiz-GFP plasmid and mPEG-*b*-P(APNBMA·HCl)$_{7.9}$. DNA solutions were prepared at 40 μg/mL in 20 mM HEPES (pH 6.0). Polyplexes were formed by dropwise addition of polymer solution to an

equal volume of DNA while vortexing. Solutions contained polymer over the range of concentrations appropriate to form polyplexes at the desired ammonium to phosphate (N/P) ratio. Polyplexes were incubated at 23 °C for 10 min prior to further analyses. DNA condensation using the ethidium bromide exclusion assay. Polyplex formation was analyzed using agarose gel electrophoresis. Polyplexes were prepared at N/P ratios from 0 to 7 by mixing 0.5 μg DNA with the appropriate amount of polymer, and the resulting mixture was added to 5 μL of gel loading dye (2.5 mg/mL bromophenol blue in 3/7 (v/v) glycerol/water). Then, the polyplex solution was added to the wells of a 1.0% agarose gel containing 0.2 μg/mL of ethidium bromide. Gels were run at 100 V for 2 h and subsequently imaged using a Biorad Gel Doc XR.

3.2.4 YOYO-1 Fluorescence Quenching Assay

gWiz-GFP plasmid was mixed with the bisintercalating dye YOYO-1 iodide (Invitrogen) at a base pair/dye ratio of 50 and incubated at room temperature for 1 h. Polyplexes were formed at N/P ratios of 0, 1, 2, 3, 4, 5, 6, and 7 by combining 1 μg YOYO-1 labeled DNA and the appropriate amount of PEG-*b*-P(APNBMA·HCl)$_{7.9}$ as described previously. Subsequently, 50 μL of polyplex solution was added to a 96-well plate, and the fluorescence was measured using a GloMax Multi Detection System reader.

3.2.5 Polymer/Polyplex Cleavage

Polymer and polyplexes were prepared such that the final polymer concentration was 0.1 mg/mL. Solutions were loaded into a chamber prepared by sealing two glass slides with a rubber gasket. The chamber was irradiated with 365 nm light at 200 W/m^2 (Omnicure S2000, Lumen Dynamics, Mississaugua, Ontario,

Canada) for 0 min, 10 min, 20 min, 40 min, and 60 min. Samples were removed from the chamber and collected for absorbance measurements (Thermo Scientific, NanoDrop 1000 Spectrophotometer) and agarose gel electrophoresis.

3.2.6 Preparation of Polyplexes for Dynamic Light Scattering (DLS)

Polyplexes (1.5 μg DNA, 75 μL of solution) were mixed with 200 μL HEPES buffer, H_2O, PBS, or Opti-MEM, and subsequently incubated at 23 °C for 60 min prior to particle size determination. DLS experiments were performed using a CNI Optoelectronics Co., Ltd. 532 nm, 427.6 mW laser, coupled with a Brookhaven Instruments Corporation BI-200SM goniometer equipped with an inline 532 nm filter from Intor, Inc. The intensity auto-correlation function was recorded at 90° and analyzed using a quadratic cumulant fit. All light scattering experiments were performed at 25 °C.

3.3 Results and Discussion

Developing structure-property relationships is critical to the design and optimization of polymeric nanocarriers, and necessitates the synthesis of polymers with well-defined characteristics. Thus, ATRP of Boc-APNBMA from a mPEG-Br macroinitiator (5,300 g/mol, $Đ = 1.05$) was used to generate well-defined mPEG-*b*-P(Boc-APNBMA) block copolymers. Boc-APNBMA content and overall copolymer molecular weight was tuned by manipulating the monomer to macroinitiator ratio. (Note: reaction time was held constant at 24 h.) The size exclusion chromatography (SEC) traces in Figure 3.1 demonstrate the shift in elution volume upon a change in the monomer to macroinitiator ratio. Narrow molecular weight distributions ($Đ \leq 1.16$) for mPEG-*b*-P(Boc-APNBMA)$_n$ (where *n* represents the calculated degree of

polymerization of the Boc-APNBMA block) supported the controlled nature of the polymerization during Boc-APNBMA chain extension.

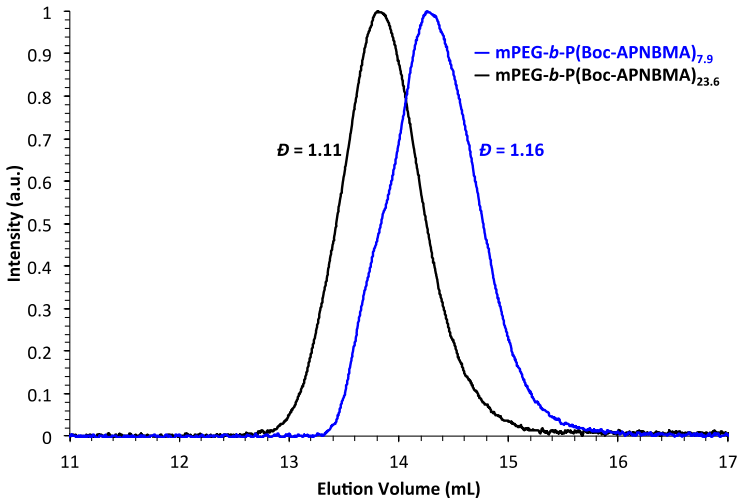

Figure 3.1 Size exclusion chromatograms of mPEG-*b*-P(Boc-APNBMA)$_n$.

Analysis of ^{1}H NMR spectroscopy data confirmed the chemical structures of the monomer, protected diblock copolymer, and cationic diblock copolymer (Figure 3.2). After ATRP, the appearance of mPEG-associated resonances at ≈ 3.6 ppm, the elimination of resonances from the methacrylate C=C bond between 5.7-6.3 ppm, and the broadened resonances that correlated to the repeat unit functional groups supported the successful synthesis of mPEG-*b*-P(Boc-APNBMA)$_n$. The disappearance of the resonances at 1.4 ppm following acid treatment indicated complete conversion of mPEG-*b*-P(Boc-APNBMA)$_n$ to mPEG-*b*-P(APNBMA·HCl)$_n$. Comparing the integrations of the terminal methoxy (3.4 ppm), PEG methylene (3.6 ppm), and Boc methylene (1.4 ppm) resonances enabled the calculation of the number-average

molecular weights (M_n)s for mPEG-*b*-P(Boc-APNBMA)$_n$, which were 8,400 g/mol and 14,600 g/mol for the two polymers depicted in Figure 3.1. Using a range of monomer to initiator ratios yielded a series of BCPs, and the two discussed herein illustrate our ability to tune and control molecular weight and dispersity. The integrations from the remaining resonances did not change following Boc deprotection, indicating that no cleavage of the pendant ester residues occurred during synthesis or workup. Table 3.1 summarizes the molecular weights obtained from ^{1}H NMR spectroscopy and the dispersities obtained from SEC for the two protected polymers and their deprotected counterparts.

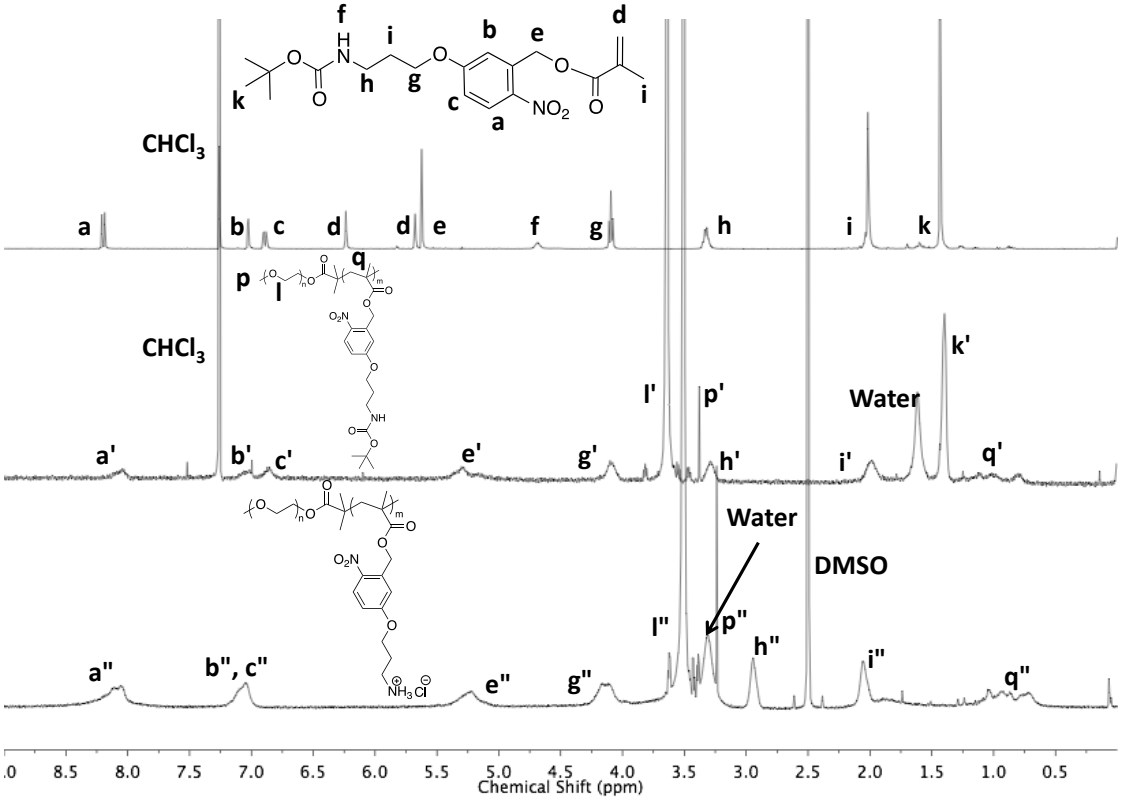

Figure 3.2 ^{1}H NMR spectroscopy of Boc-APNBMA monomer (top) in $CDCl_3$, mPEG-*b*-P(Boc-APNBMA)$_n$ (middle) in $CDCl_3$, and mPEG-*b*-P(APNBMA·HCl)$_n$ (bottom) in DMSO-*d*$_6$.

Table 3.1 Characterization of mPEG-b-P(Boc-APNBMA)n using 1H NMR spectroscopy and SEC.

	M_n[a] (g/mol)	$Đ$[b]
mPEG-Br	5,300	1.05
mPEG-*b*-P(Boc-APNBMA)$_{7.9}$	8,400	1.16
mPEG-*b*-P(APNBMA·HCl)$_{7.9}$	7,900	-
mPEG-*b*-P(Boc-APNBMA)$_{23.6}$	14,600	1.11
mPEG-*b*-P(APNBMA·HCl)$_{23.6}$	13,100	-

(a) Determined using ^{1}H NMR spectroscopy, and subsequently used to calculate the degree of polymerization for each polymer (7.9 and 23.6). (b) Determined using SEC.

It was expected that the lower molecular weight APNBMA block would provide adequate nucleic acid binding affinity based on the behavior of polymers with similar polycation valency.[11] Therefore, investigations of the DNA complexation at various N/P ratios in this chapter were conducted using the mPEG-*b*-P(APNBMA)$_{7.9}$, demonstration of DNA assembly with mPEG-*b*-P(APNBMA)$_{23.6}$ is shown in Appendix A. Two assays were employed to analyze polyplex formation in this work. The first assay, an ethidium bromide exclusion assay, probes the ability of cationic polymers to condense nucleic acids into polyplexes; ethidium bromide fluoresces upon intercalation between nucleic acid base pairs to reveal the location of the nucleic acids migrating down an electrophoresis gel. A tightly formed polyplex excludes the fluorescent dye, which reduces or eliminates fluorescence. The cationic mPEG-*b*-P(APNBMA·HCl)$_{7.9}$ complexed DNA into polyplexes at N/P $\geq$ 2, with tight polyplex formation occurring at N/P $\geq$ 5 as shown by the complete exclusion of ethidium bromide (Figure 3.3a). The second assay, a YOYO-1 iodide fluorescence quenching assay, quantitatively determined the level of fluorescence quenching induced by polyplex formation. YOYO-1 iodide labels DNA through intercalation binding interactions, and DNA packaging into polyplexes can position the bound YOYO-1 iodide fluorophores in sufficient proximity for self-quenching. DNA complexation

with mPEG-*b*-P(APNBMA·HCl)$_{7.9}$ produced decreased fluorescence as tighter polyplexes formed at higher N/P ratios (Figure 3.3b). A plateau in fluorescence occurred near N/P ≈ 5, supporting the ethidium bromide exclusion data in Figure 3.3a.

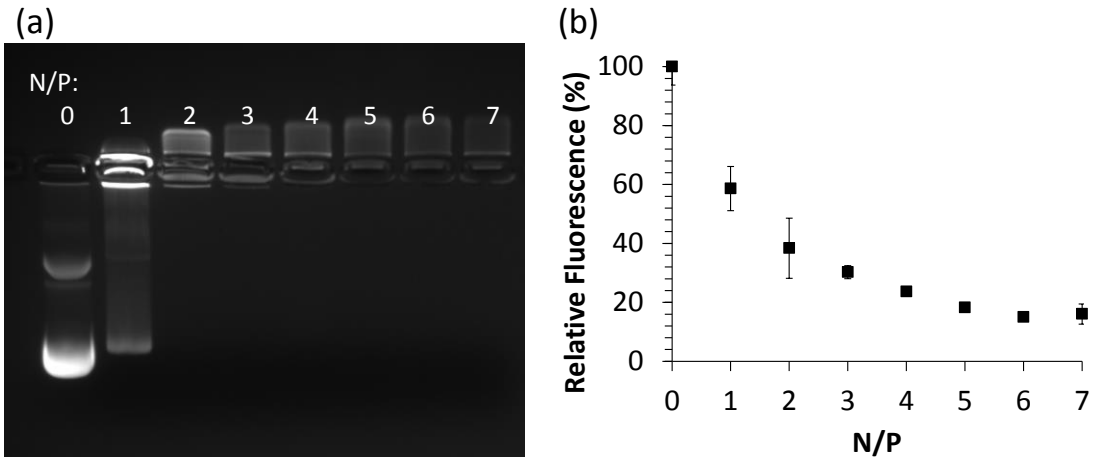

Figure 3.3 DNA condensation by mPEG-*b*-P(APNBMA·HCl)$_{7.9}$ monitored by (a) agarose gel electrophoresis and the(b) YOYO-1 fluorescence quenching assay.

These complementary results suggested tight polyplex formation at N/P ≥ 5. Thus, polyplexes were formed at N/P = 5 and further analyzed using DLS to investigate polyplex size and salt stability. DLS analyses identified hydrodynamic diameters (D_H, Figure 3.4a) of ≈150 nm for DNA/mPEG-*b*-P(APNBMA·HCl)$_{7.9}$ polyplexes at N/P > 3, suggesting potential compatibility with the size limits for endocytic internalization into cells.[38] Increasing the N/P ratio led to slight decreases in D_H, which corresponded to the tighter polyplexes as determined by fluorescence quenching.

Polyplex stability to high salt and/or serum-containing environments is an additional key criterion for predicting the *in vivo* performance of gene delivery vehicles. High salt environments can induce polyplex aggregation and precipitation, and enzymes in serum containing environments can initiate degradation of loosely bound nucleic acids.[39] The DNA/mPEG-*b*-P(APNBMA·HCl)$_{7.9}$ polyplexes exhibited no change in size following incubation in mild buffered solution (HEPES buffer), Opti-MEM or water over a period of 60 min at 23 °C. Incubation in cell-culture grade PBS solutions containing physiological saline (150 mM salt) only modestly increased polyplex D_H by ≈ 40 nm (1.4-fold), which suggested improved polyplex stability in high salt media relative to other nucleic acid carriers in the literature.[40] In comparison, Johnson *et al*. reported an increase of approximately 1 μm (10-fold) for the D_H of DNA/polyethylenimine and DNA/poly(L-lysine) polyplexes over 15 min in PBS; these two cationic polymers are common commercially available carriers used in nucleic acid delivery.[40] In the present work, the nearly constant polyplex sizes suggested greater stability in the high salt conditions commonly encountered *in vitro* and *in vivo* (Figure 3.4b), and indicated a potential for extension to cell-based applications.

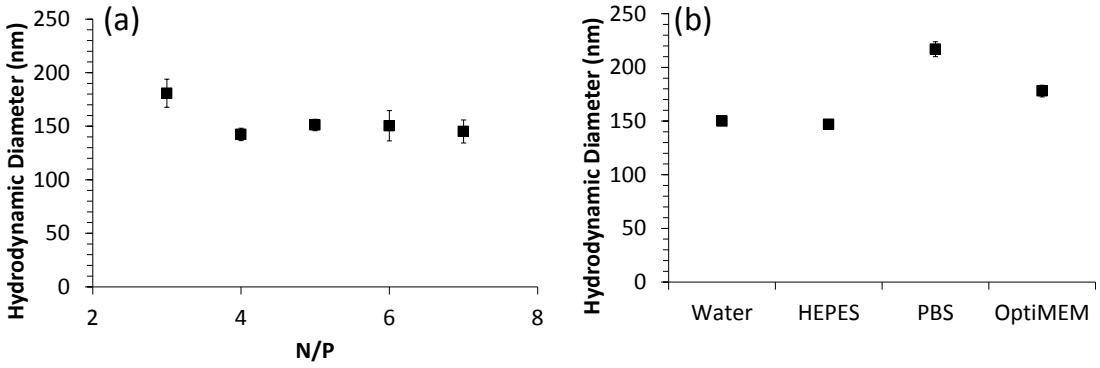

Figure 3.4 Characterization of the DNA/mPEG-*b*-P(APNBMA·HCl)$_{7.9}$ polyplex size and stability. (a) Hydrodynamic diameters of polyplexes formed at various N/P ratios in HEPES buffer. (b) Hydrodynamic diameters of polyplexes at N/P = 5 after a 60 min incubation in various salt solutions. The data in (a) and (b) were collected using DLS.

As mPEG-b-P(APNBMA•HCl)$_{7.9}$ demonstrated potential as a vehicle for nucleic acid condensation and packaging, UV irradiation studies were preformed to assess the polymer's efficacy for light-triggered nucleic acid release. mPEG-*b*-P(APNBMA•HCl)$_{7.9}$ was irradiated with 365 nm light at an intensity of 200 W/m^2 and the relative characteristic absorbance of the *o*-NB ester at 316 nm was monitored to determine the extent of photocleavage. These UV irradiation conditions have been previously used in cellular applications of photocleavable polymers with minimal toxicity.[41] The polymer absorption spectra displayed dramatic decreases up to 20 min, small changes from 20 min to 40 min, and no change in the characteristic absorbance between 40 min and 60 min (Figure 3.5a). The ability to tune the photocleavage reaction through variations in irradiation time, polymer properties, and polyplex formation introduced an additional attractive feature to this platform. The decreased absorbance as a function of irradiation time followed an exponential decay, and fitting the decay enabled the determination of an exponential decay constant (τ = 340 s for *n*

= 7.9 and τ = 220 s for n = 23.6) (Appendix A). The exponential decay constant for the DNA/mPEG-*b*-P(APNBMA·HCl)$_{7.9}$ polyplexes was 160 s. These calculated decay constants are consistent with the experimentally observed data, with nearly complete conversion occurring at approximately 3τ in all cases. In principle there is no reason to expect that the longer polymer chain should have a significantly lower decay constant than the shorter chain length, however further experiments would be needed to identify a dependence between polymer chain length and photocleavage decay constants.

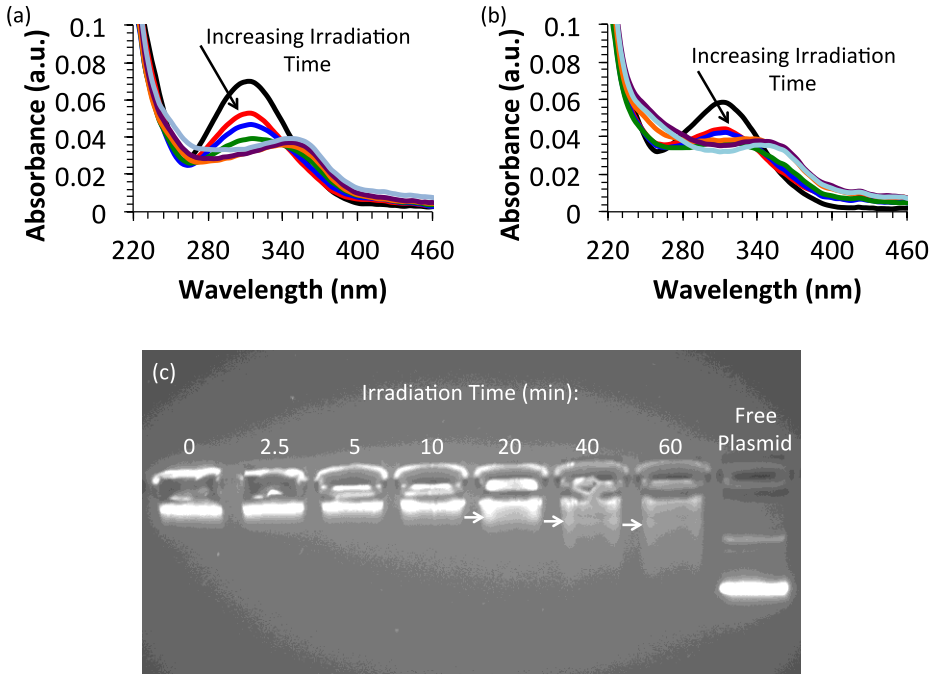

Figure 3.5 UV-visible spectroscopy of (a) mPEG-*b*-P(APNBMA·HCl)$_{7.9}$ following exposure to 200 W/m^2 for 0 (black), 2.5 (red), 5 (blue), 10 (green), 20 (orange), 40 (purple), and 60 (teal) min; and (b) DNA/mPEG-*b*-P(APNBMA·HCl)$_{7.9}$ polyplexes following exposure to 200 W m-2 for 0 (black), 2.5 (red), 5 (blue), 10 (green), 20 (orange), 40 (purple), and 60 (teal) min. (c) Gel electrophoresis of DNA/mPEG-*b*-P(APNBMA·HCl)$_{7.9}$ polyplexes following exposure to UV at varying irradiation times.

Subsequent irradiation of DNA/mPEG-*b*-P(APNBMA·HCl)$_{7.9}$polyplexes using the same irradiation conditions yielded similar UV-Vis absorbance spectra over time, and behavior similar to the polymer absorbance spectra was seen in the polyplex absorption spectra (Figure 3.5b). The UV-Vis absorption findings suggested complete cleavage of the *o*-NB ester in both the polymer and polyplex, and negligible screening of UV light from the DNA. Visualization of polyplex destabilization and unpackaging using gel electrophoresis confirmed that longer irradiation times reduced electrostatic interactions (Figure 3.5c). The DNA migrated through the gel at UV irradiation times $\geq$ 20 min, which suggested polyplex destabilization and DNA release. The reduced migration in the gel in comparison to free DNA indicated that the photocleavage reaction products either inhibited the mobility of the DNA through direct interactions or changed the gel characteristics such that migration was limited. Cowman and coworkers reported several experimental parameters that influenced the mobility of hyaluronan in agarose gels, including buffer composition, buffer salt concentration, agarose percentage (i.e. gel pore size), etc.[42] One possible explanation is that the cleaved fragments continue to interact with the DNA and screen the electric field, which would increase the apparent molecular weight and distribution. Regardless of the reduced DNA mobility, the supposition of photo-triggered polyplex disassembly remained sound based on the clear shifts in DNA migration behavior following light irradiation.

3.4 Conclusions

In summary, this work presents the synthesis of a new photo-responsive, methacrylate-based monomer using controlled polymerization techniques to generate a pair of block copolymers with tunable block lengths and narrow molecular weight

distributions. The polymer with the shorter cationic block length, mPEG-*b*-P(APNBMA·HCl)$_{7.9}$, effectively complexed DNA into salt-stable polyplexes with sizes appropriate for cellular internalization. Furthermore, the development of block copolymers with varying chain lengths introduces the possibility for tunable association with other therapeutic nucleic acids such as messenger RNA (mRNA) – with similar molecular weights as the plasmids investigated in this chapter – or short interfering RNA (siRNA) – with a significantly smaller molecular weight. Irradiation with UV light cleaved the o-NB ester and facilitated DNA release. Considering the favorable complexation and release of DNA, investigations into the spatiotemporal efficacy and control of these photocleavable block copolymers as nucleic acid delivery vehicles and the influence of cationic block length on nucleic acid encapsulation and release are discussed in the following chapter. These promising findings suggested that the mPEG-*b*-P(APNBMA·HCl)$_n$ design could address a key paradox in gene carrier design through the simultaneous incorporation of ammonium cations for strong binding and an externally-triggered mechanism to allow defined release.

REFERENCES

1. Burke, P. A.; Pun, S. H.; Reineke, T. M., Advancing Polymeric Delivery Systems Amidst a Nucleic Acid Therapy Renaissance. *ACS Macro Letters* **2013,** 2, (10), 928-934.

2. Guo, X.; Huang, L., Recent advances in nonviral vectors for gene delivery. *Acc Chem Res* **2012,** 45, (7), 971-9.

3. Namgung, R.; Kim, J.; Singha, K.; Kim, C. H.; Kim, W. J., Synergistic effect of low cytotoxic linear polyethylenimine and multiarm polyethylene glycol: study of physicochemical properties and in vitro gene transfection. *Mol Pharm* **2009,** 6, (6), 1826-35.

4. Pack, D. W.; Hoffman, A. S.; Pun, S.; Stayton, P. S., Design and development of polymers for gene delivery. *Nat Rev Drug Discov* **2005,** 4, (7), 581-93.

5. Burke, R. S.; Pun, S. H., Extracellular Barriers to in Vivo PEI and PEGylated PEI Polyplex-Mediated Gene Delivery to the Liver. *Bioconjugate Chemistry* **2008,** 19, (3), 693-704.

6. Merkel, O. M.; Librizzi, D.; Pfestroff, A.; Schurrat, T.; Buyens, K.; Sanders, N. N.; De Smedt, S. C.; Behe, M.; Kissel, T., Stability of siRNA polyplexes from poly(ethylenimine) and poly(ethylenimine)-g-poly(ethylene glycol) under in vivo conditions: effects on pharmacokinetics and biodistribution measured by Fluorescence Fluctuation Spectroscopy and Single Photon Emission Computed Tomography (SPECT) imaging. *J Control Release* **2009,** 138, (2), 148-59.

7. Abdelhady, H. G.; Allen, S.; Davies, M. C.; Roberts, C. J.; Tendler, S. J.; Williams, P. M., Direct real-time molecular scale visualisation of the degradation of condensed DNA complexes exposed to DNase I. *Nucleic Acids Res* **2003,** 31, (14), 4001-5.

8. Layman, J. M.; Ramirez, S. M.; Green, M. D.; Long, T. E., Influence of polycation molecular weight on poly(2-dimethylaminoethyl methacrylate)-mediated DNA delivery in vitro. *Biomacromolecules* **2009,** 10, (5), 1244-52.

9. Kizzire, K.; Khargharia, S.; Rice, K. G., High-affinity PEGylated polyacridine peptide polyplexes mediate potent in vivo gene expression. *Gene Ther* **2013,** 20, (4), 407-16.

10. Green, J. J.; Langer, R.; Anderson, D. G., A combinatorial polymer library approach yields insight into nonviral gene delivery. *Acc Chem Res* **2008,** 41, (6), 749-59.

11. Schaffer, D. V.; Fidelman, N. A.; Dan, N.; Lauffenburger, D. A., Vector unpacking as a potential barrier for receptor-mediated polyplex gene delivery. *Biotechnol Bioeng* **2000,** 67, (5), 598-606.

12. Choosakoonkriang, S.; Lobo, B. A.; Koe, G. S.; Koe, J. G.; Middaugh, C. R., Biophysical characterization of PEI/DNA complexes. *J Pharm Sci* **2003,** 92, (8), 1710-22.

13. Erbacher, P.; Roche, A. C.; Monsigny, M.; Midoux, P., The reduction of the positive charges of polylysine by partial gluconoylation increases the transfection efficiency of polylysine/DNA complexes. *Biochim Biophys Acta* **1997,** 1324, (1), 27-36.

14. Florea, B. I.; Meaney, C.; Junginger, H. E.; Borchard, G., Transfection efficiency and toxicity of polyethylenimine in differentiated Calu-3 and nondifferentiated COS-1 cell cultures. *AAPS PharmSci* **2002,** 4, (3), E12.

15. Hwang, S. J.; Bellocq, N. C.; Davis, M. E., Effects of structure of beta-cyclodextrin-containing polymers on gene delivery. *Bioconjug Chem* **2001,** 12, (2), 280-90.

16. Reineke, T. M.; Davis, M. E., Structural effects of carbohydrate-containing polycations on gene delivery. 1. Carbohydrate size and its distance from charge centers. *Bioconjug Chem* **2003,** 14, (1), 247-54.

17. Kelley, E. G.; Albert, J. N.; Sullivan, M. O.; Epps, T. H., 3rd, Stimuli-responsive copolymer solution and surface assemblies for biomedical applications. *Chem Soc Rev* **2013,** 42, (17), 7057-71.

18. Abbott, N. L.; Jewell, C. M.; Hays, M. E.; Kondo, Y.; Lynn, D. M., Ferrocene-containing cationic lipids: influence of redox state on cell transfection. *J Am Chem Soc* **2005,** 127, (33), 11576-7.

19. Aytar, B. S.; Muller, J. P.; Golan, S.; Hata, S.; Takahashi, H.; Kondo, Y.; Talmon, Y.; Abbott, N. L.; Lynn, D. M., Addition of ascorbic acid to the extracellular

environment activates lipoplexes of a ferrocenyl lipid and promotes cell transfection. *J Control Release* **2012,** 157, (2), 249-59.

20. Aytar, B. S.; Muller, J. P.; Kondo, Y.; Abbott, N. L.; Lynn, D. M., Spatial control of cell transfection using soluble or solid-phase redox agents and a redox-active ferrocenyl lipid. *ACS Appl Mater Interfaces* **2013,** 5, (17), 8283-8.

21. Zhao, H.; Sterner, E. S.; Coughlin, E. B.; Theato, P., o-Nitrobenzyl Alcohol Derivatives: Opportunities in Polymer and Materials Science. *Macromolecules* **2012,** 45, (4), 1723-1736.

22. Il'ichev, Y. V.; Schworer, M. A.; Wirz, J., Photochemical reaction mechanisms of 2-nitrobenzyl compounds: methyl ethers and caged ATP. *J Am Chem Soc* **2004,** 126, (14), 4581-95.

23. Zhao, Y., Light-Responsive Block Copolymer Micelles. *Macromolecules* **2012,** 45, (9), 3647-3657.

24. Thomas, S. W., New Applications of Photolabile Nitrobenzyl Groups in Polymers. *Macromolecular Chemistry and Physics* **2012,** 213, (23), 2443--2449.

25. Kim, M. S.; Diamond, S. L., Photocleavage of o-nitrobenzyl ether derivatives for rapid biomedical release applications. *Bioorg Med Chem Lett* **2006,** 16, (15), 4007-10.

26. Kloxin, A. M.; Kasko, A. M.; Salinas, C. N.; Anseth, K. S., Photodegradable hydrogels for dynamic tuning of physical and chemical properties. *Science* **2009,** 324, (5923), 59-63.

27. Jiang, J.; Tong, X.; Morris, D.; Zhao, Y., Toward Photocontrolled Release Using Light-Dissociable Block Copolymer Micelles. *Macromolecules* **2006,** 39, (13), 4633-4640.

28. Liu, G.; Dong, C. M., Photoresponsive poly(S-(o-nitrobenzyl)-L-cysteine)-b-PEO from a L-cysteine N-carboxyanhydride monomer: synthesis, self-assembly, and phototriggered drug release. *Biomacromolecules* **2012,** 13, (5), 1573-83.

29. Kumar, S.; Allard, J.; Morris, D.; Dory, Y. L.; Lepage, M.; Zhao, Y., Near-infrared light sensitive polypeptide block copolymer micelles for drug delivery. *J Mater Chem* **2012,** 22, 7252-7257.

30. Johnson, J. A.; Lu, Y. Y.; Burts, A. O.; Lim, Y. H.; Finn, M. G.; Koberstein, J. T.; Turro, N. J.; Tirrell, D. A.; Grubbs, R. H., Core-clickable PEG-branch-azide

bivalent-bottle-brush polymers by ROMP: grafting-through and clicking-to. *J Am Chem Soc* **2011,** 133, (3), 559-66.

31. Kostiainen, M. A.; Smith, D. K.; Ikkala, O., Optically Triggered Release of DNA from Multivalent Dendrons by Degrading and Charge-Switching Multivalency. *Angewandte Chemie* **2007,** 119, (40), 7744--7748.

32. Han, G.; You, C. C.; Kim, B. J.; Turingan, R. S.; Forbes, N. S.; Martin, C. T.; Rotello, V. M., Light-regulated release of DNA and its delivery to nuclei by means of photolabile gold nanoparticles. *Angew Chem Int Ed Engl* **2006,** 45, (19), 3165-9.

33. Yin, L.; Tang, H.; Kim, K. H.; Zheng, N.; Song, Z.; Gabrielson, N. P.; Lu, H.; Cheng, J., Light-responsive helical polypeptides capable of reducing toxicity and unpacking DNA: toward nonviral gene delivery. *Angew Chem Int Ed Engl* **2013,** 52, (35), 9182-6.

34. Newkome, G. R.; Shreiner, C. D., Poly(amidoamine), polypropylenimine, and related dendrimers and dendrons possessing different 1→2 branching motifs: An overview of the divergent procedures. *Polymer* **2008,** 49, (1), 1 - 173.

35. Andersson, L.; Blomberg, L.; Flegel, M.; Lepsa, L.; Nilsson, B.; Verlander, M., Large-scale synthesis of peptides. *Biopolymers* **2000,** 55, (3), 227-50.

36. Alkilany, A. M.; Murphy, C. J., Toxicity and cellular uptake of gold nanoparticles: what we have learned so far? *J Nanopart Res* **2010,** 12, (7), 2313-2333.

37. Dimitriou, M. D.; Zhou, Z.; Yoo, H. S.; Killops, K. L.; Finlay, J. A.; Cone, G.; Sundaram, H. S.; Lynd, N. A.; Barteau, K. P.; Campos, L. M.; Fischer, D. A.; Callow, M. E.; Callow, J. A.; Ober, C. K.; Hawker, C. J.; Kramer, E. J., A general approach to controlling the surface composition of poly(ethylene oxide)-based block copolymers for antifouling coatings. *Langmuir* **2011,** 27, (22), 13762-72.

38. Ogris, M.; Steinlein, P.; Carotta, S.; Brunner, S.; Wagner, E., DNA/polyethylenimine transfection particles: influence of ligands, polymer size, and PEGylation on internalization and gene expression. *AAPS PharmSci* **2001,** 3, (3), E21.

39. Millili, P. G.; Yin, D. H.; Fan, H.; Naik, U. P.; Sullivan, M. O., Formulation of a Peptide Nucleic Acid Based Nucleic Acid Delivery Construct. *Bioconjug Chem* **2010**.

40. Johnson, R. N.; Chu, D. S.; Shi, J.; Schellinger, J. G.; Carlson, P. M.; Pun, S. H., HPMA-oligolysine copolymers for gene delivery: optimization of peptide length and polymer molecular weight. *J Control Release* **2011,** 155, (2), 303-11.

41. Lee, H.; Kim, Y.; Schweickert, P. G.; Konieczny, S. F.; Won, Y. Y., A photo-degradable gene delivery system for enhanced nuclear gene transcription. *Biomaterials* **2014,** 35, (3), 1040-9.

42. Lee, H. G.; Cowman, M. K., An agarose gel electrophoretic method for analysis of hyaluronan molecular weight distribution. *Anal Biochem* **1994,** 219, (2), 278-87.

Chapter 4

LIGHT-TRIGGERED UNPACKAGING OF SIRNA POLYPLEXES FOR IMPROVED GENE SILENCING

An important challenge in gene delivery is the development of gene transfer structures that remain stably associated in the extracellular space, yet efficiently disassemble to release nucleic acid in the cytosol. This controllable release characteristic is particularly important for the delivery of short interfering RNA (siRNA), which has increased susceptibility to enzymatic degradation if released prematurely, yet lacks silencing activity if release is delayed. Chapter 3 introduced this photocleavable copolymer platform with tailorable molecular weights/ binding capacity and demonstrated the ability to create stable extracellular assemblies, promote light-induced polymer cleavage, charge reversal and subsequently weakened DNA binding. Building on the promising characteristics of this photocleavable platform, the work presented in this chapter explored the implementation of PEG-*b*-P(APNBMA)$_n$ block copolymers as controllable, stealth carriers for siRNA delivery and was aimed at defining a copolymer design and polyplex assembly conditions to promote the formation of nuclease inaccessible structures with the capacity for light-triggered release. Due to its demonstrated weaker electrostatic binding than DNA, this shorter and more rigid nucleic acid was hypothesized to allow for strong enough binding to promote tight association and stability, but weak enough binding to promote triggered siRNA release.[1] These studies aimed to controllably release siRNA in the intracellular compartment to enhance its gene silencing efficacy. The

preparation of these structures indicated tight association with siRNA and favorable cytoplasmic distribution following transfection. Furthermore, *in vitro* UV treatment facilitated ~70% reduction in protein expression compared to untreated cells, thus highlighting utility of the light-trigger in promoting siRNA transfer.

4.1 Introduction

RNA interference (RNAi) has emerged as a promising gene delivery strategy due to its ability to mediate sequence specific post-transcriptional gene silencing.[2-6] However, the direct application of siRNAs has been limited by their increased susceptibility to enzymatic hydrolysis, rapid clearance from systemic circulation, limited cellular uptake, and inability to efficiently traffic to the cytoplasm of the cell.[7, 8] Significant strides have been made to improve the nuclease stability of siRNAs including 2'-fluoro and 4'-thio chemical modifications.[5] However, efficient delivery still necessitates a packaging strategy to protect against enzymatic degradation and to overcome the anionic plasma membrane. Unfortunately the key delivery requirements of stability during circulation and efficient cytoplasmic release place contradictory demands on siRNA delivery vehicles. Specifically, carriers should provide (1) stable binding during circulation and transport to ensure extracellular stability, and (2) the capacity for intracellular unbinding to provide efficient polyplex disassembly and cytoplasmic siRNA release.

In recent years a number of strategies have been employed to improve the extracellular stability of siRNA complexes. However, the rigid structure of siRNA has made it much more difficult to package than DNA molecules and has also limited clinical translation of siRNA structures.[9] For example, in a well-known study, Davis and coworkers highlighted the importance of polyplex stability in the development of

siRNA/cyclodextrin-containing polymer (CDP) complexes for treatment of Ewing's sarcoma.[10] When introduced into systemic circulation, the siRNA/CDP polyplexes assembled at the glomerular basement membrane (GBM). Furthermore, the heterogeneity observed in confocal microscopy suggested a loss in nucleic acid content due to interactions with heparin sulfate on the GBM. Several efforts have focused on improving the stability of siRNA encapsulation including structural modifications to the cargo (through multimerization) or developing modified polymers (with increases in molecular, charge density, or by the incorporation of hydrophobic residues) to facilitate more stable binding. For example, Park and colleagues developed methods to adjust the binding association of the cationic polymer and siRNA. Specifically, with the development of self-crosslinked siRNA multimers, they were able to form more stable and compact polyplex assemblies using linear polyethylenimine (LPEI) as a carrier because of substantially increased nucleic acid molecular weight and the presence of flexible chemical linkers in the backbone.[11-13] Various publications have explored the preparation of siRNA polyplexes through the complementary approach of modifying the polymer charge density. In one such example Liu and coworkers showed efficient siRNA complexation with the use of high molecular weight chitosan in contrast to low molecular weight chitosan, which was not able to condense siRNA to form discrete NPs because of the short chain length of the polymer.[14] While some these approaches to improve affinity have proven beneficial for reducing nuclease degradation, the enhanced binding stability has the drawback of reducing intracellular release and siRNA activity.[15, 16] Specifically, in the previously mentioned work of Park and coworkers they observed low levels of gene silencing due to their tight polyplex association, despite a

demonstrated efficiency in siRNA packaging and high levels of cellular uptake. Similarly, in the preparation of linear PEI (LPEI) polyplexes for siRNA delivery, Shim and coworkers highlighted the need for mechanisms to control the unpackaging of their condensed polyplex structures, which demonstrated limited siRNA unpackaging and low gene silencing efficiency despite efficient cellular uptake and cytoplasmic localization of these structures.[15] As such, a delivery strategy that balances the requirements of strong binding stability during circulation and reduced binding stability in the cytosol is particularly attractive for improving siRNA delivery. Indeed, delivery approaches with triggered release strategies provide a method to address the requirement of strong binding and efficient release. Additionally, a triggered release strategy employing an external trigger would be particularly attractive because it would introduce the ability to provide user-defined spatiotemporal control of release.

Chapter 3 reported on a UV-cleavable polymer platform with a tunable nucleic acid binding region that combines polycationic and photosensitive units to enable triggered release of polycationic groups. By employing the tunable binding capacity of this polymer platform in the delivery of siRNA – with demonstrated weaker electrostatic association that DNA carriers,[1] this chapter identifies strong siRNA association and stability of these photocleavable structures and efficient siRNA release and gene silencing in response to a light-trigger.

4.2 Materials and Methods

4.2.1 Materials

Photocleavable mPEG-*b*-P(APNBMA)$_n$ polymers were synthesized via atom transfer radical polymerization as previously described in Chapter 3. ON-TARGETplus siRNA [anti-glyceraldehyde 3-phosphate dehydrogenase (anti-GAPDH)] as well as a non-targeting siRNA sequence were purchased from ThermoFisher Scientific (Pittsburgh, PA). A bicinchoninic acid (BCA) protein assay kit and bovine serum albumin (BSA) were purchased from Pierce (Rockford, IL). Dulbecco's modification of Eagle's medium (DMEM) and phosphate buffered saline (PBS) solutions were obtained from Corning Life Sciences - Mediatech Inc. (Manassas, VA). The ECL Plus Western Blotting Detection Kit was obtained from GE Healthcare Bioscience, Buckinghamshire, UK. Antibodies for Western blotting were obtained from AbCam (Cambridge, CA). Other Western blotting reagents and inhibitors were obtained from Pierce Biotechnology (Rockford, IL, USA). All other chemicals and reagents were purchased from Sigma (St. Louis, MO).

4.2.2 Polyplex Formulation and Characterization

Polyplexes were formed using mixtures of the ON-TARGETplus siRNAs and PEG-*b*-P(APNBMA•HCl)$_n$ polymers. Prior to complexation, siRNA solutions were prepared at 40 μg/mL in 20 mM 4-(2-hydroxyethyl)-1-piperazineethanesulfonic acid (HEPES) buffer, pH = 6.0. Polyplexes were formed by dropwise addition of polymer solution to an equal volume of siRNA while vortexing. Polymer solutions contained polymer over the range of concentrations appropriate to form polyplexes at the desired polymer nitrogen to siRNA phosphate (N/P) ratios. Polyplexes were incubated at room temperature for 10 minutes prior to further analyses.

Polyplex formation was analyzed using agarose gel electrophoresis. For electrophoresis, 25 μL of polyplex solution was added to 5 μL of loading solution (3/7 (v/v) glycerol/water). Then, the polyplex solution was added to the wells of a 4.0% agarose gel containing 0.5 μg/mL of ethidium bromide. Gels were run at 100 V for 1 h and subsequently imaged using a Biorad Gel Doc XR (Hercules, CA).

For the nuclease stability assays, 20 μL of each polyplex solution was incubated with 10 μL mouse serum for 4 h at 37°C. The nuclease activity was terminated by adding 8 μL of a buffer comprised of 0.16 M EDTA, 0.67 M NaOH, and 0.16 M NaCl, and placing the terminating solutions on ice for 10 min. The polyplex solutions were subsequently analyzed by gel electrophoresis as previously described.

A CNI Optoelectronics Co., Ltd. 532 nm, 427.6 mW laser, coupled with a Brookhaven Instruments Corporation BI-200SM goniometer equipped with an inline 532 nm filter from Intor, Inc. was used for DLS analyses. The intensity auto-correlation function was recorded at 90° and analyzed using a quadratic cumulant fit. All light scattering experiments were performed at 25 °C.

4.2.3 Photocleavage and siRNA Release

Photocleavage studies were performed using 300 μL of siRNA polyplex solution or solutions with polymer alone. Solutions were loaded into a chamber prepared by sealing two glass slides with a rubber gasket. The chamber was irradiated with 365 nm light at 200 W/m^2 (Omnicure S2000, Lumen Dynamics, Mississaugua, Ontario, Canada) for 0 min, 5 min, 10 min, 20 min, 40 min, and 60 min. Samples were removed from the chamber and collected for absorbance measurements (Thermo Scientific, NanoDrop 1000 Spectrophotometer) and agarose gel electrophoresis.

4.2.4 Cell Culture and Synchronization

The mouse embryonic fibroblast (NIH/3T3) cell line used in these studies was obtained from American Type Culture Collection (ATCC, Manassas, VA). The cells were cultured according to ATCC protocols at 37°C and 5% CO_2 in Dulbecco's modified Eagle's medium (DMEM) supplemented with 10% fetal bovine serum (FBS) and 1% penicillin-streptomycin; all cell culture chemicals were purchased from Fisher (Pittsburgh, PA).

Cells were plated at a density of 2,000 cells/cm^2 and incubated overnight. To synchronize the cells, the medium was removed the following day and replaced with fresh DMEM containing 0.75% FBS and antibiotics, according to standard procedures.[17] The cells were grown for an additional 48 h, and then the cells were released 12 h prior to transfection by replacing the low serum medium with fully supplemented growth medium.

4.2.5 Cell Transfection

For all transfections with PEG-*b*-P(APNBMA·HCl)$_n$ polymers, cells were seeded into 6-well plates at a density of 15,000 cells/cm^2. Growth medium was replaced with Opti-MEM and polyplex solutions containing 3 pmol siRNA/cm^2 were added dropwise to the cells 24 h post-seeding. After a 3 h incubation with the transfection reagents, the cells were washed once with PBS and complete growth medium was added to each well.

For transfections with UV treatment, cells were allowed to recover for 30 min in complete growth medium following the 3 h transfection. Subsequently, the medium was replaced with Opti-MEM and the samples were irradiated for 20 min at 365 nm (I_0 = 200 W/m^2). Cells were subsequently washed once with PBS and supplemented

with complete growth medium for the remainder of the culture period. Lipofectamine^{TM} RNAiMax- mediated transfections were performed according to the manufacturer's protocol.

4.2.6 Immunocytochemical (ICC) Analysis and Cellular Uptake of Polyplexes

Cells were synchronized, incubated for an additional 12 h following synchronization, and transfected using polyplex suspensions containing 3 pmol siRNA/cm^2 labeled with 1.5 eq YOYO-1 Iodide. Transfections were halted after 1, 2, or 3 hours of polyplex exposure and the cells were rinsed with PBS, washed with 10 μg/mL heparin, and washed again with PBS prior to further treatment.

To prepare the cell samples for ICC analyses, the cells were fixed with 4% paraformaldehyde in PBS for 15 min. Cells were subsequently permeabilized with 0.2% Tween-20 in PBS (PBSt) and blocked with 3% BSA in 0.2% PBSt. Cells were stained with 4 μg/mL Hoechst dye solution and stored at 4°C prior to imaging. Flow cytometry was used for quantification of cellular uptake. Cells were collected for analysis by standard trypsin-mediated collection protocols and resuspended in PBS, filtered through a 35 μm nylon mesh to remove aggregates, and stored at 4°C until analysis. Polyplex uptake efficiency was calculated as the percentage of cells containing polyplexes. Specifically, scatter plots from untransfected cells were gated for autofluorescence and the percentage of cells with fluorescence levels above the autofluroescence threshold was determined by comparison with the gate position. A total of 10,000 cells were analyzed for each sample.

4.2.7 Western Blot Analysis

Gene silencing by siRNA/PEG-*b*-P(APNBMA)$_{23.6}$ polyplexes was analyzed by standard Western blotting analyses. Forty-eight hours after the start of transfection, protein was extracted from NIH/3T3 cells by incubation of the cells with a lysis solution composed of 0.5% Triton X-100, 0.5% sodium deoxycholate, 150 mM NaCl, 5 mM Tris-HCl (pH 7.4), 5 mM ethylene diamine tetraacetic acid (EDTA), and 1×Halt Protease and Phosphatase Inhibitor cocktail. For each sample, total protein content was measured using a BCA Protein Assay Reagent Kit. Equal amounts of cellular protein from each cell extract were subjected to 4-20% sodium dodecyl sulfate polyacrylamide gel electrophoresis (SDS-PAGE), and transferred onto a polyvinylidene fluoride (PVDF) membrane. The membrane was blocked in 5% BSA in Tris-HCl buffered saline containing 0.1% Tween 20 (TBSt, pH 7.4) for 1 h at room temperature and then incubated with an anti-GAPDH rabbit monoclonal IgG primary antibody (in 1× TBSt) overnight at 4°C. Subsequently, the membrane was incubated with a solution of goat anti-rabbit polyclonal IgG antibody conjugated to horseradish peroxidase (HRP) in 1× TBSt buffer for 1 h at room temperature. Target proteins were visualized with the ECL Plus chemiluminescent substrate. The membrane was subsequently stripped using Restore Western Blot stripping buffer and reprobed for actin using an anti-actin rabbit polyclonal IgG and the HRP conjugated secondary antibody.

4.2.8 Serum and RNase 1 Stability of siRNA/PEG-*b*-P(APNBMA)$_{23.6}$ Polyplexes

Unbound siRNA (1 μg) and PEG-*b*-P(APNBMA)$_{23.6}$ polyplexes with 1 μg of siRNA were incubated in 25 μL of whole mouse serum for 2 h. The nuclease activity was terminated by adding 20 μL of a buffer comprised of 0.16 M EDTA, 0.67 M

NaOH, and 0.16 M NaCl, and placing the terminating solutions on ice for 10 min. The extent of polyplex disassembly was subsequently analyzed by gel electrophoresis. To determine the ability to resist nuclease-mediated degradation, polyplexes were incubated with 0.5 ng/μL solutions of RNase 1 for 10 minutes at 37°C. siRNA was subsequently displaced from the polyplexes using 1 μL of a 10 mg/mL solution of sodium dodecyl sulfate (SDS) in ddH_2O. The extent of siRNA degradation was subsequently analyzed by gel electrophoresis

4.2.9 Cell Toxicity

Polymer toxicity was evaluated in NIH/3T3 cells using the Alamar Blue (AB) assay according to the manufacturer's protocols. Polymer solutions were prepared in Opti-MEM at the specified concentrations. The cells were rinsed once with PBS and incubated with polymer solutions for 3 h at 37 °C, 5% CO_2. Subsequently, the cells were rinsed with PBS and the medium was replaced with complete growth medium. After 48 h, AB was added directly into culture medium to a final concentration of 10% (v/v) for viability/proliferation measurements, and the AB-containing solutions were incubated for an additional 18 h at 37 °C, 5% CO_2. AB fluorescence was measured using a GloMax-multi detection system plate reader (Promega, Madison, WI). To determine the baseline fluorescence, AB was added to media without cells.

4.3 Results and Discussion

4.3.1 Characterization of siRNA/PEG-*b*-P(APNBMA)$_n$ Polyplexes

4.3.1.1 siRNA Condensation/Ethidium Bromide Exclusion

Efficient siRNA condensation typically requires higher N/P ratios and/or higher molecular weight polycations as compared with DNA condensation.[1] Hence, we sought to test the siRNA binding capacity of PEG-*b*-P(APNBMA)$_n$ block copolymers are a function of molecular weight/cationic chain length. PEG-*b*-P(APNBMA)$_n$ block copolymers were added to siRNA at various charge ratios, as depicted in Figure 4.1, and the resulting solutions were analyzed via gel electrophoresis. As seen in Figure 4.1a, PEG-*b*-P(APNBMA)$_{7.9}$ was unable to efficiently condense siRNA based on the minimal changes that were observed in ethidium bromide fluorescence and the migration of siRNA for all tested N/P ratios. While there was an initial reduction in ethidium bromide fluorescence as PEG-*b*-P(APNBMA)$_{7.9}$ was added to siRNA, further polymer addition above an N/P ratio of 40 did not induce additional complex formation. Several research groups have indicated similar reductions in siRNA complexation efficiency for carriers demonstrating high affinity for DNA.[9, 14] In fact, poly-L-lysine (PLL) – a polycation routinely used for DNA delivery – does not form complexes with short oligonucleotides. As demonstrated in Figure 4.1b, preparation of polyplexes using PEG-*b*-P(APNBMA)$_{23.6}$ provided sufficient cationic charge for stable binding interactions and complexation with siRNA. Upon addition of PEG-*b*-P(APNBMA)$_{23.6}$ at N/P 0.5 there was an initial ~83% reduction in ethidium bromide fluorescence. Further addition of the polymer resulted in a lack of migration (N/P $\geq$ 1) but indicated low levels of fluorescence in the wells. Above an N/P of 4, the free

siRNA band and fluorescence in the wells of the gel disappeared almost completely, suggesting that PEG-*b*-P(APNBMA)$_{23.6}$ condensed siRNA with high efficiency. The high affinity PEG-*b*-P(APNBMA)$_{23.6}$ for siRNA suggests the presence of additional (non-electrostatic) interactions during association. As demonstrated in a number of similar cationic systems, siRNA is often difficult to package with linear cationic polymers. For example, as seen in work by Byrne and coworkers, the linear architecture of PLL hinders complexation of siRNA into compact structures as demonstrated by ethidium bromide accessibility and large aggregate structures revealed in DLS.[18] Similar to studies of Rice and coworkers demonstrating enhanced polyplex association through the incorporation of hydrophobic acridine groups into polycations, a possible explanation for the strong association of siRNA/ PEG-*b*-P(APNBMA)$_{23.6}$ is the combined effect of electrostatic interactions and intercalation of the hydrophobic acridine groups.[19]

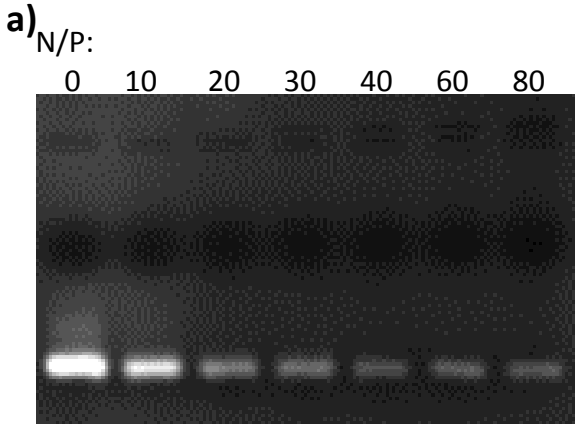

N/P	% Free siRNA
0	100
10	73.5
20	35.8
30	32.2
40	18.0
60	21.8
80	20.0

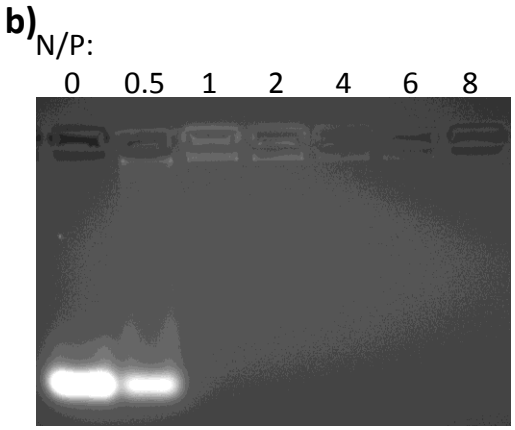

N/P	% Free siRNA
0	100
0.5	~17
1	-
2	-
4	-
6	-
8	--

Figure 4.1 Characterization of siRNA/PEG-*b*-P(APNBMA)$_n$ polyplexes. Representative siRNA mobility assay in 4 wt% agarose gels stained with ethidium bromide. Polyplexes were prepared with (a) PEG-*b*-P(APNBMA)$_{7.9}$ and (b) PEG-*b*-P(APNBMA)$_{23.6}$. Lane 1 of both gels is siRNA alone (N/P = 0) while the remaining lanes show siRNA complexed with polymer at varied N/P ratios. Tabulated values indicate integrated optical density quantification of the free siRNA band.

4.3.1.2 Physical characterization of polyplexes formed with PEG-*b*-P(APNBMA)$_{23.6}$

The hydrodynamic diameters of siRNA/PEG-*b*-P(APNBMA)$_{23.6}$ were measured by DLS (Figure 4.2a) to determine whether these structures would be

suitable for cellular uptake. Additionally, an aim of this study was to evaluate whether the polyplex sizes decreased with increased binding affinity based on the observation of decreased ethidium bromide intensity in the well with increased N/P. Polyplexes were formed at varied charge ratios ranging from N/P = 2 to 8 as these compositions enabled efficient siRNA complexation based on electrophoresis. As indicated in Figure 4.2, samples were below the size limit for endocytic uptake (< 200 nm).[20-22] Furthermore, the size of siRNA/PEG-*b*-P(APNBMA)$_{23.6}$ polyplexes was relatively constant for N/P 2 to 6 and indicated a decrease in polyplex size at N/P = 8, which corresponded to the tighter polyplex formation demonstrated in electrophoresis and indicated in previous investigations of polyplex size changes in response to increased cationic charge (N/P).

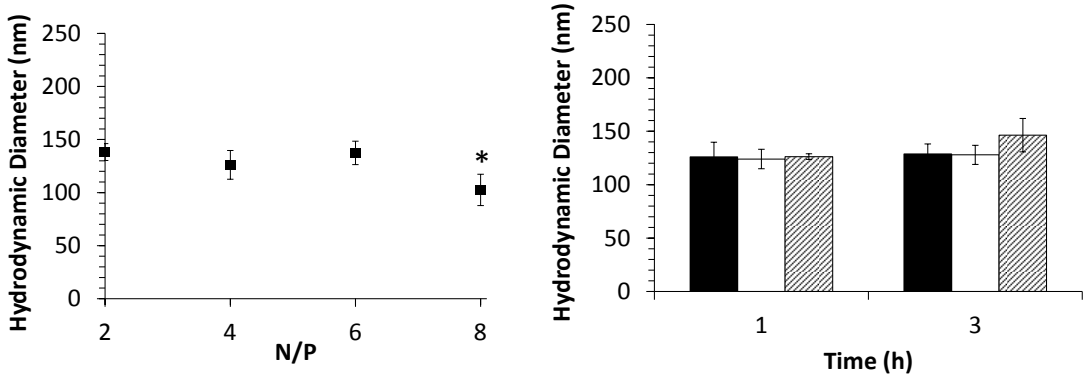

Figure 4.2 Polyplex characterization using dynamic light scattering. (a) Hydrodynamic diameters of polyplexes as determined by DLS. (b) Hydrodynamic diameters of polyplexes following 3 h incubation in polyplex formulation buffer, 20 mM HEPES pH 6 (black), Opti-MEM (white) and PBS with 150 mM salt concentration (diagonal stripes). * indicates a statistically significant difference from other samples ($p < 0.05$). Samples were analyzed by one-way analysis of variance (ANOVA).

Gene delivery polyplexes require colloidal stability to minimize salt-induced flocculation and nuclease stability to avoid non-specific protein adsorption and subsequent opsonization.[23, 24] As detailed in Chapter 1, stealth coatings such as protective PEG layers can be incorporated to promote colloidal and nuclease stability of gene delivery structures.[25-28] Thus, it was hypothesized that the protective PEG layer in these polyplexes could provide a steric barrier against aggregation and reduce the driving force for non-specific protein adsorption.

Polyplexes were incubated in PBS (150 mM salt) or Opti-MEM transfection medium to investigate their ability to remain stable during transfection. Samples were also incubated in formulation buffer (20 mM HEPES, pH 6) as a negative control. Subsequently, the average hydrodynamic diameters of the polyplexes following incubation in the various media were measured by DLS to determine whether physiological salt or serum induced appreciable changes in polyplex size (representative data for polyplexes prepared at N/P 4 shown in Figure 4.2b). Polyplexes exhibited no change in size following incubation in Opti-MEM or PBS solutions over a period of 1 h at 23 °C. Polyplex sizes also remained constant at ~130 nm after a 3 h incubation in Opti-MEM. In contrast, incubation in PBS over a 3 h period resulted in a slight but minimal increase in polyplex size (to ~ 146 nm), although polyplexes still retained sizes that were below the reported threshold for efficient endocytic uptake and gene silencing.[21] In the study of the cationic polymer PEI and N-(2-hydroxypropyl(methacrylamide)) (HPMA)-oligolysine polyplexes, Johnson *et al*. demonstrated salt-induced aggregation of PEI polyplexes with the incorporation of PEI and steric stabilization conferred by HPMA.[29] Based on the relative stability of the polyplex structures detailed in this chapter, and the minimal

increase in hydrodynamic diameter with PBS incorporation, these studies highlight the utility of the PEG block in polyplex preparation due to improved stability compared to uncoated materials.[29]

An electrophoresis assay was performed to assess the ability of PEG-*b*-P(APNBMA)$_{23.6}$ polyplexes to resist serum-mediated disassembly (Figure 4.3a). Gel mobility shift assays on free siRNA treated with mouse serum (Lane 2) demonstrated a modest broadening of the siRNA band due to degradation and no other fluorescence in the lane except for the nonspecific background present in serum samples (Figure 4.3a Lane 8). Polyplex samples treated with serum indicated the presence of siRNA in the well for all N/P ratios tested and no free siRNA band. These data suggest that the siRNA is not displaced from the polymeric delivery components with serum incorporation. Electrophoresis was similarly used to assess the ability to resist nuclease degradation (Figure 4.3b). Polyplexes prepared at N/P = 4 were incubated with RNase 1 and subsequently incubated with SDS to facilitate polyplex disassembly. In contrast to samples treated with whole mouse serum, electrophoresis of free siRNA indicated significant siRNA degradation increased mobility of the degradation product. This is likely due to the use of concentrated RNase. Treatment with SDS (Lane 4) indicated liberation of siRNA from the polyplexes and similar migration to free siRNA. Addtionally, RNase 1 incubation and subsequent treatment with SDS (Lane 5) indicated similar siRNA mobility and band intensities as compared to free siRNA (Lane 1) and siRNA released from polyplexes using SDS (Lane 4). These results and identify improved RNase 1 resistance of PEG-*b*-P(APNBMA)$_{23.6}$ polyplexes compared to free siRNA.

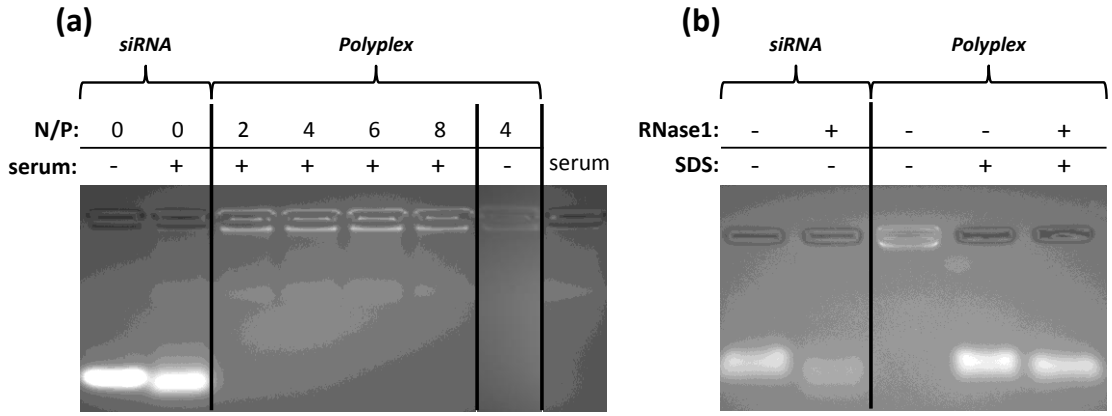

Figure 4.3 (a) Comparative stability of free siRNA and siRNA/PEG-*b*-P(APNBMA)$_{23.6}$ polyplexes in serum. Polyplexes were prepared at N/P = 2, 4, 6, 8 and analyzed via electrophoresis. (b) Stability of siRNA polyplexes (N/P = 4) against RNase 1-mediated degradation.

4.3.1.3 Effect of UV irradiation on the binding of siRNA/ PEG-*b*-P(APNBMA)$_{23.6}$ polyplexes

Given the efficient packaging and favorable properties in physiological media of siRNA/PEG-*b*-P(APNBMA)$_{23.6}$ polyplexes, UV irradiation studies were performed to assess the efficacy of siRNA release. The free PEG-*b*-P(APNBMA)$_{23.6}$ copolymer as well as siRNA/PEG-*b*-P(APNBMA)$_{23.6}$ polyplexes were irradiated with 365 nm light and the cleavage reaction was monitored in two ways. UV/Vis spectroscopy was used to monitor changes in the characteristic absorbance of the *o*-NB ester at 316 nm to investigate the extent of polymer cleavage in free *vs.* complexed polymer. Additionally, electrophoresis experiments were performed on irradiated samples to determine the amount of released siRNA.

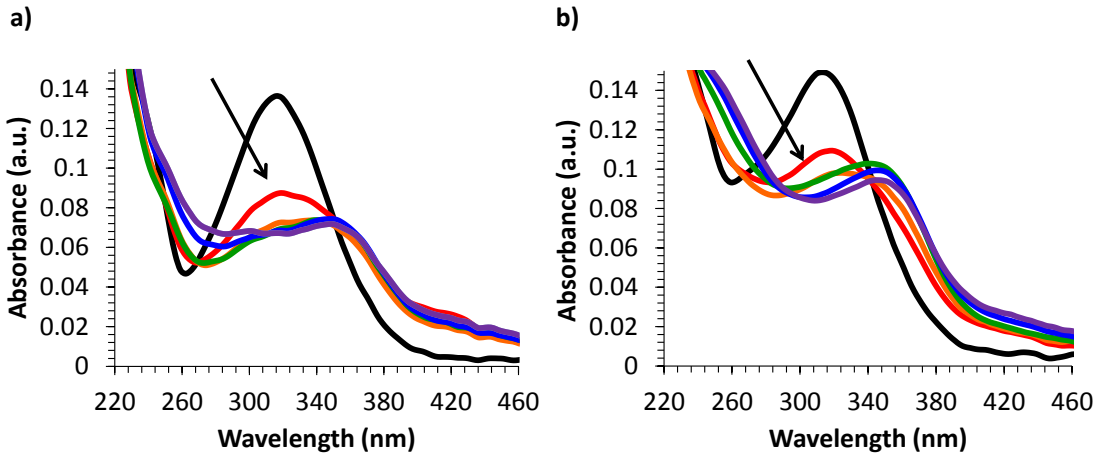

Figure 4.4 Absorbance spectral changes in (a) PEG-*b*-P(APNBMA)$_{23.6}$ and (b) siRNA/ PEG-*b*-P(APNBMA)$_{23.6}$ following exposure to UV irradiation (365 nm, 200 W/m^2) for 0 (black), 5 (red), 10 (orange), 20 (green), 40 (blue), or 60 (purple) minutes. Arrows indicate increasing irradiation time.

The polymer absorbance spectra displayed a dramatic decrease in absorbance up to 10 min of UV exposure and small changes at longer times (Figure 4.4a). Irradiation of siRNA/PEG-*b*-P(APNBMA)$_{23.6}$ polyplexes yielded similar results under the same conditions with a large decrease in absorbance within 10 min of treatment. Interestingly, the absorbance spectra of the polyplex-bound polymer showed more visible absorbance shifts than those of the free polymer following the initial 10 min exposure, indicating a slightly reduced rate of polymer cleavage within these polyplex structures. One plausible reason for this observed minimal decrease in cleavage is a reduced accessibility of the polymer due to confinement in the polyplex structure as compared with the free polymer in solution. As previously seen for the shorter cationic block length, the decreased absorbance as a function of irradiation time followed an exponential decay for both polymer and polyplex preparations. In

particular, both formulations similarly indicated ~100% cleavage of the *o*-NB group by monitoring the change in 316nm absorbance (Appendix A).

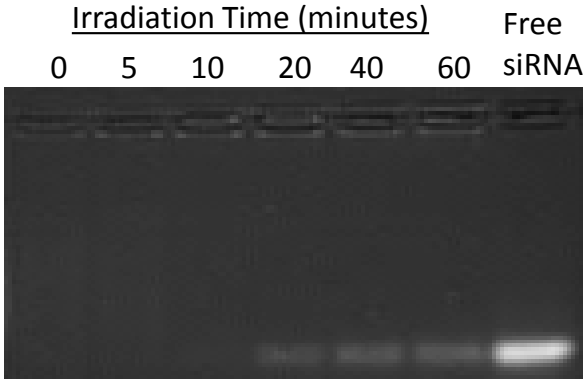

Irradiation Time (minutes)	% Free siRNA
0	-
5	1.8
10	2.9
20	15.2
40	20.7
60	23.5

Figure 4.5 Electrophoretic gel migration patterns of free siRNA (far right) or siRNA/PEG-*b*-P(APNBMA)$_{23.6}$ polyplexes after exposure to UV radiation (365 nm, 200 W/m^2) for varying periods of time (0 - 60 min).

The irradiated polyplexes were collected and analyzed via electrophoresis to determine the extent of light-induced siRNA release. While little siRNA migration was observed after short periods of light exposure (<10 min or less irradiation), free siRNA migrated down the gel after the polyplexes were exposed for 20 min or more. Quantification of free siRNA band intensities by ImageJ analysis revealed ~20% free siRNA for the 20 min irradiation condition, and increasing amounts of free siRNA were observed as a function of increasing irradiation times. As shown in Figure 4.5, siRNA release appeared to be incomplete after 60 min exposure despite indications of efficient polymer and polyplex cleavage seen in Figure 4.4. Although this apparent inconsistency may be due to incomplete polymer cleavage, it is also possible that siRNA may continue to associate with nitrobenzyl groups restricting ethidium

bromide intercalation/fluorescence. In contrast to photorelease experiments involving DNA/PEG-*b*-P(APNBMA)$_{7.9}$ polyplexes (Chapter 3), UV irradiation of siRNA polyplexes stimulated enhanced polyplex dissociation. As seen in previous studies employing siRNA as the polyplex cargo, it is likely that the shorter and more rigid structure of siRNA leads to the formation of polyplexes with weaker binding interactions and therefore facilitates more efficient dissociation.[1] While both DNA and siRNA may continue to associate with short cationic polymer fragments, this reduction in polyvalency is unlikely to provide sufficient interactions in the siRNA preparations to maintain complexation.

4.3.2 siRNA/ PEG-*b*-P(APNBMA)$_{23.6}$ Polyplexes are Internalized by Cells Gradually and at High Levels

Efficient cell uptake is an important condition for successful nucleic acid delivery. Given that PEG-*b*-P(APNBMA)$_{23.6}$ was able to form compact, salt- and serum-stable polyplexes, its ability to mediate cellular uptake in NIH/3T3 cells was tested. Polyplex uptake was visualized using fluorescence microscopy and quantified by flow cytometry. Polyplexes were formulated with siRNA that was pre-labeled with 1.5 eq YOYO-1 iodide. Microscopy images showed clear uptake of labeled polyplexes with the appearance of intracellular YOYO-1-labeled structures at short time points (<1 h; Figure 4.4a). The punctate appearance of many of these structures suggested polyplex entrapment in vesicular compartments within the cell, consistent with previous studies investigating the trafficking of siRNA polyplexes[15] and other nanostructures. Notably, even after 1 h, a diffuse polyplex staining pattern was apparent. After 3 h, there was a clear increase in intracellular YOYO-1 iodide as well

as a loss of the punctate structures and a shift to a uniformly diffuse intracellular distribution (Figure 4.4c). Although the staining pattern alone cannot confirm cytoplasmic localization of these polyplexes, as seen in multiple studies demonstrating similar staining following transfection, the release of these polyplex structures is one possible explanation for the increasingly diffuse staining pattern.[30] For example, in work by Kim and coworkers, they identify the cytoplasmic escape of siRNA/poly(cystaminebisacrylamide-diaminohexane) polyplexes through confocal imaging of Cy3 modified siRNA polyplex preparations.[30] A number of polymer and peptides with high primary amine content, including poly lysine have demonstrated a membrane penetrating capacity due to charge-based interactions with the anionic membrane. Thus it is possible that the cationic block introduces membrane penetration functionality in the polyplex structure, thus destabilizing the endosomal membrane to facilitate polyplex escape.

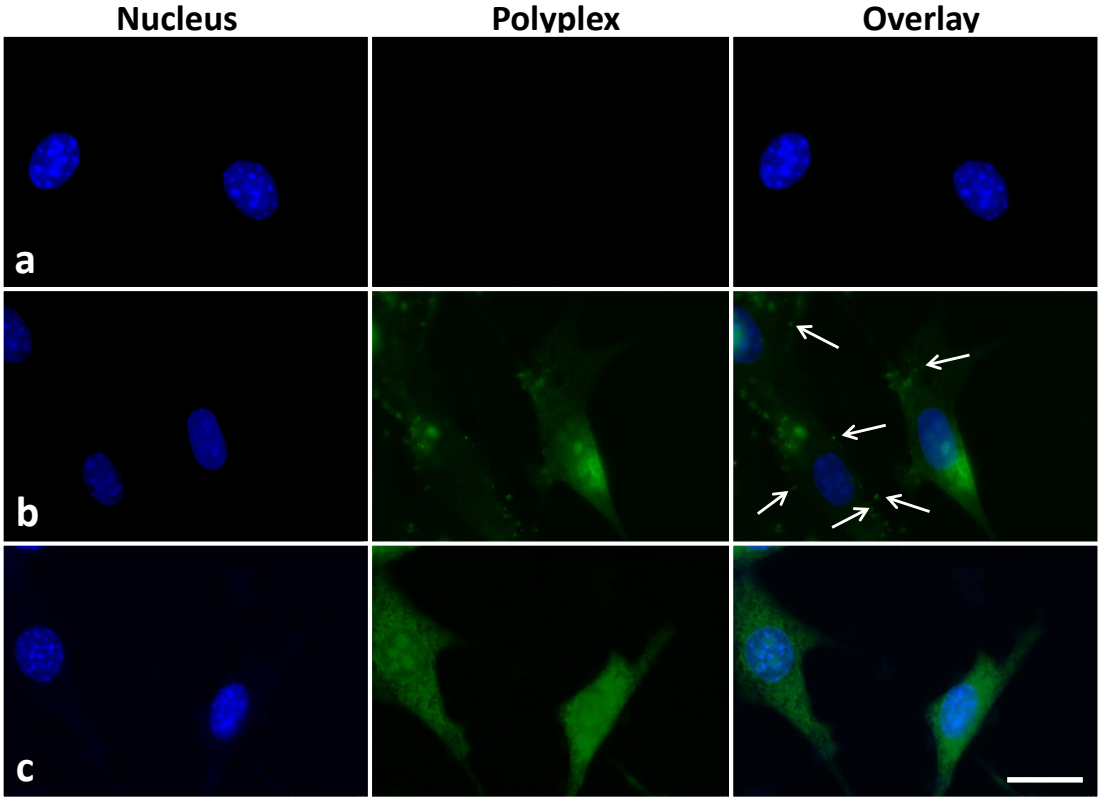

Figure 4.6 Representative images showing the internalization of siRNA polyplexes in NIH/3T3 cells, where the siRNA was labeled with YOYO-1 Iodide (green), and the nucleus was stained with Hoechst (blue). (a) Untreated cells. (b) and (c) siRNA/PEG-*b*-P(APNBMA)$_{23.6}$ polyplexes at 1 h and 3 h post-transfection, respectively. Polyplexes were formulated at N/P = 4. Arrows indicate punctate polyplex structures. The scale bar represents 25 µm.

Flow cytometry was used to quantify the efficiency of cellular uptake and the amount of intracellular YOYO-1 iodide-labeled siRNA polyplexes. Although the siRNA/PEG-*b*-P(APNBMA)$_{23.6}$ polyplexes were internalized by only a small fraction of cells by the 1 h time point (Figure 4.7), the levels of polyplex internalization were comparable to the levels observed using polyplexes prepared with commercially

available Lipofectamine RNAiMax. Notably, the uptake efficiency of siRNA/PEG-*b*-P(APNBMA)$_{23.6}$ polyplexes gradually increased compared to siRNA/Lipofectamine structures, whose uptake levels remained low after a 3 h treatment (Figure 4.7). Additionally, the average intracellular concentration of siRNA increased up to 3 h post-transfection for the PEG-*b*-P(APNBMA)$_{23.6}$ assemblies (Figure 4.8).

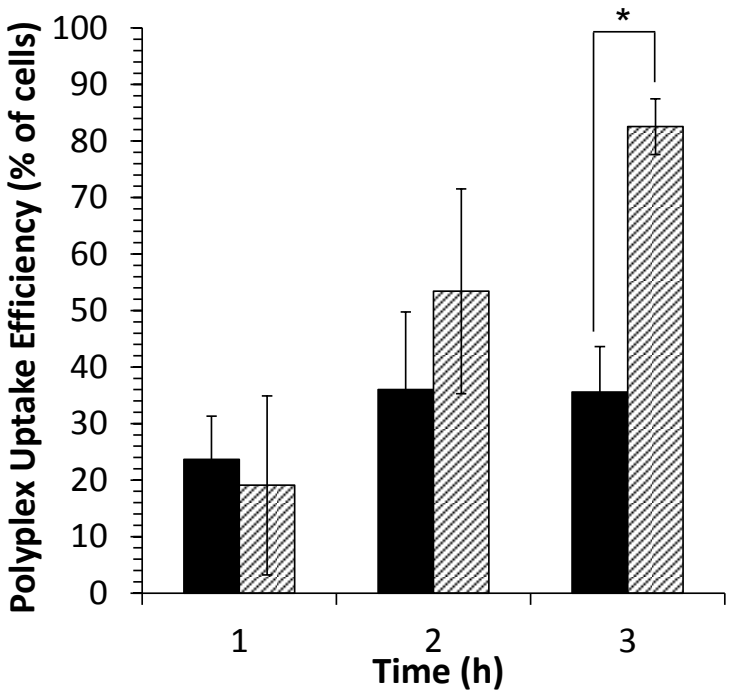

Figure 4.7 Cellular uptake of fluorescently-labeled siRNA complexes. Lipofectamine RNAiMax (black); PEG-*b*-P(APNBMA)$_{23.6}$, N/P = 4 (diagonal stripes). Polyplex uptake as a percentage of cells that internalized polyplexes. Data were obtained with flow cytometry measurements. Each data point represents the mean ± standard deviation for a total of three separately prepared samples. * indicates a statistically significant difference at a given time point between the PEG-*b*-P(APNBMA)$_{23.6}$ and Lipofectamine polyplexes ($p < 0.001$). Samples were analyzed by one-way analysis of variance (ANOVA).

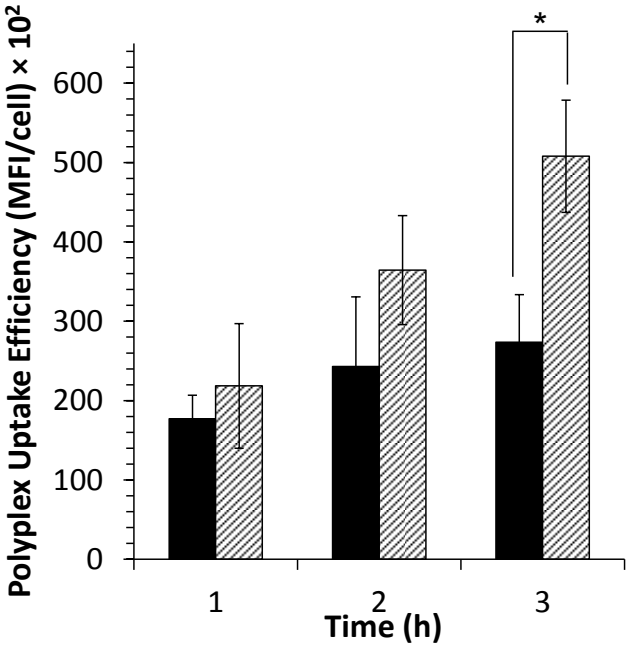

Figure 4.8 Cellular uptake of fluorescently-labeled siRNA complexes. Lipofectamine RNAiMax (black); PEG-*b*-P(APNBMA)$_{23.6}$, N/P = 4 (diagonal stripes). The mean fluorescence intensity (MFI) of the cells that had internalized polyplexes. MFI is expressed in arbitrary units. Data were obtained with flow cytometry measurements. Each data point represents the mean ± standard deviation for a total of three separately prepared samples. * indicates a statistically significant difference at a given time point between the PEG-b-P(APNBMA)$_{23.6}$ and Lipofectamine polyplexes ($p < 0.001$). Samples were analyzed by one-way analysis of variance (ANOVA).

4.3.3 Polymer, Polyplex and UV Treatment do not Compromise NIH/3T3 Cell Viability

Polyplexes can be cytotoxic due to numerous factors including molecular weight, degree of branching, ionic strength of the solution, zeta potential and particle size.[31, 32] For example, both PLL and PEI polyplexes have been shown to induce apoptosis in a number of cell lines.[33] Strategies such as the incorporation of PEG in

carrier design have been shown to reduce cellular toxicity due to reduced non-specific interactions with blood components and proteins.[34] Under the same conditions used in this work (I = 200 W/m^2, 20 min exposure), previous studies have demonstrated that the cellular viability is not influenced by the treatment with UV light.[35] However, the combined transfection and UV treatment experiment has the potential to reduce cellular viability. Hence, the Alamar Blue (AB) cell survival assay (Invitrogen) was used to determine whether the PEG-based PEG-*b*-P(APNBMA) design and/or the UV exposure conditions maintained cellular viability.

The two PEG-*b*-P(APNBMA) copolymers demonstrated substantially reduced toxicity as compared to PEI , with IC_{50} values of 1.05 μM and 0.77 μM for PEG-b-P(APNBMA)$_{7.9}$ and PEG-b-P(APNBMA)$_{23.6}$, respectively (Appendix B). In these studies, it is of note that significant PEI toxicity in the tested concentration range precluded calculation of an IC_{50} in the polymer under the conditions tested. As anticipated, PEG-b-P(APNBMA)$_{23.6}$ demonstrated modestly increased toxicity compared to the shorter cationic polymer. Increased charge molecular weight/ cationic chain length have been previously shown to correlate with greater toxicity,[36] thus the increased molecular weight (and cationic charge) in the longer cationic polymer is likely responsible for this observed increase. Previous studies have indicated significant toxicity when using the cationic polymer PEI (particularly at N/P $\geq$ 10, ~ 0.2 μM PEI working concentration),[37] thus a rapid loss of cell viability was anticipated as demonstrated in Appendix B.

The Alamar Blue cell proliferation assay was also used to investigate the effect on cellular viability of siRNA/PEG-*b*-P(APNBMA)$_{23.6}$ treatment, as well as the effect of the combined polyplex/UV transfection conditions. As anticipated, quantification

of the cellular viability in all samples revealed greater than 90% survival. Additionally, no additive/synergistic effects were observed in cells that were treated with UV light in combination with siRNA/PEG-*b*-P(APNBMA) polyplexes *vs.* UV light alone (Figure 4.9).

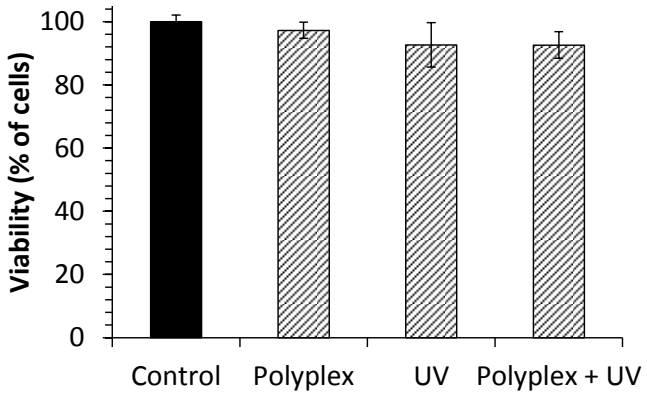

Figure 4.9 Cell viabilities 48 h after polyplex treatment, UV exposure, or the combination of polyplexes and UV exposure. Percent viabilities are relative to untreated cells. Each data point represents the mean ± standard deviation for a total of at least three separately prepared and analyzed samples. The untreated sample is shown in black as a control.

Based on observations of complete polymer cleavage at 20 min (for both short and long chain lengths) and the ability to release ~15% of siRNA from the polyplexes as indicated by ethidium bromide fluorescence, irradiation times up to 20 min (at 365 nm, 200 W/m^2) are viable for treatment with siRNA/PEG-*b*-P(APNBMA)$_{23.6}$ polyplexes. In contrast, greater than 40 min of irradiation was necessary to visualize DNA release from DNA/PEG-*b*-P(APNBMA)$_{7.9}$ polyplexes as indicated in Chapter 3 (Figure 3.5c). However, irradiation times of this length have resulted in a significant

decrease in cellular viability (Appendix B), suggesting the need for faster photocleavage and improved nucleic acid release to provide a viable platform for DNA delivery.

4.3.4 Protein Silencing Capacity of Photocleavable Polyplexes

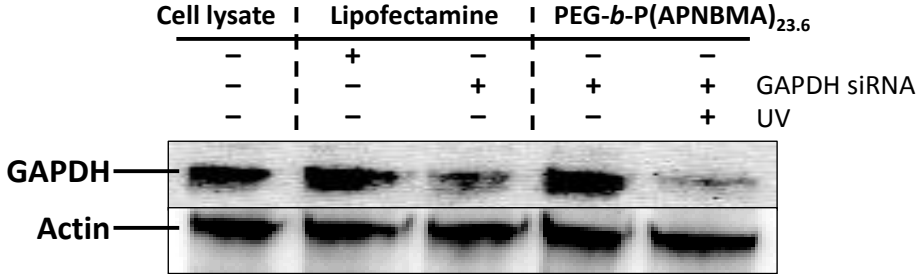

Figure 4.10 NIH/3T3 cell extracts collected 48 h post siRNA transfection and analyzed by Western blot using antibodies directed against GAPDH and actin. Cells were treated with GAPDH targeted siRNA/PEG-*b*-P(APNBMA)$_{23.6}$ polyplexes with and without UV exposure. Lipofectamine lipoplexes were prepared using non-targeting and GAPDH targeting siRNAs as negative and positive controls respectively. Samples contained 20 µg total protein as determined by the BCA assay.

siRNA/PEG-*b*-P(APNBMA)$_{23.6}$ polyplexes were assessed for their gene silencing activity in NIH/3T3 cells as shown in Figure 4.10. Samples were irradiated following a 3 h transfection based on the observation of the apparent cytoplasmic release of siRNA polyplexes by 3 h (Figure 4.6). The UV treatment of an anti-GAPDH PEG-*b*-P(APNBMA)$_{23.6}$ sample exhibited higher GAPDH inhibition than Lipofectamine, which is widely used for its high *in vitro* transfection efficiency yet demonstrates significant toxicity.[38] Specifically, quantification of the integrated optical density ImageJ analysis of the Western blot indicated ~70% and ~45%

reduction in GAPDH levels (relative to an untreated cell sample) in the siRNA/PEG-*b*-P(APNBMA)$_{23.6}$/UV sample and the Lipofectamine control, respectively. Based on the combined results of siRNA release (Figure 4.5) and protein silencing (Figure 4.10), it is of note that complete siRNA release from the irradiated polyplexes does not appear to be necessary for enhanced gene silencing. This is potentially due to the catalytic nature of siRNA delivery[5] in addition to the potential for the cell to further loosen these compromised polyplexes following user-initiated cleavage. In contrast, the non-targeted delivery strategy (ON-TARGETplus Non-targeting siRNA complexed with Lipofectamine) only minimally affected GAPDH levels, thus demonstrating the specificity of gene silencing in this study. Several investigations into the silencing effect of siRNA/Lipofectamine complexes reveal greater than 80% knock-down when monitoring mRNA levels. It is likely that investigation into the direct silencing effect on mRNA levels will further support the potency of this delivery carrier. Additionally, these results demonstrated that siRNA/PEG-*b*-P(APNBMA)$_{23.6}$ polyplexes were able to induce controlled gene silencing *in vitro*. It is possible that further enhancements in mRNA degradation/protein silencing can be demonstrated by careful timing of the UV treatment prior to quantification of mRNA and protein levels.

4.4 Conclusions

The work presented in this chapter highlighted a promising stimuli-responsive cationic carrier for gene delivery. As indicated by enhanced silencing capacity (compared to Lipofectamine and samples without UV irradiation) the stimuli-responsive aspect of this delivery platform provided significant utility for protein silencing. This siRNA delivery platform introduced several favorable features which

demonstrate a unique strategy for enhancements in current siRNA delivery strategies. Specifically, the capacity for efficient cytoplasmic release and distribution, as well as the user-controlled release mechanism incorporated in this structure introduce significant versatility into the delivery platform by allowing an on/off mechanism for siRNA release at various stages of gene delivery.

REFERENCES

1. Gary, D. J.; Puri, N.; Won, Y. Y., Polymer-based siRNA delivery: perspectives on the fundamental and phenomenological distinctions from polymer-based DNA delivery. *J Control Release* **2007,** 121, (1-2), 64-73.

2. Behlke, M. A., Progress towards in vivo use of siRNAs. *Mol Ther* **2006,** 13, (4), 644-70.

3. Dorsett, Y.; Tuschl, T., siRNAs: applications in functional genomics and potential as therapeutics. *Nat Rev Drug Discov* **2004,** 3, (4), 318-29.

4. Castanotto, D.; Rossi, J. J., The promises and pitfalls of RNA-interference-based therapeutics. *Nature* **2009,** 457, (7228), 426-33.

5. de Fougerolles, A.; Vornlocher, H. P.; Maraganore, J.; Lieberman, J., Interfering with disease: a progress report on siRNA-based therapeutics. *Nat Rev Drug Discov* **2007,** 6, (6), 443-53.

6. Jacque, J. M.; Triques, K.; Stevenson, M., Modulation of HIV-1 replication by RNA interference. *Nature* **2002,** 418, (6896), 435-8.

7. Bartlett, D. W.; Su, H.; Hildebrandt, I. J.; Weber, W. A.; Davis, M. E., Impact of tumor-specific targeting on the biodistribution and efficacy of siRNA nanoparticles measured by multimodality in vivo imaging. *Proc Natl Acad Sci U S A* **2007,** 104, (39), 15549-54.

8. Heidel, J. D.; Yu, Z.; Liu, J. Y.; Rele, S. M.; Liang, Y.; Zeidan, R. K.; Kornbrust, D. J.; Davis, M. E., Administration in non-human primates of escalating intravenous doses of targeted nanoparticles containing ribonucleotide reductase subunit M2 siRNA. *Proc Natl Acad Sci U S A* **2007,** 104, (14), 5715-21.

9. Nakamura, Y.; Kogure, K.; Futaki, S.; Harashima, H., Octaarginine-modified multifunctional envelope-type nano device for siRNA. *J Control Release* **2007,** 119, (3), 360-7.

10. Zuckerman, J. E.; Choi, C. H.; Han, H.; Davis, M. E., Polycation-siRNA nanoparticles can disassemble at the kidney glomerular basement membrane. *Proc Natl Acad Sci U S A* **2012,** 109, (8), 3137-42.

11. Jeong, J. H.; Mok, H.; Oh, Y. K.; Park, T. G., siRNA conjugate delivery systems. *Bioconjug Chem* **2009,** 20, (1), 5-14.

12. Lee, S. H.; Mok, H.; Jo, S.; Hong, C. A.; Park, T. G., Dual gene targeted multimeric siRNA for combinatorial gene silencing. *Biomaterials* **2011,** 32, (9), 2359-68.

13. Mok, H.; Lee, S. H.; Park, J. W.; Park, T. G., Multimeric small interfering ribonucleic acid for highly efficient sequence-specific gene silencing. *Nat Mater* **2010,** 9, (3), 272-8.

14. Liu, X.; Howard, K. A.; Dong, M.; Andersen, M. O.; Rahbek, U. L.; Johnsen, M. G.; Hansen, O. C.; Besenbacher, F.; Kjems, J., The influence of polymeric properties on chitosan/siRNA nanoparticle formulation and gene silencing. *Biomaterials* **2007,** 28, (6), 1280-8.

15. Shim, M. S.; Kwon, Y. J., Acid-responsive linear polyethylenimine for efficient, specific, and biocompatible siRNA delivery. *Bioconjug Chem* **2009,** 20, (3), 488-99.

16. Breunig, M.; Hozsa, C.; Lungwitz, U.; Watanabe, K.; Umeda, I.; Kato, H.; Goepferich, A., Mechanistic investigation of poly(ethylene imine)-based siRNA delivery: disulfide bonds boost intracellular release of the cargo. *J Control Release* **2008,** 130, (1), 57-63.

17. Markovits, J.; Pommier, Y.; Kerrigan, D.; Covey, J. M.; Tilchen, E. J.; Kohn, K. W., Topoisomerase II-mediated DNA breaks and cytotoxicity in relation to cell proliferation and the cell cycle in NIH 3T3 fibroblasts and L1210 leukemia cells. *Cancer Res* **1987,** 47, (8), 2050-5.

18. Byrne, M.; Victory, D.; Hibbitts, A.; Lanigan, M.; Heise, A.; Cryan, S.-A., Molecular weight and architectural dependence of well-defined star-shaped poly(lysine) as a gene delivery vector. *Biomaterials Science* **2013,** 1, (12), 1223-1234.

19. Kizzire, K.; Khargharia, S.; Rice, K. G., High-affinity PEGylated polyacridine peptide polyplexes mediate potent in vivo gene expression. *Gene Ther* **2013,** 20, (4), 407-16.

20. Ogris, M.; Steinlein, P.; Carotta, S.; Brunner, S.; Wagner, E., DNA/polyethylenimine transfection particles: influence of ligands, polymer size, and PEGylation on internalization and gene expression. *AAPS PharmSci* **2001,** 3, (3), E21.

21. Grayson, A. C.; Doody, A. M.; Putnam, D., Biophysical and structural characterization of polyethylenimine-mediated siRNA delivery in vitro. *Pharm Res* **2006,** 23, (8), 1868-76.

22. Bishop, N. E., An Update on Non-clathrin-coated Endocytosis. *Rev Med Virol* **1997,** 7, (4), 199-209.

23. Hagstrom, J. E., Self-assembling complexes for in vivo gene delivery. *Curr Opin Mol Ther* **2000,** 2, (2), 143-9.

24. Hwang, S. J.; Davis, M. E., Cationic polymers for gene delivery: designs for overcoming barriers to systemic administration. *Curr Opin Mol Ther* **2001,** 3, (2), 183-91.

25. Harris, J. M.; Chess, R. B., Effect of pegylation on pharmaceuticals. *Nat Rev Drug Discov* **2003,** 2, (3), 214-21.

26. Owens, D. E., 3rd; Peppas, N. A., Opsonization, biodistribution, and pharmacokinetics of polymeric nanoparticles. *Int J Pharm* **2006,** 307, (1), 93-102.

27. Ogris, M.; Brunner, S.; Schuller, S.; Kircheis, R.; Wagner, E., PEGylated DNA/transferrin-PEI complexes: reduced interaction with blood components, extended circulation in blood and potential for systemic gene delivery. *Gene Ther* **1999,** 6, (4), 595-605.

28. Peracchia, M. T.; Harnisch, S.; Pinto-Alphandary, H.; Gulik, A.; Dedieu, J. C.; Desmaele, D.; d'Angelo, J.; Muller, R. H.; Couvreur, P., Visualization of in vitro protein-rejecting properties of PEGylated stealth polycyanoacrylate nanoparticles. *Biomaterials* **1999,** 20, (14), 1269-75.

29. Sharma, V. K.; Thomas, M.; Klibanov, A. M., Mechanistic studies on aggregation of polyethylenimine-DNA complexes and its prevention. *Biotechnol Bioeng* **2005,** 90, (5), 614-20.

30. Kim, S. H.; Jeong, J. H.; Kim, T. I.; Kim, S. W.; Bull, D. A., VEGF siRNA delivery system using arginine-grafted bioreducible poly(disulfide amine). *Mol Pharm* **2009,** 6, (3), 718-26.

31. Kunath, K.; von Harpe, A.; Fischer, D.; Petersen, H.; Bickel, U.; Voigt, K.; Kissel, T., Low-molecular-weight polyethylenimine as a non-viral vector for DNA delivery: comparison of physicochemical properties, transfection efficiency and in vivo distribution with high-molecular-weight polyethylenimine. *J Control Release* **2003,** 89, (1), 113-25.

32. Kircheis, R.; Schuller, S.; Brunner, S.; Ogris, M.; Heider, K. H.; Zauner, W.; Wagner, E., Polycation-based DNA complexes for tumor-targeted gene delivery in vivo. *J Gene Med* **1999,** 1, (2), 111-20.

33. Hunter, A. C., Molecular hurdles in polyfectin design and mechanistic background to polycation induced cytotoxicity. *Adv Drug Deliv Rev* **2006,** 58, (14), 1523-31.

34. Neu, M.; Fischer, D.; Kissel, T., Recent advances in rational gene transfer vector design based on poly(ethylene imine) and its derivatives. *J Gene Med* **2005,** 7, (8), 992-1009.

35. Lee, H.; Kim, Y.; Schweickert, P. G.; Konieczny, S. F.; Won, Y. Y., A photo-degradable gene delivery system for enhanced nuclear gene transcription. *Biomaterials* **2014,** 35, (3), 1040-9.

36. Hwang, S. J.; Bellocq, N. C.; Davis, M. E., Effects of structure of beta-cyclodextrin-containing polymers on gene delivery. *Bioconjug Chem* **2001,** 12, (2), 280-90.

37. Reilly, M. J.; Larsen, J. D.; Sullivan, M. O., Histone H3 tail peptides and poly(ethylenimine) have synergistic effects for gene delivery. *Mol Pharm* **2012,** 9, (5), 1031-40.

38. Wu, Y.; Wang, W.; Chen, Y.; Huang, K.; Shuai, X.; Chen, Q.; Li, X.; Lian, G., The investigation of polymer-siRNA nanoparticle for gene therapy of gastric cancer in vitro. *Int J Nanomedicine* **2010,** 5, 129-36.

Chapter 5

DEVELOPMENT OF A CELL-RESPONSIVE SIRNA CONJUGATE FOR TARGETED CANCER TREATMENT

5.1 Introduction

As mentioned in the previous chapters, siRNAs have a unique ability to induce gene silencing through RNA interference (RNAi), and have enormous therapeutic potential in the treatment of a range of acquired and heritable diseases.[1-3] The use of siRNAs presents a particularly attractive cancer treatment strategy due to the wide range of protein targets associated with this cellular dysfunction.[4-7] In one particular approach, Alnylam Pharmaceuticals investigate the use of lipid nanoparticles (LNP) delivering siRNA for the treatment of transthyretin-related amyloidosis (ATTR). These siRNA/LNPs (drug name ALN-TTR02) enabled rapid dose-dependent gene knockdown in Phase II trials and showed tremendous potential for continued clinical investigation due to their capacity for efficient siRNA encapsulation, scalable and reproducible development, and blocked 85% of the expression of the disease-causing TTR protein.[8] siRNAs have exhibited similar promise in a current clinical study by Calando Pharmaceuticals. In their approach, using transferrin receptor-targeted cyclodextrin-based polymer (CALAA-01) for solid tumor directed delivery against the M2 subunit of ribonucleotide reductase (RRM2) – a protein involved in DNA replication) – they demonstrated enhanced tumor targeting capability and efficient RRM2 knockdown.[9] Despite the tremendous strides towards the successful application of gene silencing for cancer treatment, it is of note that there are currently

no siRNA treatments on the market and limited clinical applications of siRNA for cancer treatment. Based on the design features of these current clinical strategies, it is evident that future clinical success relies upon detailed consideration of the functional and practical requirements on the delivery vehicle to design improved structures.

As outlined in Chapters 1 and 4, the functional requirements for siRNA delivery vehicles include improved extracellular stability, targeted cellular localization and uptake, controlled cytoplasmic release, and siRNA liberation from the carrier. Furthermore, the delivery vehicle faces the practical requirement of scalable and reproducible formulation, as well as a facile delivery strategy. Building on the discussions in the previous chapters, the work presented herein aims to develop a well-defined siRNA delivery vehicle to combine targeted delivery with controlled siRNA release. Specifically, the siRNA delivery vehicle presented in this chapter contains multiple functional components as outlined in Figure 5.1 including: (1) a non-fouling scaffold to facilitate improved stability during circulation, (2) cell-targeting/binding capability for improved uptake in cancer cells, (3) endosomal destabilizing capability to facilitate cytoplasmic release, and finally (4) a controlled siRNA release mechanism to allow for siRNA liberation from the delivery structure.

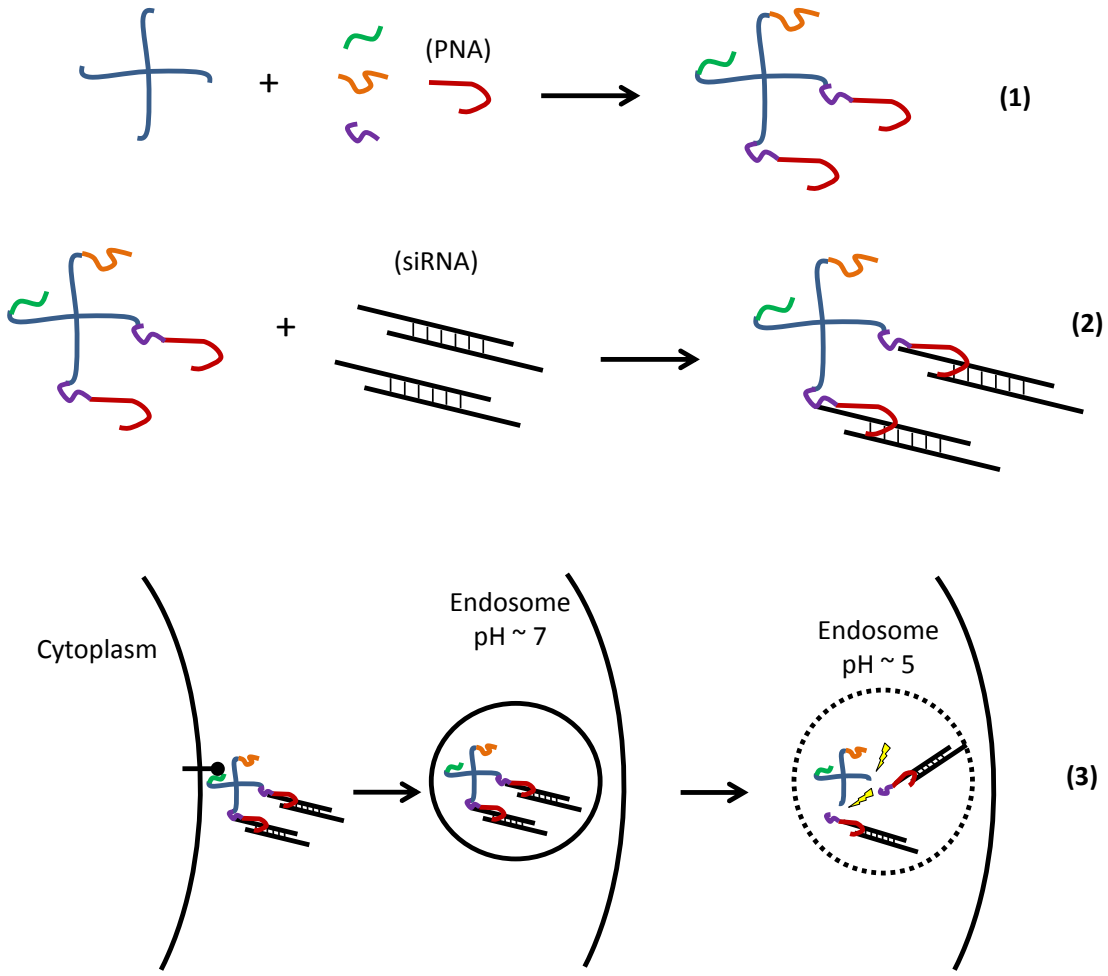

Figure 5.1 **Versatile PNA-peptide-PEG (PPP) for siRNA delivery. (a) Peptides and PNA (red) assemble on a PEG scaffold (blue) to form PPP. (b) PPP conjugates self-assemble with siRNA via hydrogen bonding between PNA arms and 5'-sense extensions on siRNA. (c) Cell-binding arms (green) stimulate endocytosis, and endosomolytic arms (orange) promote endosomal rupture and carrier release. The lysosomal endopeptidase cathepsin L (lightning bolt) releases the siRNA from the conjugates via cleavage of the cathepsin L-cleavable peptide (purple).**

The presented nanoconjugate provides numerous functional capabilities for siRNA delivery. A four-arm star polyethylene glycol (PEG) scaffold provides

multiple reactive sites to incorporate biological functionalities. PEG has previously been included in a number of gene delivery carriers for its ability to enhance *in vivo* resistance to salt aggregation and protein adsorption.[10-12] Thus, the incorporation of PEG in this structure is hypothesized to provide enhanced stability during delivery. The cell-binding arm is incorporated in the conjugate to facilitate efficient cellular uptake. Targeting strategies have been utilized in a number of cancer therapies due to observed differences in expressed proteins associated with numerous cellular dysfunctions.[13] For example, transferrin (TF) is widely used as a tumor-targeting ligand for the delivery of anticancer drugs, such as the aforementioned CALAA-01 strategy, because the TF receptor is overexpressed on the surface of various fast-growing cancer cells.[14, 15] Similarly, the $\alpha_v\beta_3$ integrin is overexpressed not only on tumor endothelium, but also on cancer cells in a number of malignancies. As such, the arginine-glycine-aspartic acid (RGD) tripeptide, which serves as a ligand for $\alpha_v\beta_3$, has been used in a number of cancer therapies to deliver associated therapies by targeting tumor endothelium and subsequently targeting cancer cells following extravasation of the therapeutics.[16, 17] The carrier design presented in this work involved either the RGD tripeptide or the cell penetrating trans-activating transcriptional activator (Tat) peptide due to its known ability to enhance cellular uptake of attached cargo.[18-21] The addition of this cell-binding arm in the nanoconjugate design presents an attractive feature in the delivery vehicle to improve and direct cellular uptake.

As mentioned is Chapter 4, the unpackaging of siRNA delivery structures is a primary hurdle towards efficient gene silencing.[22] As such, the conjugate design included a cathepsin L-cleavable linker peptide to confer cell-responsive siRNA release functionality into the delivery vehicle. Cathepsin L is a lysosomal

endopeptidase that is expressed at high levels within tumor cells;[23-25] and thus it was hypothesized that the incorporation of this cleavable sequence would provide a cell-triggered approach for siRNA release. siRNA-binding capability was conferred through the incorporation of a peptide nucleic acid (PNA) due to its demonstrated sequence-specific binding to complementary nucleic acids in other applications.[26]

This tailorable, multifunctional construct addresses the need for well-defined siRNA delivery vehicles to promote efficacious delivery. The work presented in this chapter presents a series of synthetic strategies aimed towards the successful development of this multifunctional structure due to its potential to synergistically enhance siRNA delivery as a cancer treatment strategy.

5.2 Materials and Methods

5.2.1 Materials

All fluorenylmethyloxycarbonyl (Fmoc)-protected amino acids were purchased from EMD Chemicals (Darmstadt, Germany). The bis-PNA (maleimide-OOTCTCTCTC-OOO-JTJTJTJT-$CONH_2$, where O = 8-amino-3,6-dioxaoctanoic acid and J = pseudoisocytosine) was obtained with greater than 90% purity from Panagene (Daejeon, Korea) for solution-based coupling. Custom siRNAs were designed to provide silencing capability against glyceraldehyde 3-phosphate dehydrogenase (GAPDH) (sense: 5'-GUGUGAACCACGAGAAAUAUU-3'; extended sense: 5'-AGAGAGAGUUUGUGUGAACCACGAGAAAUAUU-3'; antisense: 5'P-UAUUUCUCGUGGUUCACACUU-3'). The sequences were designed with 5'-phosphorylation on the antisense strand and 3' UU characteristic of endogenous siRNAs .[27-29] The sequences also included 2'-fluoro modifications to provide

increased stability, increased specificity and reduced immunogenicity of the siRNA duplex in cellular studies.[30, 31] Sequences were annealed according to the manufacturer's protocols. The PNA-binding sequence contained a 5'-sense extension to facilitate siRNA/PNA hybridization. All custom siRNAs were prepared by ThermoFisher Scientific (Pittsburgh, PA). Fmoc and Benzhydryloxycarbonyl (Bhoc) peptide nucleic acid (PNA) monomers were purchased from PolyOrg, Inc (Leominster, MA). 10 kDa 4-arm PEG was purchased from Creative PEGworks (Winston Salem, NC) and used without further purification. All other chemicals were purchased from Sigma (St. Louis, MO) unless otherwise noted.

5.2.2 Methods

5.2.2.1 Peptide Synthesis and Purification

Peptide synthesis was performed by standard Fmoc-mediated solid phase strategies with a Protein Technologies, Inc. (Tucson, AZ) Tribute series peptide synthesizer. Peptides were synthesized on a rink-amide ChemMatrix resin (PCAS Biomatrix, Inc., Saint-Jean-sur-Richelieu, Canada). Cleavage of the peptides from the resin was performed using a cocktail consisting of 5 wt% phenol in 95 vol% trifluoroacetic acid (TFA), 2.5 vol% double distilled H_2O (ddH_2O), and 2.5 vol% triisopropyl silane for 2-4 h. The peptides were precipitated from the cleavage solution using ice-cold diethyl ether and centrifuged at 3,220g for 4 min at 4 ºC. The ether was decanted and the peptides were redissolved in ddH_2O, frozen and lyophilized to remove any trace amounts of ether. Purification of the peptides was performed by reverse-phase high performance liquid chromatography (RP-HPLC), on an UFLC 20 series instrument from Shimadzu, Inc. (Columbia, MD) with 0.1% TFA in ddH_2O and

0.1% TFA in acetonitrile as the mobile phase. Purification was performed using gradient flow through the column at a rate of 5 mL/min through a Viva C18 (21 mm × 150 mm, 5 μm particle diameter) column from Restek (Lancaster, PA). Peptide elution was monitored by absorbance measurements at 210 nm.

Protected peptides were synthesized using a slightly modified strategy. Peptide fragments were prepared on a 2-Chlorotrityl Resin ChemMatrix resin (PCAS Biomatrix, Inc., Saint-Jean-sur-Richelieu, Canada). Cleavage of the peptides from the resin was performed using a 1:1:8 by volume mixture of acetic acid/trifluoroethanol/dichloromethane for 30 min. The peptides were precipitated in water, filtered and washed to yield protected fragments.

5.2.2.2 PNA Synthesis

PNA synthesis was performed in a similar fashion, but with slight modifications. Synthesis was performed by Fmoc/Bhoc strategies on a rink-amide ChemMatrix resin. Cleavage of PNA from the resin was performed using a cocktail consisting of trifluoromethane sulphonic acid:TFA:*m*-cresol (2:8:1) for 90 minutes on ice prior to ether precipitation and purification.

5.2.2.3 Formation of Cell-responsive Conjugates

5.2.2.3.1 Solution Phase Thiol-acrylate Reaction

A thiol-acrylate coupling reaction was utilized for peptide-PEG conjugation as previously described.[32] The reactants were dissolved in a 0.1 M sodium phosphate (pH = 8.0) buffer solution at the desired molar ratio and was allowed to proceed for at least 90 min, with 25 μL samples removed every 15 min to enable assessment of the progress of the reaction. To monitor the extent of the reaction, the reaction samples

were placed in a solution containing 521 μL of 0.1 M sodium phosphate (pH 8.0) and 10 μL of a 4 mg/mL solution of 5,5'-dithiobis-(2-nitrobenzoic acid) (DTNB or Ellman's Reagent), and were incubated for 15 min at room temperature. The absorbance of these solutions was analyzed at 412 nm on a Nanodrop 1000 Spectrophotometer (Thermo Scientific, Wilmington, DE). The peptide thiol concentration was determined using a calibration curve made with acetyl cysteine. After 90 min, the samples were stored at -20 °C until purification. Purification and characterization of conjugates were performed using RP-HPLC and mass spectrometry analyses as previously described.

5.2.2.3.2 PNA-siRNA Hybridization and Characterization

PNA-binding siRNA was incubated with maleimide-PNA in a 20 mM HEPES buffer (pH 7.4) overnight at 37 °C. After incubation, the samples were analyzed by gel electrophoresis on a 4% agarose gel containing 0.5 μg ethidium bromide/mL and visualized on a Bio-Rad Gel Doc XR (Hercules, CA).

5.2.2.4 Mass Spectrometry

The molecular weight of the peptides, polymers and conjugate structures was determined using either electrospray ionization (ESI) mass spectrometry (MS) on a Thermo Finnigan LCQ MS or matrix assisted laser desorption ionization time of flight (MALDI-TOF) MS on a Bruker Daltonics Omniflex System. For ESI analysis, samples were dissolved at ~0.01 mg/mL in acetonitrile or methanol based on the solubility of the product to be analyzed. The matrix utilized for MALDI-TOF analysis was α-cyano-4-hydroxycinnamic acid (HCCA) (Sigma, St. Louis, MO) dissolved at a

concentration of 32 mg/mL in 50% ddH_2O and 50% acetonitrile. MS analysis was performed using a Bruker Daltonics Omniflex System (Billerica, MA).

5.2.3 Results and Discussion

Synthesis of PPP conjugates was approached by: (1) solution-phase and (2) solid-phase synthetic strategies. The following sections discuss some of the main points in each preparation.

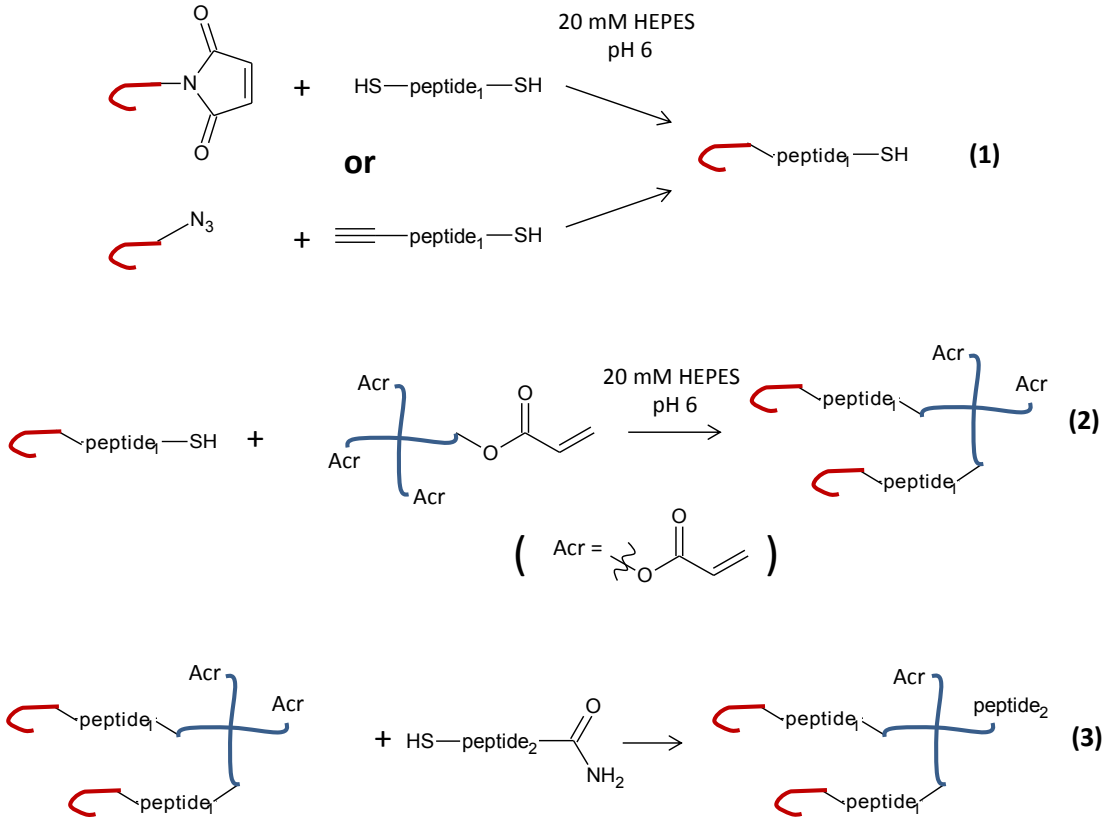

Figure 5.2 Solution-based approach to PPP conjugate formation. PNA (red); 4-arm star PEG (blue); peptide$_1$ = cathepsin L-cleavable peptide; peptide$_2$ = targeting/endosomolytic peptide sequence.

5.2.3.1 Solution-based Methods for PPP Preparation

The solution-phase approach to PPP preparation is shown in Figure 5.2. As outlined in this approach, the first stage of conjugate formation involves the coupling of a PNA and peptide via either a thiol-maleimide or alkyne-azide coupling strategy, which have both demonstrated high efficiency in preparation of bioconjugates.[33, 34] A cysteine terminated TAT peptide (TAT-C: NH_2-CGRKKRRQRRR-COOH) was used for initial proof of concept verification of the thiol-maleimide reaction. Thiol groups spontaneously react and couple preferentially with maleimides at acidic pH (e.g. pH < 6.5-7.5), however at higher pH (>8.0), maleimides will favor a reaction with primary amines (such as those on lysine and arginine residues).[35] Thus the reaction between maleimide-PNA and TAT-C peptide was performed in 20 mM HEPES, pH 7.4 to obtain the conjugate structure. RP-HPLC indicated complete conversion of maleimide PNA when using a 2-fold molar excess of thiol-functionalized peptide, which can be recovered for further reaction following RP-HPLC purification (Figure 5.3).

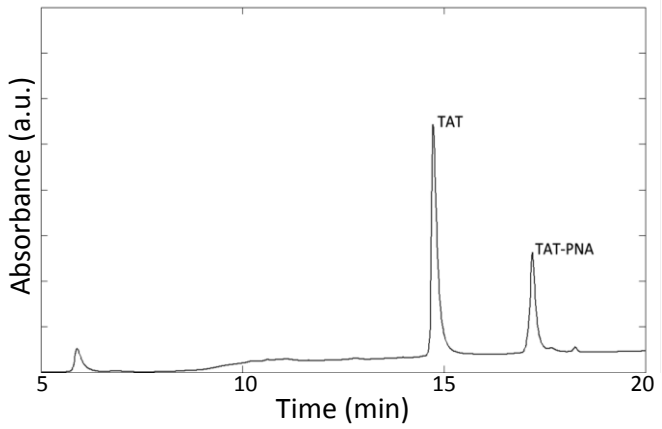

Figure 5.3 RP-HPLC of model thiol-maleimide reaction using TAT-C peptide and PNA-mal. The product was purified by RP-HPLC with a gradient of 0.1% TFA in ddH_2O (A) and 0.1% TFA in acetonitrile (B) as the mobile phase on a Viva C18 (4.2 mm × 150 mm, 5 µm diameter) column from Restek.

As a result of the successful demonstration of maleimide-thiol chemistry for PNA-peptide formation, the cathepsin L-cleavable peptide was prepared by SPPS. An important concern in the synthesis of the cathepsin L-cleavable sequence in this scheme (peptide$_1$: NH_2-CRDAKLKWGDRC-$CONH_2$) is its potential to either form dimers due to the multiple cysteines or undergo head-to-tail cyclization as a result of terminal cysteines. RP-HPLC of this cleavable sequence indicated a high purity peptide, which was collected for MS analysis. The peptide had an expected molecular weight of 1506.8 g/mol (Figure 5.4), however, mass spectrometry revealed ionization states corresponding to the formation or a disulfide bridged ring structure ($[M + H]^+$: 1504.7 g/mol,$[M + 2H]^{2+}$: 752.86, $[M + 3H]^{3+}$: 502.27) and quantification of free thiols suggested that < 10% free thiols were available for the reaction (Appendix C).

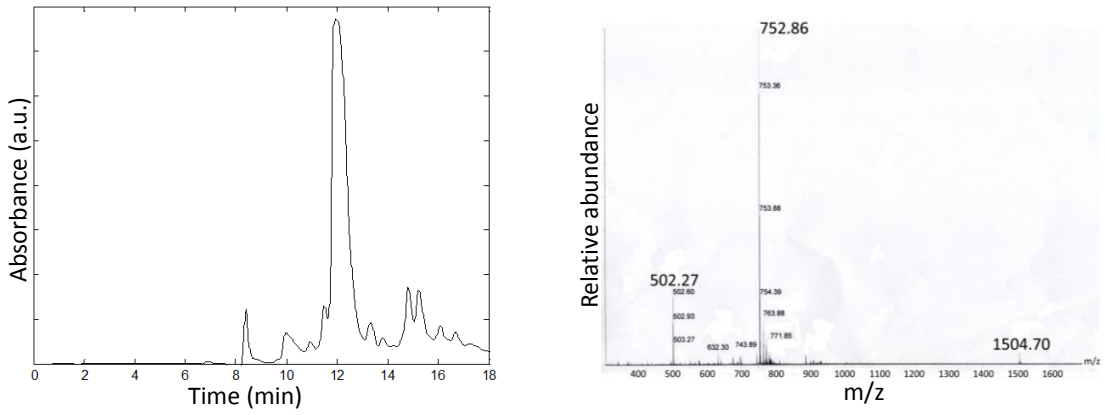

Figure 5.4 (a) RP-HPLC and (b) MALDI-TOF MS of cathepsin L-cleavable peptide (NH_2-CRDAKLKWGDRC-$CONH_2$).

Opening the ring via the use of a reducing agent is one potential route to enable this synthetic strategy for preparing the PNA-peptide conjugate. The reducing agent

tris-(2-carboxyethyl) phosphine (TCEP) was used to obtain a reduced peptide (Appendix C); however, removal of TCEP through RP-HPLC led to re-cyclization of the peptide. Furthermore, the known reactivity between maleimides and TCEP precluded the inclusion of the reducing agent in the PNA-peptide reaction (Appendix C).[36] Based on these results, an alternative coupling approach – alkyne-azide cycloaddition – was proposed for PNA-peptide conjugation.

The alkyne functionalized cathepsin L-cleavable sequence (NH_2-GCRDGAKLKĠG-$CONH_2$, where Ġ = propargylglycine) was prepared via SPPS and purified by RP-HPLC (Appendix C). The copper catalyzed Huisgen azide-alkyne cycloaddition (CuAAC) reaction (Scheme 2, step 1) has been used extensively in peptide chemistry due to the favorable reaction conditions, high efficiency and versatility of this chemical reaction.[37, 38] Additionally, the triazole formed in the reaction is particularly attractive due to its resistance to enzymatic degradation, hydrolysis, and oxidation.[38] CuAAC has been employed in peptide conjugation to biomolecules, polymers, nano-particles as well as in the preparation of cyclic peptides.[34, 39, 40] Thus, this synthetic scheme has the potential to provide improved efficacy for PPP formation following the CuAAC reaction.

Additional steps towards the solution phase preparation of PPP conjugates involved sequential conjugation and purification thiol-acrylate reactions between cysteine-containing peptides and a four-arm PEG acrylate. This 4-arm star polymer has previously demonstrated utility in the preparation of multifunctional carriers for gene delivery through efficient thiol-acrylate Michael's-type coupling.[32] Specifically, in the preparation of multifunctional DNA conjugates, Sakiyama-Elbert *et al*. investigated the effects of various peptide functionalities on the rates of conjugate

internalization, trafficking, and subsequent transfection.[32] As mentioned in Chapter 1, a number of peptide ligands have demonstrated significant utility in facilitating uptake of conjugated molecules.[41] For example, in the preparation of PEGylated siRNA/PEI nanoparticles with an RGD peptide ligand attached at the distal end of the polyethylene glycol (PEG), Woodle and coworkers effectively targeted tumor neovasculature to deliver siRNA inhibiting vascular endothelial growth factor receptor-2 (VEGF R2) expression. Specifically, through intravenous administration into tumor-bearing mice they demonstrated tumor-specific uptake, specific inhibition of protein expression within the tumor and inhibition of both tumor angiogenesis and growth rate.[41] Thus, an integrin binding 'RGD' peptide sequence, and the cell-penetrating TAT-C peptide were used in the preparation of peptide-PEG conjugates. The integrin binding sequence used in this study was NH_2-G**RGDSP**GDRCG-$CONH_2$, where serine and proline sequences were included due to conservation in the native motif of fibronectin, which has been implicated in carcinoma development.[42, 43]

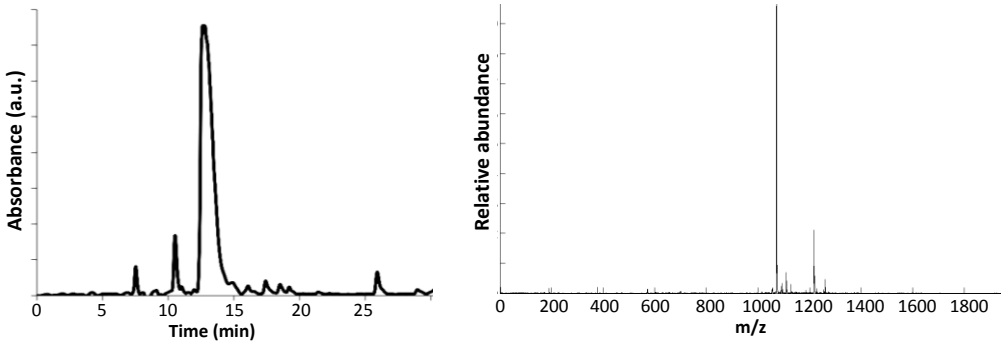

Figure 5.5 (a) RP-HPLC and (b) MALDI-TOF MS of integrin binding peptide (NH_2-GRGDSPGDRCG-$CONH_2$).

The integrin binding sequence was prepared by SPPS and subsequently purified via RP-HPLC and characterized by MS (Figure 5.5). Peptide-PEG conjugates were prepared using the TAT-C peptide via thiol-acrylate chemistry using a three-fold molar excess of peptide to preferentially target the preparation of a three-arm functionalized conjugate. Monitoring the extent of the thiol-acrylate reaction showed that the majority of free thiols reacted over the course of 90 min as shown in Figure 5.6. Quantification of peptide conversion indicated ~75 ± 6% conversion of free thiols in the TAT-C preparation. In the absence of PEG, disulfide bridge formation between peptides can possibly consume free thiols. However, the free thiol concentration remained constant based on Ellman's assay quantification of sulfhydryl groups suggesting that disulfide formation is significantly slower than the thiol-acrylate reaction.

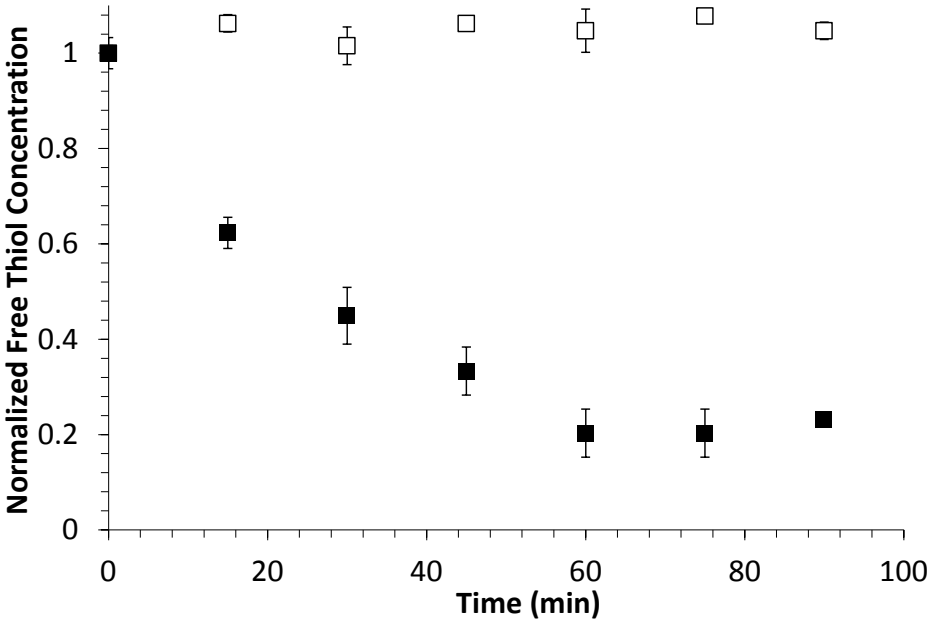

Figure 5.6 Representative data of normalized free thiol concentration over time when forming TAT-PEG conjugates. The concentration was determined using an Ellman's assay, and the thiol concentrations were normalized to the initial concentration in the solution. Experiments were performed with solutions of TAT peptide (white) and a mixture of TAT and PEG (solid). The data represent the mean ± std. error (n=3).

RP-HPLC of TAT-PEG conjugates indicated a mixture of structures. As shown in Figure 5.7, the peptide eluted off the column at approximately 12 min, and the PEG eluted off the column at approximately 38 min with a gradient of 1.25% acetonitrile/min. Various peptide-PEG derivatizations eluted between the peptide and PEG samples. A similar elution profile was seen for RGD-PEG conjugate structures (Appendix C).

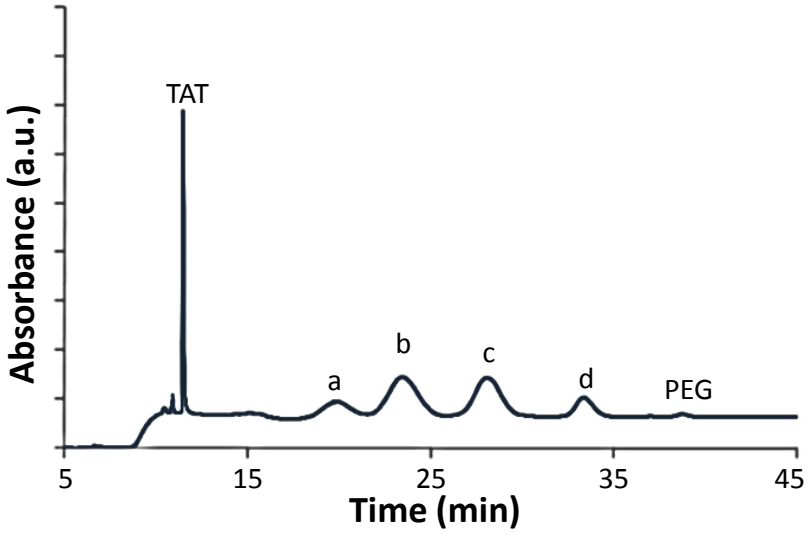

Figure 5.7 The RP-HPLC trace of a representative peptide-PEG reaction. The absorbance of the elutant was measured at 210 nm over time. Peptide-PEG fractions are (a) tetra-, (b) tri-, (c) di-, and (d) mono-functionalized PEG-peptides.

The various peaks were collected and analyzed by MALDI-TOF MS to confirm the identity of the compounds seen in RP-HPLC. As shown in Fig. 5.8, the various peptide-PEG conjugates were identified by the spacing of approximately 1,500 Da, which is the approximate molecular weight of the TAT-C peptide (1499.8 Da). It was found that the PEG with 4-arms functionalized with the TAT conjugate is peak a in Fig. 5.7, 3-arm functionalized PEG is peak b, 2-arm functionalized PEG is peak c, and 1-arm functionalized PEG is peak d. These purified structures can then be further reacted with additional peptide to create multi-functional vehicles.

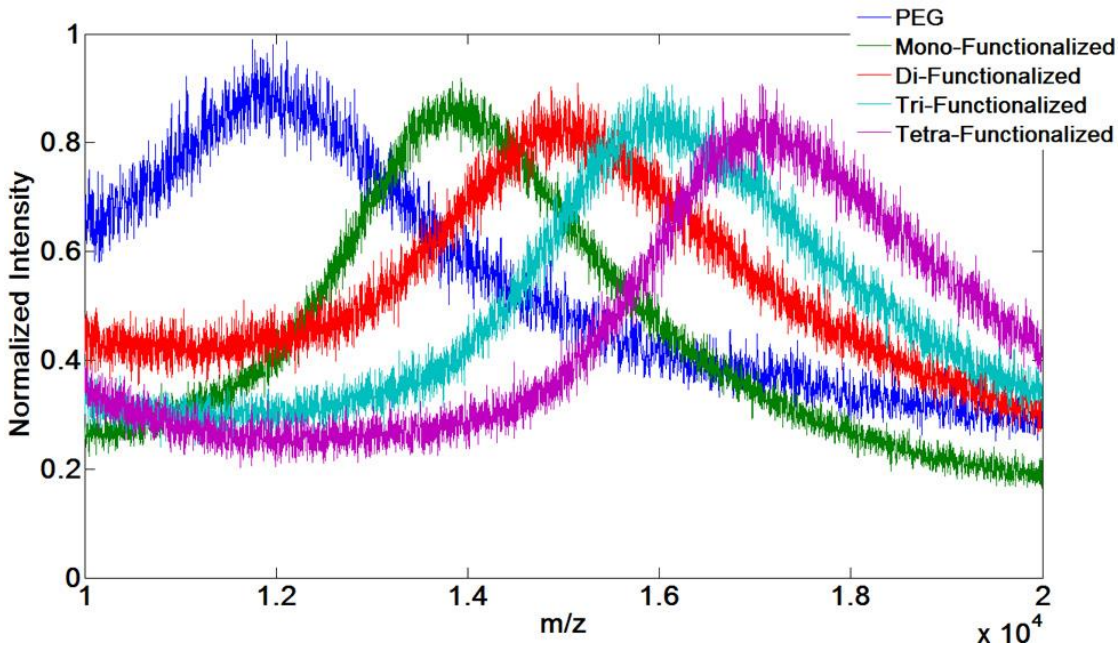

Figure 5.8 Molecular weight of the TAT-PEG conjugates as determined by MALDI-MS.

5.2.3.2 Partial Solid-phase Methods for PPP Preparation

Although solution-phase approaches provide a high efficiency coupling strategy for the preparation of bioconjugates, solid-phase preparation techniques are particularly attractive due to the ease of purification of prepared structures, the amenability to automation, and the potential to minimize losses due to the attachment to solid support. Specifically, the immobilization and conjugate growth on a resin bead during this process allows for easier removal of excess reactant or byproducts. PPP preparation using a solid-phase approach is outlined in Figure 5.9.

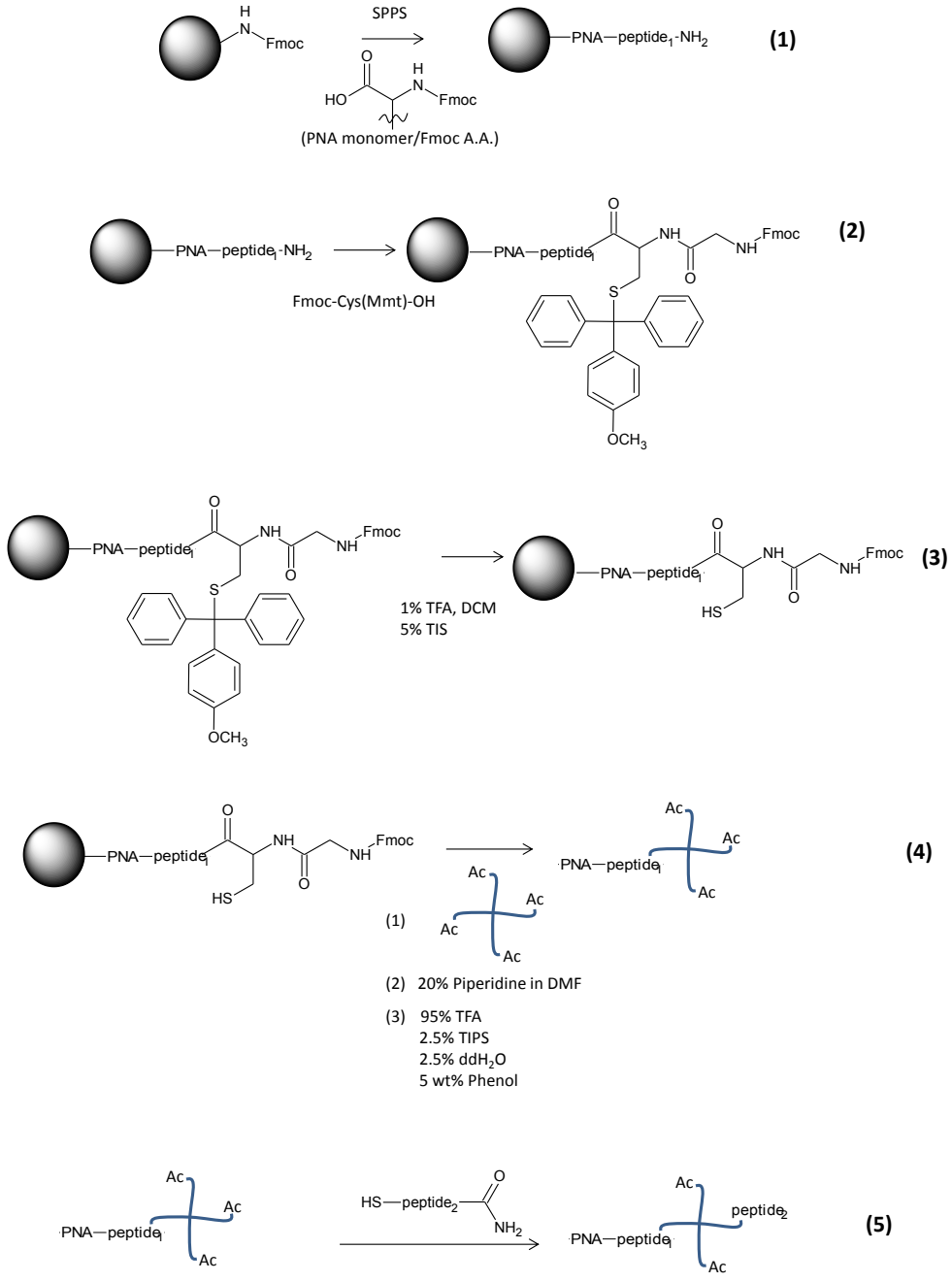

Figure 5.9 Solid-phase approach to PPP conjugate formation. PNA (red); 4-arm star PEG (blue); peptide$_1$ = cathepsin L-cleavable peptide; peptide$_2$ = targeting/endosomolytic peptide sequence.

The synthesis starts with the SPPS of the PNA (NH_2-OOTCTCTCTC-OOO-JTJTJTJT-$CONH_2$) followed by the addition of the cathepsin L-cleavable segment (or a linker fragment to be used as a control in cellular studies). Although stepwise elongation, in which the amino acids are connected step-by-step in turn, may be ideal for a number of short peptides less than 50 residues in length, a number of peptides resist facile synthesis. The difficulty in the preparation of these peptides may arise due to unfavorable solvation of the peptide chains on the solid support, as well as the structure of the growing peptide fragment up to that point of synthesis.[44] For example, sequences containing alanine, valine, isoleucine, methionine, aspartic acid or glutamine are prone to aggregation during chain growth.[44, 45] A number of strategies can be employed to improve the yield and efficiency of synthesis, such as the use of solid-phase resins demonstrating higher degrees of swelling during synthesis to better solvate the growing peptide chain. Fragment condensation provides another approach to improve the yield and efficiency of synthesis. Using this technique, protected peptide fragments are coupled in solution or to a growing peptide chain on the solid support allowing for rapid preparation of larger peptides.[46, 47] The use of purified fragments in this way can be particularly advantageous for synthesis and purification of long/difficult to synthesize peptides as the side products from incomplete couplings may be more easily removed as they differ by the size of the size of the fragment. Thus, in the preparation of PPPs using a solid-phase synthetic route, the cleavable peptide and non-cleavable control were synthesized on a hyperlabile H-glycine-2-chlorotrityl (H-Gly-2-ClTrt) resin so that they would be amenable to the fragment condensation approach.

The linker sequence (Fmoc-GGG-COOH) and protected cathepsin L-cleavable fragment (Fmoc-AK(Boc)LK(Boc)G-COOH) were synthesized via SPPS using a H-Gly-2-ClTrt resin to provide a carboxylic acid functionality of the C-terminus of the peptide for further coupling. These fragments were subsequently cleaved from the resin using mild conditions to ensure the preparation of protected fragments. The MS analysis of protected peptide fragments presents a challenge when the charged residues are shielded by protecting groups. In particular, these peptides become more difficult to ionize. As such, salt-doping techniques can be employed to direct the ionization of these fragments by adding an excess of the doping agent. Salt-doping of the protected linker and cleavable fragments using potassium chloride gave rise to intentionally formed K^+ adducts (Figure 5.9) demonstrating the successful preparation of these protected fragments.

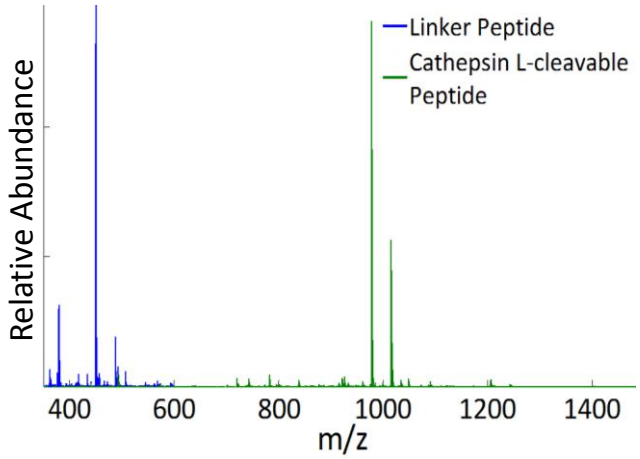

Figure 5.10 Linker (Fmoc-GGG-COOH) and Cathepsin L-cleavable (Fmoc-AK(Boc)LK(Boc)G-COOH) sequences were synthesized on a H-Gly-2-ClTrt resin. Peptides were dissolved at 10 mg/mL in DMF. MALDI-TOF mass spectra were obtained for the peptides using α–Cyano-3-hydroxycinnamic acid as the matrix with KCl as an additive, giving rise to intentionally formed K^+ adducts.

Synthesis of the PNA was subsequently performed on the ChemMatrix rink amide resin due to its demonstrated improved solvation compared to polystyrene-based solid-phase supports used in traditional synthesis approaches.[48] The preparation of PNAs is often a difficult and laborious process involving repeated couplings and a large excess of Fmoc/Bhoc monomers to obtain a high purity product.[49, 50] However, strategies such as lowered resin loading (lower functional amines on resin surface for PNA growth), repeated coupling steps, and increased monomer concentration have demonstrated utility in improving PNA synthesis yields.[49, 50] Additionally, yields may be improved by incorporating capping steps in the synthetic strategy. This involves the treatment of unreacted/truncated fragments with a large excess of a highly reactive, unhindered acid derivative, usually acetic anhydride or benzoyl chloride and pyridine, to limit subsequent growth of unwanted deletion sequences.[51] The PNA chain was prepared via SPPS and a small fraction was cleaved from resin for characterization prior to the fragment condensation reaction.

As shown in Figure 5.10, analysis of synthesized PNA resulted in a broad RP-HPLC peak of the crude PNA. The main fraction (10 - 25 min) was collected for subsequent MS analysis. It is of note that PNA sequences are much more difficult to analyze than their peptide analogues due to their neutral backbone. The synthesized PNA showed limited ionization in MS techniques despite the addition of numerous doping salts. A number of studies have reported the development of PNAs with charged groups flanking the PNA sequence. Improved ionization may potentially be possible by the incorporation of additional cationic residues in the peptide nucleic acid, which would involve a slight modification in the synthetic strategy. Cationic

residues may be incorporated at either terminus of the PNA to promote improved ionization.

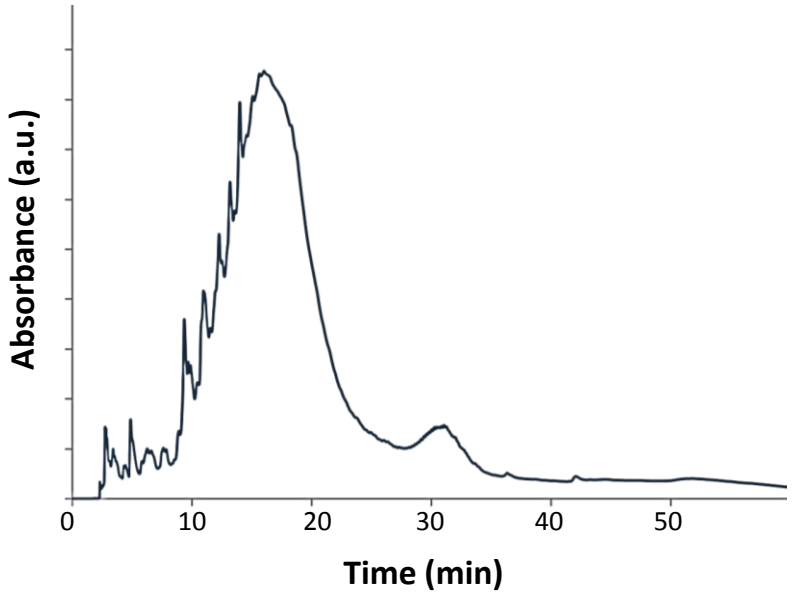

Figure 5.11 Validation of PNA synthesis via RP-HPLC. (PNA: maleimide-OOTCTCTCTC-OOO-JTJTJTJT-CONH2, where O = 8-amino-3,6-dioxaoctanoic acid and J = pseudoisocytosine).

5.2.3.3 PNA-siRNA Hybridization and Characterization

PNAs are nucleic acid analogs that contain a peptide backbone and can hydrogen bond to complementary DNA (or RNA) via either conventional Watson-Crick base pairing in the anti-parallel direction or Hoogsteen base pairing in the parallel direction. An attractive feature of PNA hybridization is the improved thermal stability conferred onto duplexes formed by these structures due to the lack of electrostatic interactions.[52] Furthermore, symmetric PNA oligomers linked by a flexible spacer have been shown to form a stable triplex with complementary nucleobases.[26, 52] Studies have demonstrated that conjugation of molecules to the 5'

end of the sense strand of siRNA does not alter intracellular activity and RNAi.[53-55] Thus, siRNAs were designed with a 5'-sense extension to facilitate hybridization with PNA.

PNA-binding and non-binding siRNA sequences were incubated with PNA over a range of ratios and the resulting mixtures were analyzed via electrophoresis to validate the hybridization reaction (Figure 5.12). As anticipated, there was no observed change in mobility of the non-binding siRNA (left), yet hybridization using a PNA-binding siRNA(right) indicated a reduced mobility of migrating siRNA with PNA incorporation. Furthermore, continued addition of PNA resulted in a disappearance of the original sense-extended siRNA band as more of the siRNA/PNA triplex is formed. Saturation of siRNA is observed at mole ratios above 1, which is anticipated given the single binding site (consisting of 8 nucleotides) on each siRNA molecule.

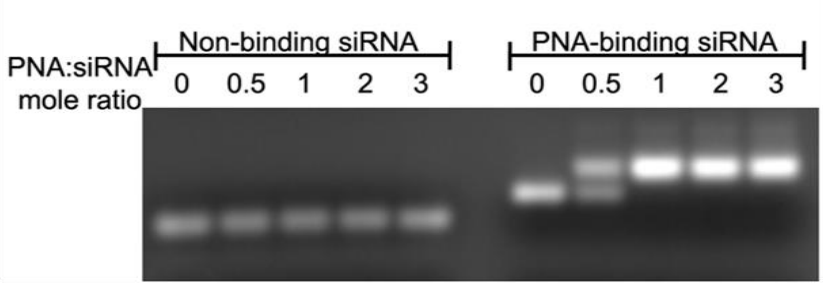

Figure 5.12 siRNA-PNA Conjugation. Anti-GAPDH PNA-binding and non-PNA-binding siRNAs were incubated with PNA and analyzed by agarose gel electrophoresis.

5.2.3.4 Advantages and Disadvantages of Selected Solution- and Solid-phase PPP Preparation Techniques

While the synthetic approaches outlined in this chapter both demonstrate utility in PPP preparation, several factors should be considered for further pursuit of either method. Solution-phase approaches offer high coupling yields during individual coupling steps. However, approaches that are entirely solution-based require careful consideration of reaction conditions (and reactive groups) that are compatible with the peptide side chains and PNA nucleobases to limit unwanted byproducts that may be difficult (or impossible) to remove. Additionally, the development of complicated structures – with numerous functional segments and reaction steps – necessitates repetitive purification, which may cause substantial losses in product preparation.

Solid-phase methods for PNA-peptide synthesis have seen increased use as a facile strategy for preparing bionconjugate strutcures.[56-58] However, the small losses in each of the coupling and deprotection steps place a practical limit on the final conjugate length. Additionally, truncations during synthesis may result in difficult purification and a low overall yield. The fragment condensation/block coupling approach outlined in this work offers a promising strategy to circumvent challenges resulting from truncated sequences and coupling losses. However, a number of factors must be considered in using this approach. Specifically, the protected peptide block may have limited solubility in the synthesis solvent leading to slow coupling and poor yields. Additionally, protected fragments place steric constraints on fragment condensation.

It is of note that the solid phase approach detailed in this work offers improved versatility over the purely solution-based synthetic approach, and provides a promising strategy for PPP preparation. Specifically, the synthesis can be performed on the solid

support as well as validated on resin at steps throughout the PNA-peptide chain growth. Additionally, modified amino acids – such as those with alkyne or azide functionalized residues – can be incorporated to allow for an efficient orthogonal conjugation strategy. In this way the preparation of the full multi-functional conjugate can realize the benefits of both solution- and solid-phase strategies.

REFERENCES

1. Shen, H.; Sun, T.; Ferrari, M., Nanovector delivery of siRNA for cancer therapy. *Cancer Gene Ther* **2012,** 19, (6), 367-73.

2. Okumura, A.; Pitha, P. M.; Harty, R. N., ISG15 inhibits Ebola VP40 VLP budding in an L-domain-dependent manner by blocking Nedd4 ligase activity. *Proc Natl Acad Sci U S A* **2008,** 105, (10), 3974-9.

3. Morrissey, D. V.; Lockridge, J. A.; Shaw, L.; Blanchard, K.; Jensen, K.; Breen, W.; Hartsough, K.; Machemer, L.; Radka, S.; Jadhav, V.; Vaish, N.; Zinnen, S.; Vargeese, C.; Bowman, K.; Shaffer, C. S.; Jeffs, L. B.; Judge, A.; MacLachlan, I.; Polisky, B., Potent and persistent in vivo anti-HBV activity of chemically modified siRNAs. *Nat Biotechnol* **2005,** 23, (8), 1002-7.

4. Resnier, P.; Montier, T.; Mathieu, V.; Benoit, J. P.; Passirani, C., A review of the current status of siRNA nanomedicines in the treatment of cancer. *Biomaterials* **2013,** 34, (27), 6429-43.

5. Aagaard, L.; Rossi, J. J., RNAi therapeutics: principles, prospects and challenges. *Adv Drug Deliv Rev* **2007,** 59, (2-3), 75-86.

6. Jana, S.; Chakraborty, C.; Nandi, S.; Deb, J. K., RNA interference: potential therapeutic targets. *Appl Microbiol Biotechnol* **2004,** 65, (6), 649-57.

7. Takei, Y.; Kadomatsu, K.; Yuzawa, Y.; Matsuo, S.; Muramatsu, T., A small interfering RNA targeting vascular endothelial growth factor as cancer therapeutics. *Cancer Res* **2004,** 64, (10), 3365-70.

8. Adams, D.; Coelho, T.; Suhr, O.; Conceicao, I.; Waddington-Cruz, x. M.; Schmidt, H.; Campistol, J.; Pouget, J.; Buades, J.; Falzone, R.; Harrop, J.; De Frutos, R.; Butler, J.; Cehelsky, J.; Nochur, S.; Vaishnaw, A.; Gollob, J., Interim results form Phase II trial of ALN-TTR02, a novel RNAi therapeutic for the treatment of familial amyloidotic polyneuropathy. In *2013 Periferal Nerve Society Meeting*, Brittany, France, 2013.

9. Davis, M. E.; Zuckerman, J. E.; Choi, C. H.; Seligson, D.; Tolcher, A.; Alabi, C. A.; Yen, Y.; Heidel, J. D.; Ribas, A., Evidence of RNAi in humans from systemically administered siRNA via targeted nanoparticles. *Nature* **2010,** 464, (7291), 1067-70.

10. Wu, W.; Jiang, X., Long-Circulating Polymeric Drug Nanocarriers. In *Functional Nanoparticles for Bioanalysis, Nanomedicine, and Bioelectronic Devices*, 2012; Vol. 2, pp 27-36.

11. Kunath, K.; von Harpe, A.; Petersen, H.; Fischer, D.; Voigt, K.; Kissel, T.; Bickel, U., The structure of PEG-modified poly(ethylene imines) influences biodistribution and pharmacokinetics of their complexes with NF-kappaB decoy in mice. *Pharm Res* **2002,** 19, (6), 810-7.

12. Shi, J.; Schellinger, J. G.; Pun, S. H., Engineering biodegradable and multifunctional peptide-based polymers for gene delivery. *J Biol Eng* **2013,** 7, (1), 25.

13. Zhou, J.; Shum, K. T.; Burnett, J. C.; Rossi, J. J., Nanoparticle-Based Delivery of RNAi Therapeutics: Progress and Challenges. *Pharmaceuticals (Basel)* **2013,** 6, (1), 85-107.

14. Hubbell, J. A.; Langer, R., Translating materials design to the clinic. *Nat Mater* **2013,** 12, (11), 963-6.

15. Choi, C. H.; Alabi, C. A.; Webster, P.; Davis, M. E., Mechanism of active targeting in solid tumors with transferrin-containing gold nanoparticles. *Proc Natl Acad Sci U S A* **2010,** 107, (3), 1235-40.

16. Desgrosellier, J. S.; Cheresh, D. A., Integrins in cancer: biological implications and therapeutic opportunities. *Nat Rev Cancer* **2010,** 10, (1), 9-22.

17. Zitzmann, S.; Ehemann, V.; Schwab, M., Arginine-glycine-aspartic acid (RGD)-peptide binds to both tumor and tumor-endothelial cells in vivo. *Cancer Res* **2002,** 62, (18), 5139-43.

18. Frankel, A. D.; Pabo, C. O., Cellular uptake of the tat protein from human immunodeficiency virus. *Cell* **1988,** 55, (6), 1189-93.

19. Lee, J. Y.; Choi, Y. S.; Suh, J. S.; Kwon, Y. M.; Yang, V. C.; Lee, S. J.; Chung, C. P.; Park, Y. J., Cell-penetrating chitosan/doxorubicin/TAT conjugates for efficient cancer therapy. *Int J Cancer* **2011,** 128, (10), 2470-80.

20. Green, M.; Loewenstein, P. M., Autonomous functional domains of chemically synthesized human immunodeficiency virus tat trans-activator protein. *Cell* **1988,** 55, (6), 1179-88.

21. Niu, R.; Zhao, P.; Wang, H.; Yu, M.; Cao, S.; Zhang, F.; Chang, J., Preparation, characterization, and antitumor activity of paclitaxel-loaded folic acid modified and TAT peptide conjugated PEGylated polymeric liposomes. *J Drug Target* **2011,** 19, (5), 373-81.

22. Shim, M. S.; Kwon, Y. J., Acid-responsive linear polyethylenimine for efficient, specific, and biocompatible siRNA delivery. *Bioconjug Chem* **2009,** 20, (3), 488-99.

23. Zhang, W.; Wang, S.; Wang, Q.; Yang, Z.; Pan, Z.; Li, L., Overexpression of cysteine cathepsin L is a marker of invasion and metastasis in ovarian cancer. *Oncol Rep* **2014,** 31, (3), 1334-42.

24. Jean, D.; Rousselet, N.; Frade, R., Expression of cathepsin L in human tumor cells is under the control of distinct regulatory mechanisms. *Oncogene* **2006,** 25, (10), 1474-84.

25. Turk, V.; Turk, B.; Guncar, G.; Turk, D.; Kos, J., Lysosomal cathepsins: structure, role in antigen processing and presentation, and cancer. *Adv Enzyme Regul* **2002,** 42, 285-303.

26. Millili, P. G.; Yin, D. H.; Fan, H.; Naik, U. P.; Sullivan, M. O., Formulation of a Peptide Nucleic Acid Based Nucleic Acid Delivery Construct. *Bioconjug Chem* **2010**.

27. Elbashir, S. M.; Lendeckel, W.; Tuschl, T., RNA interference is mediated by 21- and 22-nucleotide RNAs. *Genes Dev* **2001,** 15, (2), 188-200.

28. Cioca, D. P.; Aoki, Y.; Kiyosawa, K., RNA interference is a functional pathway with therapeutic potential in human myeloid leukemia cell lines. *Cancer Gene Ther* **2003,** 10, (2), 125-33.

29. Lau, N. C.; Lim, L. P.; Weinstein, E. G.; Bartel, D. P., An abundant class of tiny RNAs with probable regulatory roles in Caenorhabditis elegans. *Science* **2001,** 294, (5543), 858-62.

30. Chiu, Y. L.; Rana, T. M., siRNA function in RNAi: a chemical modification analysis. *Rna* **2003,** 9, (9), 1034-48.

31. Choung, S.; Kim, Y. J.; Kim, S.; Park, H. O.; Choi, Y. C., Chemical modification of siRNAs to improve serum stability without loss of efficacy. *Biochem Biophys Res Commun* **2006,** 342, (3), 919-27.

32. Schmieder, A. H.; Grabski, L. E.; Moore, N. M.; Dempsey, L. A.; Sakiyama-Elbert, S. E., Development of novel poly(ethylene glycol)-based vehicles for gene delivery. *Biotechnol Bioeng* **2007,** 96, (5), 967-76.

33. Ghosh, S. S.; Kao, P. M.; McCue, A. W.; Chappelle, H. L., Use of maleimide-thiol coupling chemistry for efficient syntheses of oligonucleotide-enzyme conjugate hybridization probes. *Bioconjug Chem* **1990,** 1, (1), 71-6.

34. Presolski, S. I.; Hong, V. P.; Finn, M. G., Copper-Catalyzed Azide-Alkyne Click Chemistry for Bioconjugation. *Curr Protoc Chem Biol* **2011,** 3, (4), 153-162.

35. Brewer, C. F.; Riehm, J. P., Evidence for possible nonspecific reactions between N-ethylmaleimide and proteins. *Analytical Biochemistry* **1967,** 18, (2), 248 - 255.

36. Shafer, D. E.; Inman, J. K.; Lees, A., Reaction of Tris(2-carboxyethyl)phosphine (TCEP) with maleimide and alpha-haloacyl groups: anomalous elution of TCEP by gel filtration. *Anal Biochem* **2000,** 282, (1), 161-4.

37. Presolski, S. I.; Hong, V.; Cho, S. H.; Finn, M. G., Tailored ligand acceleration of the Cu-catalyzed azide-alkyne cycloaddition reaction: practical and mechanistic implications. *J Am Chem Soc* **2010,** 132, (41), 14570-6.

38. Li, X., Click to join peptides/proteins together. *Chem Asian J* **2011,** 6, (10), 2606-16.

39. Kaiser, J.; Kinderman, S. S.; van Esseveldt, B. C.; van Delft, F. L.; Schoemaker, H. E.; Blaauw, R. H.; Rutjes, F. P., Synthetic applications of aliphatic unsaturated alpha-H-alpha-amino acids. *Org Biomol Chem* **2005,** 3, (19), 3435-67.

40. El-Sagheer, A. H.; Brown, T., Click nucleic acid ligation: applications in biology and nanotechnology. *Acc Chem Res* **2012,** 45, (8), 1258-67.

41. Schiffelers, R. M.; Ansari, A.; Xu, J.; Zhou, Q.; Tang, Q.; Storm, G.; Molema, G.; Lu, P. Y.; Scaria, P. V.; Woodle, M. C., Cancer siRNA therapy by tumor selective delivery with ligand-targeted sterically stabilized nanoparticle. *Nucleic Acids Res* **2004,** 32, (19), e149.

42. Garrigues, H. J.; Rubinchikova, Y. E.; Dipersio, C. M.; Rose, T. M., Integrin alphaVbeta3 Binds to the RGD motif of glycoprotein B of Kaposi's sarcoma-associated herpesvirus and functions as an RGD-dependent entry receptor. *J Virol* **2008,** 82, (3), 1570-80.

43. Han, S.; Khuri, F. R.; Roman, J., Fibronectin stimulates non-small cell lung carcinoma cell growth through activation of Akt/mammalian target of rapamycin/S6 kinase and inactivation of LKB1/AMP-activated protein kinase signal pathways. *Cancer Res* **2006,** 66, (1), 315-23.

44. Krchnak, V.; Flegelova, Z.; Vagner, J., Aggregation of resin-bound peptides during solid-phase peptide synthesis. Prediction of difficult sequences. *Int J Pept Protein Res* **1993,** 42, (5), 450-4.

45. van Woerkom, W. J.; van Nispen, J. W., Difficult couplings in stepwise solid phase peptide synthesis: predictable or just a guess? *Int J Pept Protein Res* **1991,** 38, (2), 103-13.

46. Nyfeler, R., Peptide synthesis via fragment condensation. *Methods Mol Biol* **1994,** 35, 303-16.

47. Narita, M.; Isokawa, S.; Nagasawa, S.; Ishijima, T., Peptide synthesis by fragment condensation on a soluble polymer support. 8. Maximum peptide chain lengths of carboxyl component peptides for effective coupling reactions with amino component peptides anchored to soluble and cross-linked polystyrene supports. *Macromolecules* **1987,** 20, (9), 2306-2307.

48. Garcia-Martin, F.; Quintanar-Audelo, M.; Garcia-Ramos, Y.; Cruz, L. J.; Gravel, C.; Furic, R.; Cote, S.; Tulla-Puche, J.; Albericio, F., ChemMatrix, a

poly(ethylene glycol)-based support for the solid-phase synthesis of complex peptides. *J Comb Chem* **2006,** 8, (2), 213-20.

49. Thomson, S. A.; Josey, J. A.; Cadilla, R.; Gaul, M. D.; Hassman, C. F.; Luzzio, M. J.; Pipe, A. J.; Reed, K. L.; Ricca, D. J.; Wiethe, R. W.; Noble, S. A., Fmoc mediated synthesis of Peptide Nucleic Acids. *Tetrahedron* **1995,** 51, (22), 6179 - 6194.

50. Joshi, R.; Jha, D.; Su, W.; Engelmann, J., Facile synthesis of peptide nucleic acids and peptide nucleic acid-peptide conjugates on an automated peptide synthesizer. *J Pept Sci* **2011,** 17, (1), 8-13.

51. Amblard, M.; Fehrentz, J. A.; Martinez, J.; Subra, G., Methods and protocols of modern solid phase Peptide synthesis. *Mol Biotechnol* **2006,** 33, (3), 239-54.

52. Chakrabarti, M. C.; Schwarz, F. P., Thermal stability of PNA/DNA and DNA/DNA duplexes by differential scanning calorimetry. *Nucleic Acids Res* **1999,** 27, (24), 4801-6.

53. McNamara, J. O., 2nd; Andrechek, E. R.; Wang, Y.; Viles, K. D.; Rempel, R. E.; Gilboa, E.; Sullenger, B. A.; Giangrande, P. H., Cell type-specific delivery of siRNAs with aptamer-siRNA chimeras. *Nat Biotechnol* **2006,** 24, (8), 1005-15.

54. Endoh, T.; Sisido, M.; Ohtsuki, T., Cellular siRNA delivery mediated by a cell-permeant RNA-binding protein and photoinduced RNA interference. *Bioconjug Chem* **2008,** 19, (5), 1017-24.

55. Lorenz, C.; Hadwiger, P.; John, M.; Vornlocher, H. P.; Unverzagt, C., Steroid and lipid conjugates of siRNAs to enhance cellular uptake and gene silencing in liver cells. *Bioorg Med Chem Lett* **2004,** 14, (19), 4975-7.

56. Sazani, P.; Gemignani, F.; Kang, S. H.; Maier, M. A.; Manoharan, M.; Persmark, M.; Bortner, D.; Kole, R., Systemically delivered antisense oligomers upregulate gene expression in mouse tissues. *Nat Biotechnol* **2002,** 20, (12), 1228-33.

57. Awasthi, S. K.; Nielsen, P. E., Parallel synthesis of PNA-peptide conjugate libraries. *Comb Chem High Throughput Screen* **2002,** 5, (3), 253-9.

58. Tian, X.; Wickstrom, E., Continuous solid-phase synthesis and disulfide cyclization of peptide-PNA-peptide chimeras. *Org Lett* **2002,** 4, (23), 4013-6.

Chapter 6

CONCLUSIONS AND FUTURE RECOMMENDATIONS

6.1 Summary and Future Directions

Extensive research surrounding non-viral carriers has led to several promising strategies for delivering nucleic acids, and has highlighted multiple potential opportunities for improved design. However, an incomplete understanding and control of the assembly, subcellular trafficking, and disassembly of these carriers has limited their clinical and commercial realization. This dissertation presents novel design approaches and mechanistic studies to improve the current understanding of nucleic acid assembly-and-release behavior in non-viral carriers. Specifically, a systematic exploration of a model delivery approach highlighted the impact of structural changes on polyplex assembly and stability. Additionally, two novel stimuli-responsive approaches were investigated to provide improved spatiotemporal control in the delivery of siRNA. The general outline of this work can be seen in Figure 6.1.

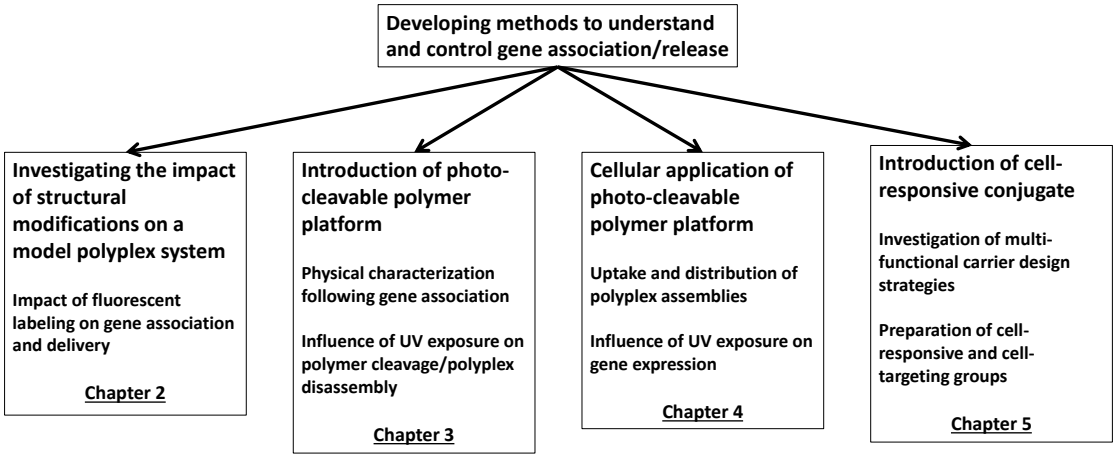

Figure 6.1 Outline of investigations of the gene association and release of non-viral carriers

Numerous to attempts to elucidate the intracellular trafficking of non-viral vehicles have involved the development of modified carriers – with fluorescent, radioactive or electron-dense markers – to probe cellular delivery and endocytic processing, yet few studies explore the effects of these structural modifications on their ultimate function. Thus, in Chapter 2, the importance of understanding structure/function relationships in gene delivery carriers was highlighted. Specifically, a systematic study of a dye-labeled model delivery vehicle, DNA-PEI-Oregon Green 488, was performed to determine the effects on endocytic processing of routinely used hydrophobic probes. Polyplexes were prepared at varying N/P ratios where the amine/cationic component contained mixtures of PEI and PEI-488 (reported as the % of incorporated PEI-488).

In these studies, weakened gene association was observed as a result of the incorporation of the hydrophobic fluorescent label. Thus, the effects of reduced binding interactions and increased hydrophobicity on extra- and intracellular polyplex

stability and endocytic processing were determined. Through DLS analysis, this weakened packaging efficiency was manifested in structures with similar size but increasing dispersity. Furthermore, *in vitro* studies showed that the cellular environment was able to prematurely unpackage the loosened structures. These studies exposed instabilities and differences in hydrophobicity in the polyplexes that were not detectable by DLS. Specifically, fluorescence microscopy revealed the formation of extracellular aggregates in formulations prepared with greater than 50% PEI-488 label that were unable to efficiently enter cells (Figure 6.2).

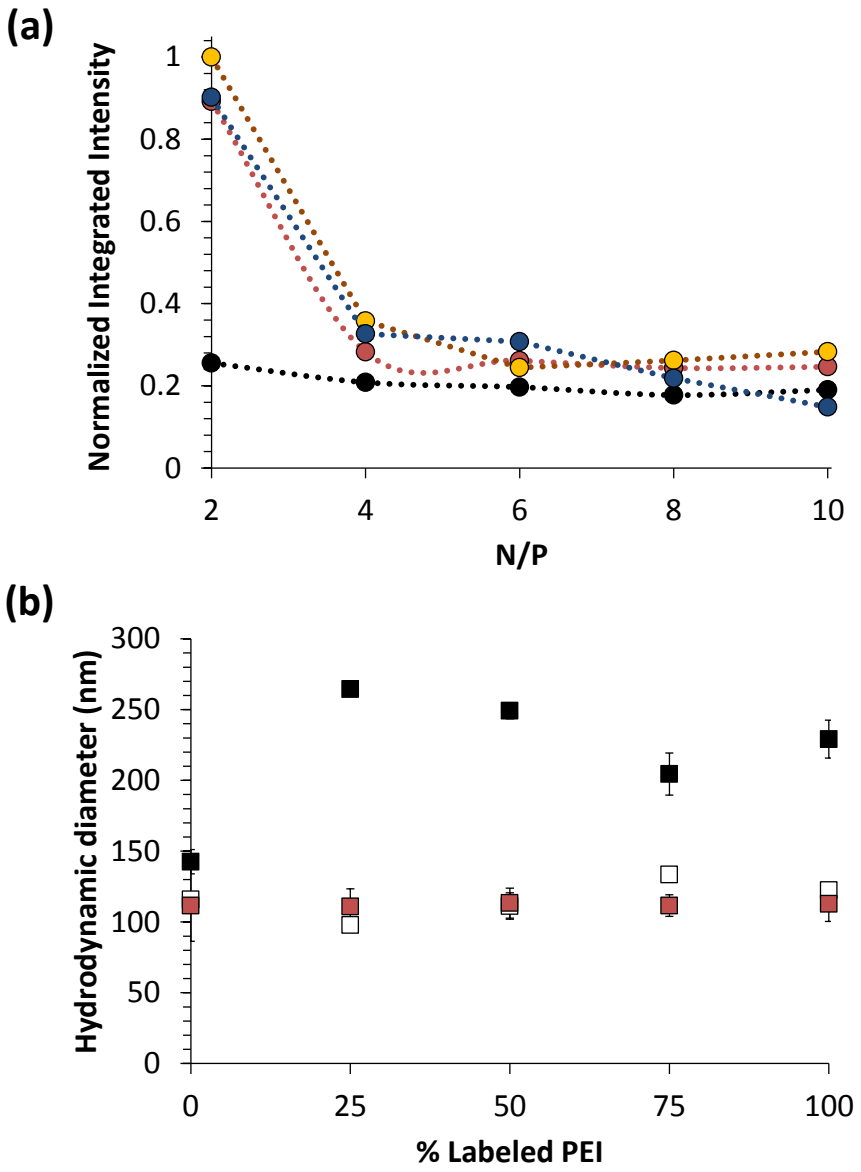

Figure 6.2 **Exploring the structure/function relationship of fluorescent polymer carriers. (a) Quantification of ethidium bromide fluorescence for polyplexes containing unmodified PEI (black), 25% PEI-488 (red), 50% PEI-488 (yellow), and 100% PEI-488 (blue). (b) Uptake of modified DNA delivery structures at N/P 4 (black), N/P = 6 (white), and N/P = 8 (red).**

These results indicate that understanding structure/function relationships is a critical requirement in designing model materials to explore the assembly and endocytic processing of current nucleic acid delivery strategies. Furthermore, these studies identify the need for continued exploration of polyplex assembly and trafficking. Numerous studies have noted heterogeneity in polyplex structures as a result of standard vortex or pipet mixing techniques.[1] Thus, the step-wise preparation of these polyplexes through the vortex mixing technique outlined in Chapter 2 is one potential area for study. Systematic changes in the formulation method of these polyplexes – adjustments in the order of mixing, etc. – and subsequent analysis using the studies outlined in Chapter 2 may identify improved preparation methods for controlling the delivery of these non-viral carriers. Additionally, a logical next step in this study is to explore the trafficking of these structures through intracellular organelle staining techniques using the "pulse-chase" strategy as outlined in Chapter 2.

Having identified the importance of understanding and controlling gene association, material structures were developed to both stably binding and controllably release nucleic acids. Thus, in Chapter 3, fundamental engineering tools were extended to the rational design of block copolymers (BCPs) for controlling gene association and nucleic acid presentation to cells. In this study, a novel cationic polymer was designed with functional capabilities for (1) efficient nucleic acid complexation into polyplexes; (2) minimized charge content to retain binding; (3) salt and serum stability; and (4) triggered nucleic acid release.

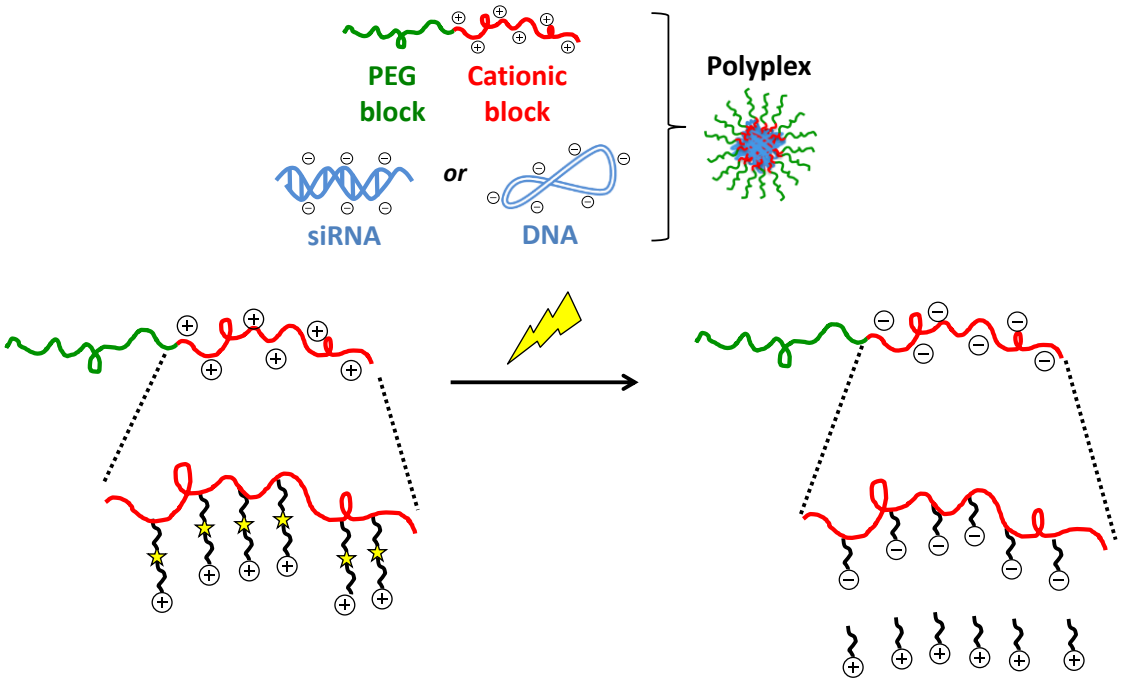

Figure 6.3 A photo-cleavable polymer carrier for controlling DNA/siRNA association and release.

The polymer consisted of a non-fouling PEG block to form a stealth coating corona following complexation and a novel photo-responsive block with pendant amines to facilitate tunable, salt-stable NA complexation and light-activated release as shown in Figure 6.3. The polymer was synthesized with tunable block lengths and narrow molecular weight distributions. Furthermore, electrophoresis and scattering studies indicated the ability to effectively complex DNA into salt-stable polyplexes with sizes appropriate for cellular internalization. In studies aimed at promoting polyplex disassembly, irradiation with UV light cleaved the *o*-NB ester and facilitated DNA release. Considering the favorable complexation and release of DNA, Chapter 4 discusses the influence of cationic block length on nucleic acid encapsulation and

release, and the ability of these materials to provide spatiotemporal release in NIH/3T3 cells.

In Chapter 4, a copolymer design and polyplex assembly condition were sought to promote the formation of nuclease inaccessible siRNA structures with the capacity for light-triggered intracellular release. Based on the weaker binding of siRNA assemblies compared to DNA delivery structures, [2] it was hypothesized that PEG-*b*-P(APNBMA)$_n$ would form polyplexes with both strong electrostatic association and an enhanced capacity for light-triggered release. As anticipated, electrophoresis analysis of preparations using PEG-*b*-P(APNBMA)$_{23.6}$ revealed efficient siRNA complexation. Conversely, PEG-*b*-P(APNBMA)$_{7.9}$ interactions were insufficient to yield efficient polyplex structures. Further study of siRNA/PEG-*b*-P(APNBMA)$_{23.6}$ revealed that these salt- and serum-stable structures could effectively liberate siRNA, as seen in electrophoresis, following as little as 20 min of light exposure. Additionally, the internalization of fluorescently labeled structures revealed favorable cytoplasmic distribution of these polyplexes following a 3 h transfection and high levels of uptake compared to transfections performed with Lipofectamine lipoplexes. Thus, combining electrophoresis and microscopy observations, gene silencing experiments were performed to determine the effects on gene silencing of UV-induced polyplex disassembly. These experiments showed that triggered siRNA release within the cytoplasm stimulated a ~50% reduction in targeted protein levels (Figure 6.4).

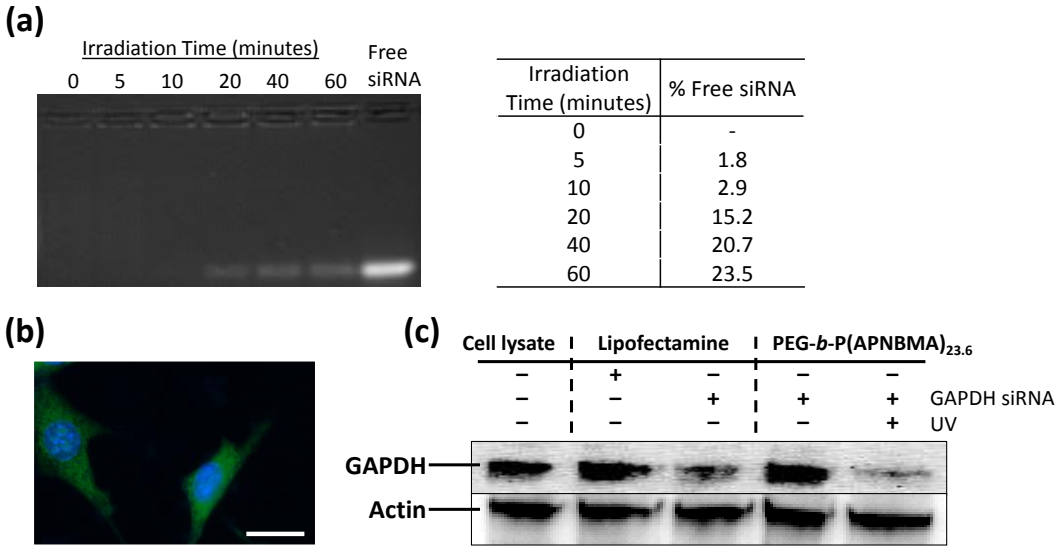

Irradiation Time (minutes)	% Free siRNA
0	-
5	1.8
10	2.9
20	15.2
40	20.7
60	23.5

Figure 6.4 Application of photo-cleavable PEG-*b*-P(APNBMA)$_{23.6}$ for siRNA release. (a) Representative image of siRNA release and quantification of ethidium bromide fluorescence intensity of siRNA band, (b) cellular distribution of YOYO-1 iodide labeled siRNA polyplexes (green) following 3 hour transfection, and (c) protein expression following UV irradiation of treated cells. Cell nuclei stained with Hoescht dye (blue).

The favorable results of these studies necessitate further exploration of the PEG-*b*-P(APNBMA)$_n$ platform for NA delivery. First, the unpackaging of these structures in cell-free and *in vitro* settings should be investigated in additional detail. Through the use of fluorescent tags for nucleic acid and polymer labeling, Förster resonance energy transfer (FRET) studies can be utilized to provide detailed information on the disassembly of these structures following exposure to a UV trigger.

In vitro studies can provide complementary details on the unpackaging of these structures. In previous studies in the Sullivan group nuclear microinjection enabled the exploration of the kinetics of DNA unpackaging and subsequent protein expression using green fluorescent protein (GFP) encoding DNA as therapeutic cargo.[3] Similar

studies using this UV cleavable polymer could provide valuable insight into the utility of this photo-cleavable group (and UV treatment) on DNA expression. Furthermore, the use of the microinjection technique provides an elegant approach to directly control the localization of the therapeutic nucleic acid immediately prior to irradiation. Fluorescence microscopy revealed distinct differences in the intracellular distributions of siRNA/PEG-*b*-P(APNBMA)$_{23.6}$ polyplexes after a 1 h and 3 h transfection. Based on this observation, it is likely that employing UV treatment at varying transfection times could impact the efficacy of protein silencing. A study of this nature can be performed to optimize the timing of siRNA release to provide enhanced protein silencing. Additionally, quantitative real-time polymerase chain reaction (qRT-PCR) may provide additional insight into the activity of these materials through direct measurement of the levels of the mRNA substrate.

Another potential area of improvement for delivery from these structures is modification of the polymer design. Tuning the molecular structure of the integrated photolabile group modifies the efficiency of the photolysis reaction. For example, incorporating an α-methyl group onto the benzylic carbon has been shown to enhance the relative cleavage kinetic rate by a factor of at least five.[4] Thus, modifications to the polymer structures have the potential to dramatically enhance cleavage and subsequent protein expression/gene silencing, and can be applied to the aforementioned studies. Additionally, targeting ligands may be incorporated as another functional modification to this delivery platform to improve its potential for *in vivo* application.

Following the introduction of a system to control gene association through stimuli-responsive polymer cleavage, the work of Chapter 5 introduced the design of a

novel nanoconjugate with combined features for cellular targeting and controlled assembly/release. Specifically, cell-binding moieties are incorporated to allow for interactions with cell surface receptors and direct cellular uptake; endosomolytic arms introduce a method to control the cytoplasmic release of the nanoconjugate; and finally, siRNA-binding arms allow for nucleic acid association through non-electrostatic interactions and cell-triggered liberation of siRNA from these structures due to the incorporation of cleavable linker (shown in Figure 6.5).

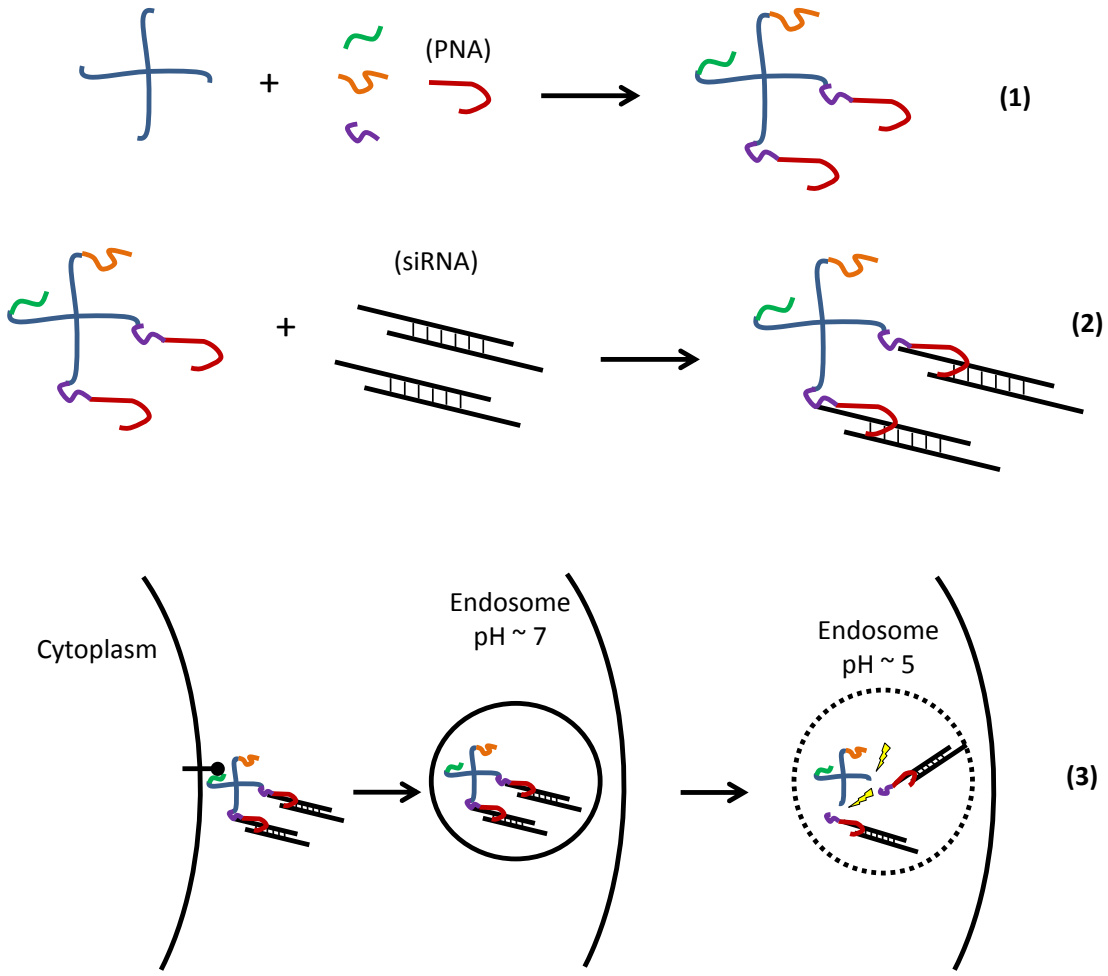

Figure 6.5 Versatile PNA-peptide-PEG (PPP) for siRNA delivery. (a) Peptides and PNA (red) assemble on a PEG scaffold (blue) to form PPP. (b) PPP conjugates self-assemble with siRNA via hydrogen bonding between PNA arms and 5'-sense extensions on siRNA. (c) Cell-binding arms (green) stimulate endocystosis, and endosomolytic arms (orange) promote endosomal rupture. The lysosomal endopeptidase cathepsin L (lightning bolt) releases the siRNA from the conjugates via cleavage of the cathepsin L-cleavable peptide (purple).

Solution-based methods afforded efficient preparation of PNA-peptide and peptide-PEG conjugates towards the preparation of the full PNA-peptide-PEG (PPP)

assembly. High conversion of peptide thiols was demonstrated (75 ± 6% for TAT-C peptide) in the preparation of TAT-functionalized PEG. Furthermore, RP-HPLC purification and MALDI-TOF MS demonstrated the successful preparation of varying derivatizations of TAT-PEG conjugates. However, these solution-based studies highlighted the need for multiple rounds of purification in the preparation of the full PPP assembly. A solid-phase strategy was similarly investigated as a more facile approach to PPP preparation. Using this method, PNA and a protected Cathepsin L-cleavable peptide precursor were prepared for on-resin PPP preparation. However, the neutral nature of the prepared PNA hindered attempts at MS characterization. Separately from the solution- and solid-phase PPP preparation strategies, a siRNA sequence was designed and revealed sequence-specific hybridization with PNA afforded by a 5'-sense extension.

The investigations detailed in this Chapter highlighted the potential for efficient conjugate design and preparation by using a combined solution- and solid-phase strategy to minimize the losses that may be encountered during the purifications of the solution-phase approach. In fact, the synthesis of the PNA-peptide arm and PEG conjugation on resin affords the potential to improve the yields and efficiency of conjugate preparation with fewer intermediate purification steps. The PPP designed in the studies of Chapter 5 is primarily proof of principle. Thus, further exploration of the construct will be necessary to provide full comprehension of this delivery system. Importantly, a detailed understanding of the functional utility of the individual components in the PPP conjugate is still needed.

Following the preparation of this nanoconjugate, initial studies should investigate its ability to promote *in vitro* gene silencing in a cancer cell line. Due to

the demonstration of the Cathepsin L upregulation in a range of cancer cells,[5-7] the B16-F0 cancer cells previously used in the Sullivan lab would provide a useful system for study. Despite the overexpression of Cathepsin L in cancer cells this protease exists in range of cell lines. Thus, the cell-specificity of the system should be investigated in multiple cell lines to explore the potential for off-target silencing. An additional area for exploration is the unpackaging of these PPP structures. Thus, cell-free studies using the Cathepsin L protein, and conjugates prepared with FRET labels on both siRNA and the PPP scaffold would provide valuable insight into their the disassembly and subsequent siRNA release. Additionally, similar studies using a scrambled sequence would be particularly useful in understanding the release profile from the PPP construct. *In vitro* investigations into the utility of the RGD targeting ligand may involve pre-saturation of cell surface receptors with an RGD peptide prior to the delivery of the targeted conjugate.

6.2 Final Perspective

Due to the complex nature of the gene delivery pathway a better understanding of the assembly and subsequent trafficking of gene delivery carriers is necessary to realize the potential of nucleic acids as therapeutics. Thus, strategies to control gene association and release from these carriers are particularly attractive for therapeutic delivery. Stimuli-responsive carriers introduce the favorable feature of controlled methods to release nucleic acids and enhance the efficiency of nucleic acid presentation to cells. However, the challenges associated with *in vivo* delivery highlight the need to develop structures that address the extra- and intracellular barriers to delivery including stable extracellular association, prolonged circulation, and controlled intracellular destabilization at an intracellular target. With the observed

laboratory and clinical successes of DNA and siRNA delivery, collaborative efforts in non-viral carrier design and delivery have the potential to significantly enhance the field of non-viral gene delivery.

REFERENCES

1. Fant, K.; Norden, B.; Lincoln, P., Using ethidium to probe nonequilibrium states of DNA condensed for gene delivery. *Biochemistry* **2011,** 50, (7), 1125-7.
2. Gary, D. J.; Puri, N.; Won, Y. Y., Polymer-based siRNA delivery: perspectives on the fundamental and phenomenological distinctions from polymer-based DNA delivery. *J Control Release* **2007,** 121, (1-2), 64-73.
3. Larsen, J. D.; Reilly, M. J.; Sullivan, M. O., Using the epigenetic code to promote the unpackaging and transcriptional activation of DNA polyplexes for gene delivery. *Mol Pharm* **2012,** 9, (5), 1041-51.
4. Kim, M. S.; Diamond, S. L., Photocleavage of o-nitrobenzyl ether derivatives for rapid biomedical release applications. *Bioorg Med Chem Lett* **2006,** 16, (15), 4007-10.
5. Zhang, W.; Wang, S.; Wang, Q.; Yang, Z.; Pan, Z.; Li, L., Overexpression of cysteine cathepsin L is a marker of invasion and metastasis in ovarian cancer. *Oncol Rep* **2014,** 31, (3), 1334-42.
6. Jean, D.; Rousselet, N.; Frade, R., Expression of cathepsin L in human tumor cells is under the control of distinct regulatory mechanisms. *Oncogene* **2006,** 25, (10), 1474-84.
7. Turk, V.; Turk, B.; Guncar, G.; Turk, D.; Kos, J., Lysosomal cathepsins: structure, role in antigen processing and presentation, and cancer. *Adv Enzyme Regul* **2002,** 42, 285-303.

I

PREPARATION AND CHARACTERIZATION OF PHOTOCLEAVABLE POLYMERS

Materials. Di-*tert*-butyl dicarbonate (Boc_2O), 5-Hydroxy-2-nitrobenzaldehyde (HNBA), bromopropylamine hydrobromide, 18-crown-6, sodium borohydride ($NaBH_4$), triethylamine (Et_3N), methacryloyl chloride, concentrated hydrochloric acid (HCl), anisole, copper bromide (Cu(I) Br), N,N,N',N',N"-pentamethyldiethylenetriamine (PMDETA), methoxy PEG (mPEG), bromoisobutyryl bromide, calcium hydride (CaH_2) and anhydrous 4.0 N HCl in dioxane were purchased from Sigma Aldrich and used as received. Potassium carbonate (K_2CO_3) was purchased from Sigma Aldrich and dried at 120 ˚C for at least 18 h before use. Tetrahydrofuran (THF), sodium bicarbonate ($NaHCO_3$), diethyl ether, sodium sulfate (Na_2SO_4), methanol, acetone, ethyl acetate, and hexanes were purchased from Fisher Scientific and used as received. Dichloromethane (DCM) was purchased from Fisher Scientific and distilled from CaH_2 prior to use. Deionized water (DI water) used during monomer and polymer synthesis and for dialysis was obtained from an in-house source. Water used in characterization was obtained from a Milli-Q water purification system (resistivity = 18.2 MΩ·cm). 1× Dulbecco's phosphate buffered saline (DPBS) (150 mM NaCl, with calcium and magnesium) was purchased from Fisher, Opti-MEM® I Reduced Serum Media (buffered with HEPES and sodium bicarbonate, and supplemented with hypoxanthine, thymidine, sodium pyruvate, L-glutamine, trace elements, and growth factors) was purchased from Life Technologies. *4*-(*2*-hydroxyethyl)-*1*-piperazineethanesulfonic acid (HEPES) sodium salt was

purchased from Fisher and dissolved at 20 mM in ultrapure water, and then the pH was adjusted to ≈6 using 1.0 M HCl or 1.0 M NaOH.

Synthesis of *tert*-butyl(3-bromopropyl)carbamate. Bromopropylamine hydrobromide salt (10.03 g, 45.8 mmol) was dissolved in 300 mL of THF in a 500 mL round-bottomed flask. A solution of $NaHCO_3$ (7.77 g, 92.4 mmol) in DI water (180 mL) was added, and the solution became cloudy. Boc_2O (10.04 g, 46.0 mmol) was weighed out in a scintillation vial, dissolved in 10 mL THF, and added to the round-bottomed flask. The solution was stirred at 23 ˚C for 18 h. Afterward, the reaction was quenched with 300 mL of DI water to form two clear, colorless layers. This mixture was extracted with diethyl ether (100 mL, 3×), and the organic phase was washed with brine (100 mL, 3×). Then, the organic phase was dried over Na_2SO_4 and concentrated on a rotary evaporator to yield a clear, slightly yellow liquid. The product was recrystallized from hexanes 3× at -20 ˚C, yielding white crystals. Then, the product was dried under reduced pressure, and characterized using ^{1}H NMR spectroscopy. ^{1}H NMR (600 MHz, $CDCl_3$) δ 4.66 (s, 1H), 3.44 (t, J = 6.5 Hz, 2H), 3.27 (q, J = 6.3 Hz, 2H), 2.05 (p, J = 6.4 Hz, 2H), 1.44 (s, 9H).

Synthesis of 3-(hydroxymethyl)-4-nitrophenol (HMNP). HNBA (10.01 g, 59.8 mmol) was dissolved in 300 mL of methanol and cooled to 0 ˚C. $NaBH_4$ (4.64 g, 122.6 mmol) was added slowly over 20 min. **The reaction bubbles violently upon $NaBH_4$ addition, take caution!** The reaction proceeded for 2 h after $NaBH_4$ addition. Afterward, the reaction was quenched with 70 mL of 5% $HCl_{(aq)}$, and the solvent was removed using a rotary evaporator to yield a white solid. The product was

characterized with ^{1}H NMR spectroscopy. ^{1}H NMR (600 MHz, DMSO) δ 10.92 (s, 1H), 8.05 (d, *J* = 9.0 Hz, 1H), 7.26 (d, *J* = 2.7 Hz, 1H), 6.79 (dd, *J* = 9.0, 2.8 Hz, 1H), 5.52 (d, *J* = 4.8 Hz, 1H), 4.82 (d, *J* = 3.8 Hz, 2H).

Synthesis of *tert*-butyl(3-(3-(hydroxymethyl)-4-nitrophenoxy)propyl)carbamate (HNPC). HMNP (3.52 g, 20.8 mmol) and dried K_2CO_3 (7.21 g, 52.1 mmol) were dissolved in 100 mL of acetone and heated for 15 min at 60 ˚C in a two-neck round-bottomed flask equipped with a reflux condenser and a Teflon-coated septum. Then, a solution of *tert*-butyl(3-bromopropyl)carbamate (7.44 g, 31.2 mmol) in minimal acetone was added using a syringe, and the solution was stirred for 10 min. Subsequently, a solution of 18-crown-6 (0.55g, 2.0 mmol) in minimal acetone was added via syringe, and the solution was heated under reflux for 18 h. Following the reaction, the solution was concentrated using a rotary evaporator to yield a brown liquid. The product was dissolved in 50 mL of DCM and washed with DI water (50 mL, 3×). Then, the organic phase was dried over Na_2SO_4 and removed using a rotary evaporator, yielding a brown oil. The oil was added to hexanes resulting in two phases: a brown oil and cloudy supernatant. The mixture was heated until the supernatant became clear (40-50 ˚C), after which the supernatant was discarded. The oil was washed twice more to yield the purified product, which was dried under vacuum to yield a brown solid. The product was characterized using ^{1}H NMR spectroscopy. ^{1}H NMR (600 MHz, DMSO) δ 8.13 (d, *J* = 9.1 Hz, 1H), 7.33 (d, *J* = 2.6 Hz, 1H), 7.01 (dd, *J* = 9.1, 2.8 Hz, 1H), 6.95 (t, *J* = 5.3 Hz, 1H), 5.60 (t, *J* = 5.5 Hz, 1H), 4.85 (d, *J* = 5.5 Hz, 2H), 4.11 (t, *J* = 6.1 Hz, 2H), 3.08 (q, *J* = 6.6 Hz, 2H), 1.86 (p, *J* = 6.5 Hz, 2H), 1.36 (s, 12H).

Synthesis of 5-(3-(Boc-amino)propoxy)-2-nitrobenzyl methacrylate (Boc-APNBMA). Et_3N (2.51 g, 24.8 mmol) and HNPC (4.20 g, 12.8 mmol) were dissolved in 400 mL of DCM in a 500 mL round-bottomed flask and cooled to 0 ˚C. Methacryloyl chloride (1.50 g, 14.4 mmol) was added slowly, and the solution was stirred for 23 h. After the reaction, the solution was washed with 5% $HCl_{(aq)}$ (75 mL, 3×), saturated $NaHCO_{3(aq)}$ (100 mL, 3×), and DI water (70 mL, 3×). The organic layer was dried over Na_2SO_4 and concentrated on a rotary evaporator to yield a brown oil. The product was further purified using silica gel column chromatography (1/1 ethyl acetate/hexanes mobile phase) to yield a white solid, which was dried under vacuum and characterized using ^{1}H NMR spectroscopy (final yield 2.55 g). ^{1}H NMR (600 MHz, DMSO) δ 8.21 – 8.16 (d, 1H), 7.15 – 7.09 (m, 2H), 6.94 (t, J = 5.5 Hz, 1H), 6.11 (s, 1H), 5.79 – 5.74 (m, 1H), 5.51 (s, 2H), 4.12 (t, J = 6.1 Hz, 2H), 3.08 (q, J = 6.5 Hz, 2H), 1.93 (s, 3H), 1.85 (p, J = 6.3 Hz, 2H), 1.36 (s, 11H).

Synthesis of methoxy poly(ethylene glycol) isobutyryl bromide (mPEG-Br). mPEG (5.0 g, 1.0 mmol) and Et_3N (0.38 g, 3.7 mmol) were dissolved in 25 mL of dry DCM in a 50 mL round-bottomed flask equipped with a magnetic stir bar and cooled to 0 ˚C. To this solution, α-bromoisobutyryl bromide (0.4 mL, 3.2 mmol) was added dropwise, and the solution was allowed to warm to 23 ˚C and stirred for 18 h. After the reaction, the solution was quenched with 1 mL of water and washed with a saturated $NaHCO_3$ solution (aq; 25 mL, 3×). The organic layer was dried over Na_2SO_4 and concentrated on a rotary evaporator. Then, mPEG-Br was dissolved in methanol, precipitated in cold diethyl ether, and pelleted via centrifugation at 4000

rpm at 4 ˚C for 15 min. The precipitation and centrifugation steps were repeated twice to yield a white powder. ^{1}H NMR (600 MHz, $CDCl_3$) δ 4.35 - 4.29 (m, 2H), 3.64 (s, 459H), 3.37 (s, 3H), 1.93 (s, 6H).

Synthesis of mPEG-*b*-P(Boc-APNBMA)$_n$. As an example, for the synthesis of mPEG-*b*-P(Boc-APNBMA)$_{7.9}$, Boc-APNBMA (0.60 g, 1.5 mmol) and mPEG-Br (0.54 g, 0.10 mmol) were weighed out and transferred into a glove box. Inside a glove box, a solution of Cu(I)Br (15 mg, 0.10 mmol) and PMDETA (21 mg, 0.12 mmol) in 4 mL of anisole was prepared in a 25 mL round-bottomed flask equipped with a magnetic stir bar. Then, mPEG-Br and Boc-APNBMA were dissolved in 4 mL of anisole and transferred into the round-bottomed flask, which was then sealed with a rubber septum. The flask was transferred out of the glove box and heated to 70 ˚C. After 24 h, the diblock copolymer was precipitated in cold diethyl ether, and pelleted via centrifugation at 4000 rpm at 4 ˚C for 15 min. The pellet was dissolved in minimal methanol and the precipitation and centrifugation were repeated twice to yield a white powder. Then, the polymer was added to DI water, yielding a cloudy solution. mPEG-*b*-P(Boc-APNBMA)$_n$ was pelleted via centrifugation at 4000 rpm at 4 ˚C for 25 min, which removed residual mPEG-Br macroinitiator.

Synthesis of mPEG-*b*-P(APNBMA·HCl)$_n$. As an example, for the synthesis of mPEG-*b*-P(APNBMA•HCl)$_{7.9}$, mPEG-*b*-P(Boc-APNBMA)$_{7.9}$ (0.72 g, 0.09 mmol) was placed in a 25 mL round-bottomed flask equipped with a magnetic stir bar and sealed with a rubber septum. The flask was purged with Ar (gas) for 10 min, and then cooled to 0 ˚C. An anhydrous 4 N HCl solution in 1,4-dioxane (15 mL) was added,

and the solution was stirred for 2 h. After the reaction, the polymer was precipitated in cold diethyl ether, redissolved in DI water and dialyzed (3500 MWCO) against DI water for 24 h with three solvent exchanges.

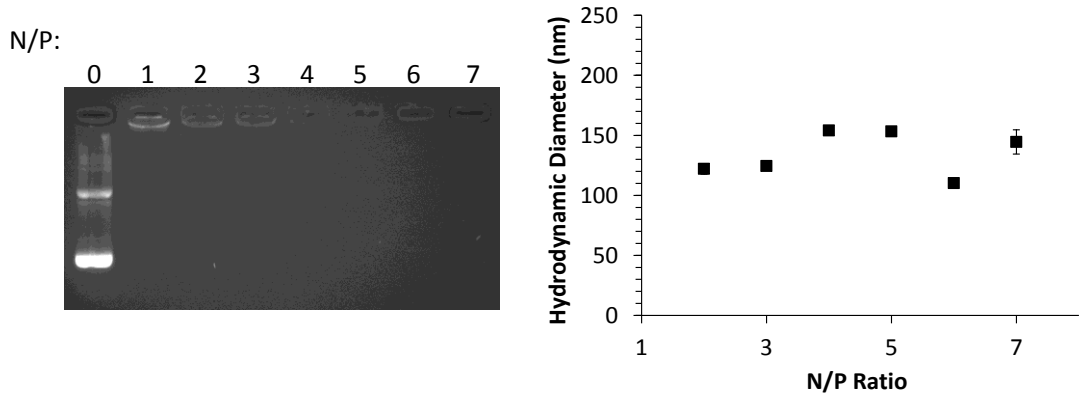

Figure A.1 DNA condensation by mPEG-*b*-P(APNBMA·HCl)$_{23.6}$ monitored by (a) agarose gel electrophoresis and the (b) YOYO-1 fluorescence quenching assay.

Determination of Exponential Decay Constant. The relative absorbance data was fit with an exponential decay. The decay follows the relationship:

$$I = \exp\frac{-t}{\tau},$$

in which I is the relative absorbance, t is time (s), and τ is the decay constant (s). Increasing the molecular weight of the cationic block caused a decrease in the decay constant (340 s for n = 7.9 and 220 s for n = 23.6), which suggested an accelerated photocleavage. Furthermore, the use of mPEG-*b*-P(APNBMA·HCl)$_{7.9}$ to encapsulate DNA into polyplexes decreased the decay constant to 160 s.

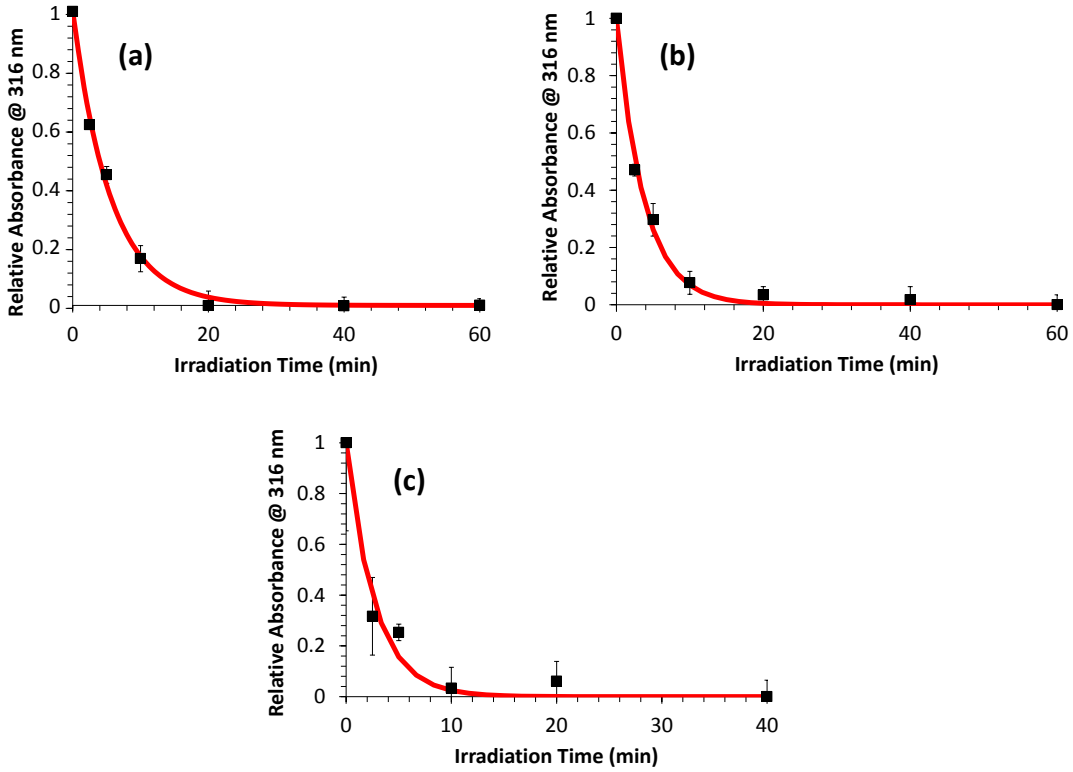

Figure A.2 Normalized absorbance at 316 nm for (a) mPEG-*b*-P(APNBMA·HCl)$_{7.9}$, (b) mPEG-*b*-P(APNBMA·HCl)$_{23.6}$, and (c) DNA/mPEG-*b*-P(APNBMA·HCl)$_{7.9}$ polyplexes as a function of UV irradiation time. The log of the normalized intensity was plotted against time to determine τ [$I = \exp(-t/\tau)$, in which I is normalized absorbance, t is time, and τ is the exponential decay constant].

I

CELLULAR TOXICITY OF PHOTOCLEAVABLE POLYMERS

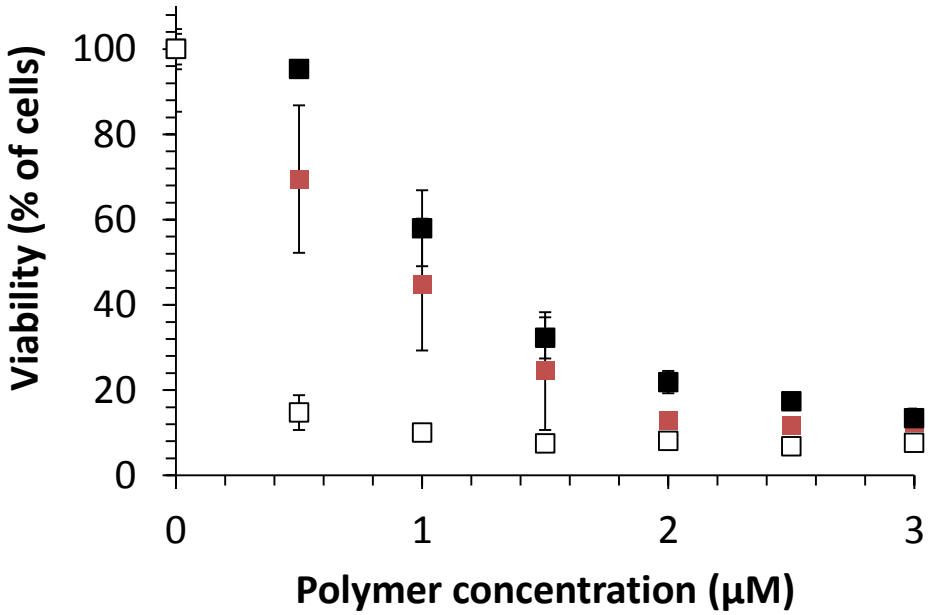

Figure B.1 **Cell viability upon exposure to mPEG-*b*-P(APNBMA·HCl)$_{7.9}$ (black), mPEG-*b*-P(APNBMA·HCl)$_{23.6}$ (red), and PEI (white) at various concentrations. IC$_{50}$ values of mPEG-*b*-P(APNBMA·HCl)$_{7.9}$ and mPEG-*b*-P(APNBMA·HCl)$_{23.6}$ are 1.05 µM and 0.77 µM respectively.**

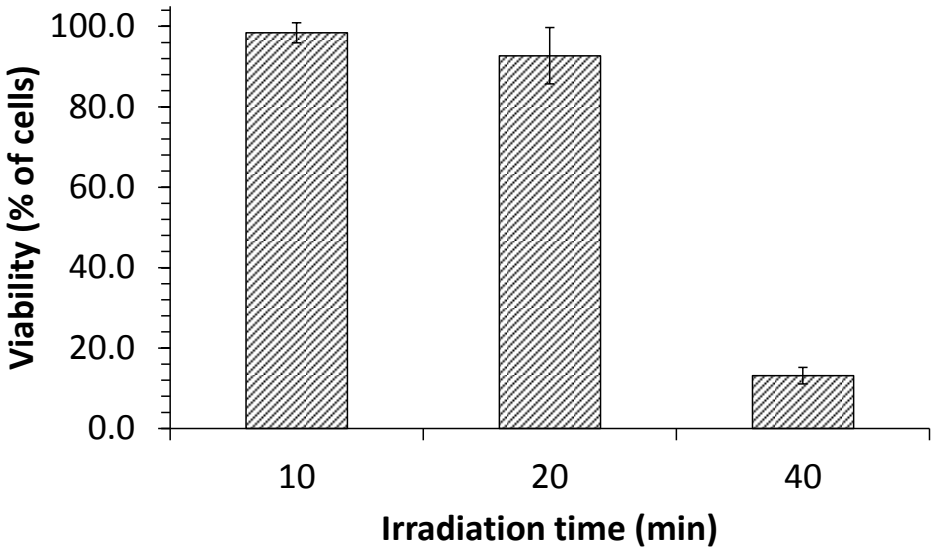

Figure B.2 Cell viability upon exposure to 365 nm light at 200 W/m^2 for 10, 20, and 40 min.

I

CHARACTERIZATION OF FUNCTIONAL PEPTIDES AND CONJUGATES

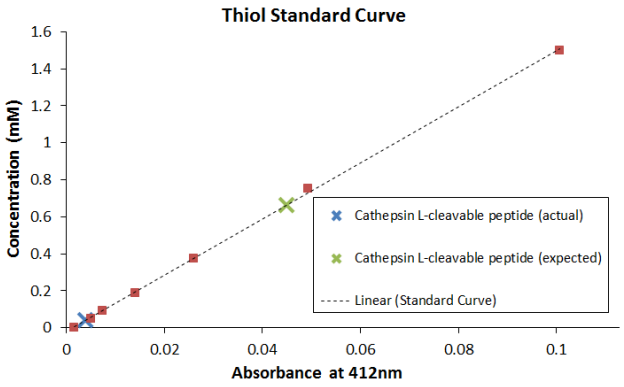

Figure C.1 Quantification of free thiols in cathepsin L-cleavable peptide (NH_2-CRDAKLKWGDRC-$CONH_2$).

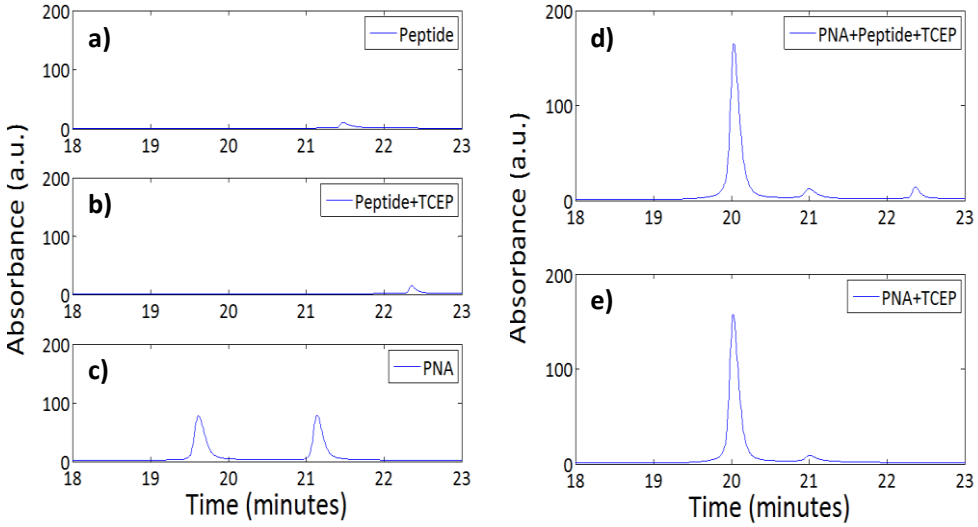

Figure C.2 RP-HPLC demonstration of PNA/TCEP side reaction showing (a) cathepsin L-cleavable peptide, (b) reduced peptide, (c) PNA, (d) PNA-peptide preparation with TCEP included, and (d) PNA and TCEP.

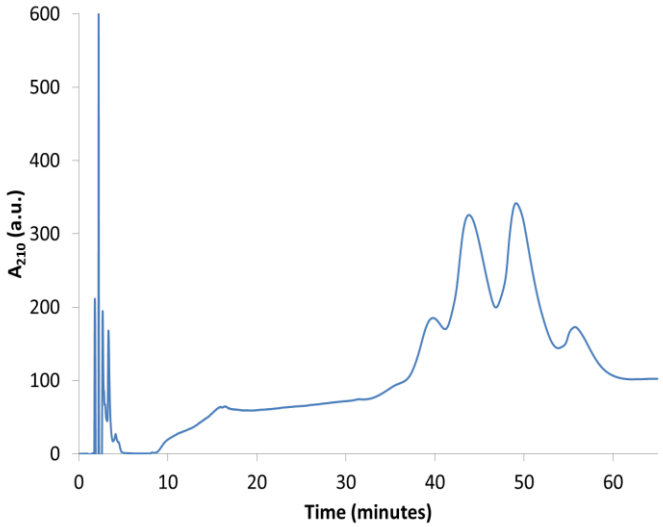

Figure C.3 The RP-HPLC trace of a representative RGD peptide-PEG reaction. The absorbance of the elutant was measured at 210 nm over time.